National Library of Canada
Canadian Theses Service
Ottawa, Canada
K1A 0N4

Bibliothèque nationale du Canada
Services des thèses canadiennes

CANADIAN THESES

THÈSES CANADIENNES

NOTICE

The quality of this microfiche is heavily dependent upon the quality of the original thesis submitted for microfilming. Every effort has been made to ensure the highest quality of reproduction possible.

If pages are missing, contact the university which granted the degree.

Some pages may have indistinct print especially if the original pages were typed with a poor typewriter ribbon or if the university sent us an inferior photocopy.

Previously copyrighted materials (journal articles, published tests, etc.) are not filmed.

Reproduction in full or in part of this film is governed by the Canadian Copyright Act, R.S.C. 1970, c. C-30. Please read the authorization forms which accompany this thesis.

AVIS

La qualité de cette microfiche dépend grandement de la qualité de la thèse soumise au microfilmage. Nous avons tout fait pour assurer une qualité supérieure de reproduction.

S'il manque des pages, veuillez communiquer avec l'université qui a conféré le grade.

La qualité d'impression de certaines pages peut laisser à désirer, surtout si les pages originales ont été dactylographiées à l'aide d'un ruban usé ou si l'université nous a fait parvenir une photocopie de qualité inférieure.

Les documents qui font déjà l'objet d'un droit d'auteur (articles de revue, examens publiés, etc.) ne sont pas microfilmés.

La reproduction, même partielle, de ce microfilm est soumise à la Loi canadienne sur le droit d'auteur, SRC 1970, c. C-30. Veuillez prendre connaissance des formules d'autorisation qui accompagnent cette thèse.

THIS DISSERTATION
HAS BEEN MICROFILMED
EXACTLY AS RECEIVED

LA THÈSE A ÉTÉ
MICROFILMÉE TELLE QUE
NOUS L'AVONS REÇUE

NL 339 (r. 86/01)

Canada

National Library of Canada | Bibliothèque nationale du Canada

Ottawa, Canada
K1A 0N4

55

TC –

0-315-22921-7

CANADIAN THESES ON MICROFICHE SERVICE – SERVICE DES THÈSES CANADIENNES SUR MICROFICHE

PERMISION TO MICROFILM – AUTORISATION DE MICROFILMER

• Please print or type – Écrire en lettres moulées ou dactylographier

AUTHOR – AUTEUR

Full Name of Author – Nom complet de l'auteur

OMOTAYO ABAYOMI FAKINLEDE

Date of Birth – Date de naissance

APRIL 1, 1956

Canadian Citizen – Citoyen canadien

☐ Yes / Oui ☑ No / Non

Country of Birth – Lieu de naissance

NIGERIA

Permanent Address – Résidence fixe

80 OYEMEKUN ROAD
AKURE, NIGERIA

THESIS – THÈSE

Title of Thesis – Titre de la thèse

SOME FACTORS AFFECTING FATIGUE CRACK PROPAGATION

Degree for which thesis was presented
Grade pour lequel cette thèse fut présentée

PH. D

Year this degree conferred
Année d'obtention de ce grade

1985

University – Université

UNIVERSITY OF ALBERTA

Name of Supervisor – Nom du directeur de thèse

DR F. ELLYIN

AUTHORIZATION – AUTORISATION

Permission is hereby granted to the NATIONAL LIBRARY OF CANADA to **microfilm** this thesis and to **lend** or **sell copies of the film.**

The author reserves other publication rights, and neither the thesis nor extensive extracts from it may be printed or otherwise reproduced without the author's written permission.

L'autorisation est, par la présente, accordée à la BIBLIOTHÈQUE NATIONALE DU CANADA de **microfilmer** cette thèse et de **prêter** ou de **vendre des exemplaires du film.**

L'auteur se réserve les autres droits de publication; ni la thèse ni de longs extraits de celle-ci ne doivent être imprimés ou autrement reproduits sans l'autorisation écrite de l'auteur.

ATTACH FORM TO THESIS – VEUILLEZ JOINDRE CE FORMULAIRE À LA THÈSE

Signature

Date

October 9, 1985

NL-91 (r. 84/03)

Canada

THE UNIVERSITY OF ALBERTA

SOME FACTORS AFFECTING FATIGUE CRACK PROPAGATION

by

(C) OMOTAYO ABAYOMI FAKINLEDE

A THESIS

SUBMITTED TO THE FACULTY OF GRADUATE STUDIES AND RESEARCH

IN PARTIAL FULFILMENT OF THE REQUIREMENTS FOR THE DEGREE

OF DOCTOR OF PHILOSOPHY

DEPARTMENT OF MECHANICAL ENGINEERING

EDMONTON, ALBERTA

FALL 1985

THE UNIVERSITY OF ALBERTA

RELEASE FORM

NAME OF AUTHOR OMOTAYO ABAYOMI FAKINLEDE

TITLE OF THESIS SOME FACTORS AFFECTING FATIGUE CRACK PROPAGATION

DEGREE FOR WHICH THESIS WAS PRESENTED DOCTOR OF PHILOSOPHY

YEAR THIS DEGREE GRANTED FALL 1985

Permission is hereby granted to THE UNIVERSITY OF ALBERTA LIBRARY to reproduce single copies of this thesis and to lend or sell such copies for private, scholarly or scientific research purposes only.

The author reserves other publication rights, and neither the thesis nor extensive extracts from it may be printed or otherwise reproduced without the author's written permission.

(SIGNED) .....

PERMANENT ADDRESS:

80 Oyemekun Road

Akure, Ondo State,

NIGERIA

DATED October 2 1985

THE UNIVERSITY OF ALBERTA

FACULTY OF GRADUATE STUDIES AND RESEARCH

The undersigned certify that they have read, and recommend to the Faculty of Graduate Studies and Research, for acceptance, a thesis entitled Some Factors affecting Fatigue Crack Propagation submitted by Omotayo Abayomi Fakinlede in partial fulfilment of the requirements for the degree of Doctor of Philosophy

.....

Supervisor

.....

.....

.....

.....

External Examiner

Date..October 7, 1985.....

ABSTRACT

The slow stable growth of a fatigue crack is modelled from a damage accumulation viewpoint. The crack-tip vicinity is treated as a chain of uniaxial fatigue elements subjected to the stress/strain level at the positions they occupy in each crack configuration. The cyclic stress/strain field for each level of applied loading range is derived using the well known plastic superposition principle from the results obtained based on monotonic loading solutions. The singularity generated at the origin by the latter has often led to the removal of the crack-tip damage from the failure criterion by previous investigators. In this work, the cyclic stress/strain distribution is modified to conform to experimental observation on the bounds of the stress/strain levels sustainable on a fatigue element. The crack growth rate law thus obtained contains some of the well known laws as special cases.

The modelling of the crack-tip as a chain of material elements is suitable for the probabilistic simulation of fatigue crack growth. A modified form of the weakest-link theory of Weibull is used as the crack growth criterion. In the absence of an exact stochastic failure criterion, asymptotic consideration led to the use of a form of the statistical Miner's law for linear damage accumulation. The stochastic simulation process is a marked improvement over the memoriless probabilistic models previously

attempted. The damage history of each fatigue element is fully accounted for in the application of the failure criterion. The historical damage on each element due to previous crack advances is quantified, and shown to be a significant portion of the linear damage process.

One major weak point of the fatigue crack-tip growth modelling similar to the one presented is in the derivation of cyclic properties using equations derived from strictly monotonic loading analysis. Such quantities like the stress/strain field and the cyclic J-integral are usually obtained from the plastic superposition principle. An alternative approach to this is shown to exist using the results from dislocation theory. This is unfortunately restricted to the elastic-perfectly plastic case. In order to extend this to include the work-hardening material, it is necessary to derive the monotonic loading dislocation field based on a friction stress that is dependent on the displacement at each position. The unloading of the dislocation field using the same nonlinear friction stress facilitates the treatment of the work-hardening unloading problem in a way that accounts for the Bauschinger effects. The special cases of isotropic, kinematic and corner hardening are highlighted.

Acknowledgements

The author expresses his deepest gratitude to his supervisor, Dr. F. Ellyin, for his academic moral and financial support during the course of this thesis. He is also thankful to the members of the supervisory committee especially Dr. F. H. Vitovec for the many helpful suggestions received at various times. Several colleagues and friends gave their time in helping to prepare the thesis. Their help is gratefully acknowledged. Special thanks to Mrs. Shelley Lorimer who proofread the final draft, and to Miss Ruth Hodges and Ms. Gail Anderson for typing the manuscript.

The author will also like to express his gratitude to his family especially his wife, Ono, whose patience and encouragement at some critical moments was instrumental to a successful completion of this work.

Table of Contents

Chapter		Page
1.	INTRODUCTION	1
	1.1 General Concepts	1
	1.2 Fracture and Fatigue	4
	1.3 Damage Accumulation	9
	1.4 Probabilistic Considerations	11
	1.5 Scope	14
	1.6 Organization of this Work	17
2.	SELECTED WORK RELATED TO DAMAGE ACCUMULATION MODELLING	19
	2.1 The Plastic Superposition Method	20
	2.2 Deterministic Cumulative Damage Models	24
	2.3 Weakest-Link Modelling of Fatigue Crack Growth	30
	2.4 Dislocation Model of the Stress/Strain Field	36
	2.5 Unloading and Cyclic J-Integral	41
	2.6 Numerical Solutions of Integral Equations	44
3.	DAMAGE ACCUMULATION AND STOCHASTIC MODELLING OF CRACK GROWTH	47
	3.1 Crack-Tip Modelling	47
	3.2 Probabilistic Growth Rate Law	56
	3.3 Simulation Process	68
	3.4 Results	71
4.	DISLOCATION MODEL OF NON-LINEAR HARDENING	92
	4.1 Introduction	92
	4.2 A Non-Linear Work-Hardening Model	95
	4.3 Conditions for Inversion of Equilibrium Equation	98

4.4 Displacement Integral Equations 109

4.5 Numerical Solution of the Work-Hardening Equations 113

4.6 Results and Discussion 122

4.7 Comparison With Continuum Models 130

5. UNLOADING FIELD AND CYCLIC J-INTEGRAL 143

5.1 Introduction 143

5.2 Work Hardening Unloading Problem 145

5.3 Solution of the Unloading Displacement Equations 155

5.4 The Unloading J-Integral 157

5.5 Results and Discussion 160

6. DISCUSSION AND CONCLUSIONS 174

6.1 Deterministic Model 174

6.2 Probabilistic Simulation 175

6.3 Dislocation Modelling of Cyclic Field 177

6.4 Future Work 179

List of References 181

Appendix 189

List of Tables

Table		Page
3.1	Material properties	84
3.2	Threshold stress intensity factor range	84
4.1	Variation in crack-tip displacement due to external loading and hardening	123

List of Figures

Figure		Page
1.1	Through thickness crack in an infinite plate	5
2.1	Derivation of cyclic distribution from monotonic field	22
2.2	Stress-strain relationship in reversed axes	25
2.3	Edge dislocations ahead of a loaded crack	38
3.1	Stress-strain field in the plastic zone	49
3.2	Random microstructural deformation zones	57
3.3	Stages of damage accumulation	60
3.4	Trend and statistical equilibrium	62
3.5	Cumulative damage and fatigue damage resistance	63
3.6	Modified continuum stress-strain ranges	69
3.7	Historical damage vs distance for 2219-T851-Aluminium	72
3.8	Historical damage vs distance for A516-Gr 70Steel	73
3.9	Historical damage vs distance for A533B Steel	74
3.10	Historical damage vs ΔK for 2219-T851-Aluminium	75
3.11	Historical damage vs ΔK for A516-Gr 70-Steel	76
3.12	Historical damage vs ΔK for A533B Steel	77
3.13	Weibull probability plot	80
3.14	Extreme value probability plot	81
3.15	Log-normal probability plot	82

Figure Page

3.16 Comparison of experimental and predicted crack propagation rate vs stress intensity factor range 85

3.17 Comparison of experimental and predicted crack propagation rate vs stress intensity factor range 86

3.18 Comparison of experimental and predicted crack propagation rate vs cyclic J-integral (A533 B Steel) 87

3.19 Estimation of crack ΔJ from stress-strain hysteresis loops 89

4.1 Holder condition for a step function 105

4.2 The effect of hardening on crack-tip displacement 124

4.3 The effect of hardening on crack-tip stress 125

4.4 The effect of hardening on crack-tip strain energy density 127

4.5 The effect of hardening on the J-integral 129

4.6 Crack-line strain comparison (negligible hardening) 131

4.7 Crack-line stress comparison (negligible hardening) 132

4.8 Crack-line strain energy density comparison (negligible hardening) 133

4.9 Crack-line strain comparison (mild hardening) 134

4.10 Crack-line stress comparison (mild hardening) 135

4.11 Crack-line strain energy density comparison (mild hardening) 136

4.12 Crack-line strain comparison (high hardening) 137

Figure Page

4.13 Crack-line stress comparison (high hardening) 138

4.14 Crack-line strain energy density comparison (high hardening) 139

4.15 Crack-line strain comparison with continuum results on log-log scale 140

5.1 Reversed yield point for various hardening rules - one dimensional case 147

5.2 Loading and unloading dislocation density functions 150

5.3 Loading sequence 158

5.4 Variation of dislocation density with monotonic and cyclic loading 161

5.5 Cyclic J-integral vs applied strain energy density 166

5.6 Effect of hardening on the crack-tip strain energy density 168

5.7 Variation of crack-tip displacement range with hardening and mean applied stress 169

5.8 Variation of crack-tip stress range with hardening and mean applied stress 170

5.9 Variation of crack-tip strain energy density range with hardening and mean applied stress 171

5.10 Variation of cyclic J-integral with hardening and mean applied stress 173

Nomenclature

Variables

α	inverse of the number of cycles N, coefficient of basis functions
β	cyclic hardening function
δ	small distance, extent of reversed dislocation motion
ε	strain component
ϵ	belongs to
ϕ	cycle ratio, basis functions
λ	Holder's index
η	Residual function
μ	Rigidity Modulus
ρ	microstructural parameter
σ	stress component
γ	shear stress
a	extent of crack-tip plasticity, half crack length
b	Burger's vector
c	half crack length
f	yield surface function
r	plastic zone size
Φ	large number
E	Elastic modulus
H	Holder class
H*	Supplementary Holder class

K	Hardening function
M	Holder's constant
W	Strain Energy
T	Traction Vector
U	Union of sets of points
P	Probability that
[a,b]	closed interval $a \leq x \leq b$
(a,b]	open interval $a < x \leq b$

Subscripts and superscripts

i,j,k,l,m,n	Tensor indices
∞	far field or nominal quantity
p	plastic zone
f	failure
L	lower bound

Chapter 1

INTRODUCTION

1.1 General Concepts

A solid body responds to extreme loading by undergoing large deformations which may or may not be accompanied by a loss of contact between parts of the body. The second phenomenon is called "fracture", and modelling of it is the topic of primary concern in fracture mechanics. It is immediately obvious that the fracture process can be "local" or "global". The latter is often associated with the idea of "catastrophe". A response that leads to a sudden large scale fracture in a real material often literally implies just that - catastrophe - with all its ramifications. It is well known that such a phenomenon is usually accompanied with low plastic deformation and consequently, low energy dissipation. Such a situation has been classified as "brittle fracture". The term brittle may refer to the nature of the material in question itself - but this is not always so. In general, this term refers to the nature of the fracture process also. The converse terminology is "ductile fracture". The two situations they describe refer to events on the micro or on the macro scale. The latter describes situations where the fracture process is attended by large plastic deformations, and consequently, large energy dissipation.

A large section of fracture mechanics studies is based on the idea of the dominant crack. Even though a real material may consist of several cracks nucleating and/or propagating simultaneously, it is still reasonable to consider a single crack in that material. The assumption is that this particular crack "dominates" the others, either in the fact that it is the largest, or it is positioned and oriented in such a way that the stress/displacement field leads to a faster growth to failure than the other cracks in the material. The effect of other cracks and crack-like discontinuities can be dealt with in two possible ways. Firstly, it may be assumed that the other cracks of similar dimensions, and their growth paths are so far away that they do not interact or coalesce with the dominant crack. Their presence could thus be ignored in dealings with the dominant crack. Secondly, for the microcracks and voids that exist along the path of growth, a small region, defined as the fracture process zone is considered, where the continuum laws from the dominant crack do not apply. This is a zone in the neighbourhood of the crack-tip where fracture develops through the successive stages of inhomogeneous slip, void growth, interactions and coalescence, accompanied by bond breaking in the atomic scale. The definition of the fracture process zone is not rigorous, as we shall see later, but it is generally taken as small in size compared to other relevant parameters

like the crack length and other material dimensions.

The broad classifications of fracture as either ductile or brittle can be from a local or global perspective. Within the process zone, brittle fracture can be understood to be the cleavage of grains and/or a separation along grain boundaries, such that the grain structure will appear in a microscopic view of the fractured faces. A locally ductile fracture on the other hand depends more on the nucleating growth and coalescence of voids formed around inclusions and grain boundaries. The fractured faces in such a growth is fibrous. It is to be noted that it is quite possible that a locally ductile fracture may eventually lead to a global brittle fracture. This would happen if the geometrical factors serve to concentrate sufficient energy at a separation site which later acts as the nucleations point for such a phenomenon.

Two other terminologies commonly used in the literature can be clarified here. They are the "initiation" and the "propagation" stages of fracture. These terms occur from the dilemma in fracture mechanics to form macroscopic viewpoint of an evidently microscopic process. The time required for a material to nucleate and propagate a crack to a macroscopically detectable size can be considered the initiation stage. The rest of crack life to the final failure of the material will then be depicted as "propagation" stage. How much of the crack life is classified as initiation may then be solely dependent on

the crack-detection method used. In a situation where the size of the crack is such that its presence does not affect macromechanical properties of the material, it can be classified as initiated crack but non-propagating.

1.2 Fracture and Fatigue

An attempt to relate the stress/displacement field magnitude and distribution in the vicinity of the crack-tip to the nominal stess applied to the structure, to the size, shape and orientation of the crack, or crack-like discontinuity, and to material properties has led to the definition of the stress intensity factor. For a uniform infinite plate subject to uniform tensile load P^{∞} per unit length, containing a through thickness crack of length 2a. (See Figure 1.1) this is defined as:

$$K_I = \sigma\sqrt{\pi a} \qquad 1.1$$

where $\sigma = P^{\infty}/\text{thickness}$, is the nominal stress.
Certain correction factors can be applied to evaluate this quantity for many finite sized material configurations. If the applied loading were in-plane shear, or out-of-plane shear, the equation 1.1 will define the mode II and mode III stress intensity factors K_{II} and K_{III}, respectively.

This definition can now be used to quantify and classify what was loosely termed "extreme loading" in section 1.1. If for a particular value K_{IC} of K_I,

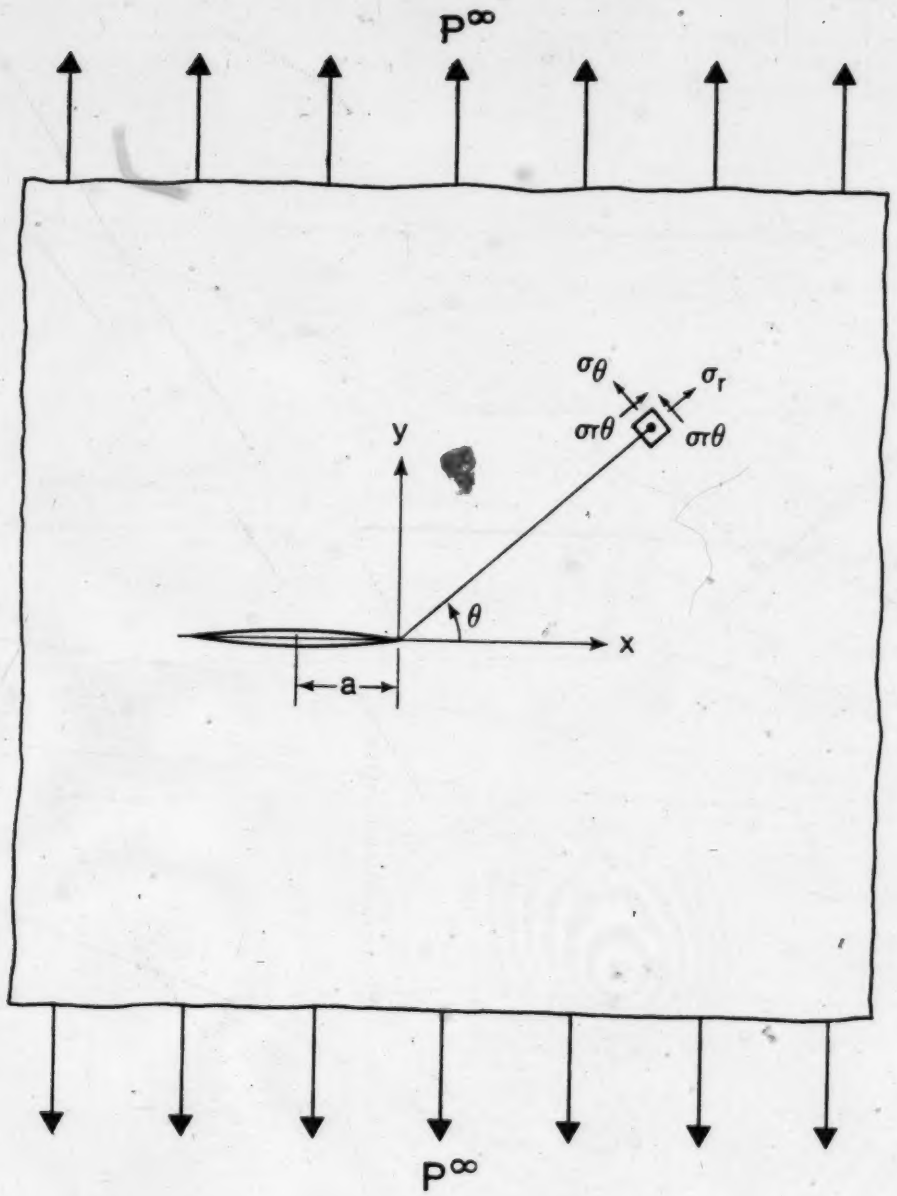

Figure 1.1 Through thickness crack in an infinite plate

instability' occurs, then depending on the applications, the loading leading to a stress intensity factor of K_{IC} may be the extreme loading in question. The latter quantity has been used in the literature to quantify the resistance of a material containing a crack or a crack-like discontinuity, to fracture. It is called "fracture toughness".

However, in many applications, the determination of a single load that could lead to instability or failure is not the primary problem. Situations often arise when the time required for a benign crack to become unstable, under the repeated application of external loads far below the critical loading, is the issue. It may be the converse problem, finding the maximum loading that can be sustained for a given period of time without instability. Such considerations lead to the application of fracture mechanics to fatigue problems. The equivalent expression to equation 1.1 for application in a fatigue setting is:

$$\Delta K_I = \Delta\sigma \sqrt{\pi a} \qquad 1.2$$

where $\Delta\sigma = \Delta P^{\infty}$/thickness, is the applied nominal stress range,

ΔP^{∞} = applied loading range per unit length

and, ΔK_I = the stress intensity factor range.

' A crack on the verge of sudden large extension is said to be unstable.

It is customary practise in the experimental determination of fatigue crack growth rate to express the results graphically as a function of the stress intensity factor range as defined. This has also led to the definition of a ΔK_{IC}, which is the value of ΔK_I at which the growth rate becomes very large and leads to instability. On the other extreme is the value ΔK_{ITH}, or threshold stress intensity factor range, which has been observed for several materials. It corresponds to the value at which the growth rate of a fatigue crack is negligible. If the application is such that it is critical that there be no crack extension at all, any loading leading to a value of the stress intensity factor range higher than ΔK_{ITH} would be considered "extreme" for the crack length in question.

Now, it must be realized that the use of K, or ΔK as defined to characterize the crack-tip activity is valid only when the plasticity region is small compared to the crack length. Such a case would arise when the crack length is large and the external load is small. These are the conditions of linear elastic fracture mechanics, L.E.F.M. The word "elastic" in this terminology is often misunderstood. It does not refer to the situation where the nominal loading is elastic. It is quite possible for the nominal loading to be well within the elastic limit, and still we can have crack-tip plasticity of considerable size compared to the crack length. In such a situation,

even though the body is under nominally "elastic" conditions, the crack-tip activity cannot be described with the linear elastic fracture mechanics theory.

Several alternative theories exist under the broad classification of Nonlinear fracture mechanics. An up-to-date resume of the state of the art in this area has been given by Hutchinson [1]. A parameter that parallels the L.E.F.M. definition of K is the Rice's [2] J-integral, defined by

$$J = \int_{\Gamma} W dy - T_m \frac{\partial u_m}{\partial x} ds \qquad 1.3$$

where W is the strain energy density = $\int_{o}^{\varepsilon_{k\ell}} \sigma_{k\ell}\, d\varepsilon_{k\ell}$, $\sigma_{k\ell}$, $\varepsilon_{k\ell}$ are the stress and strain tensors, respectively, T_m is the traction vector, u_m is the displacment vector ds is the element of length along a path Γ defined in the counter clockwise direction, while dx, dy are cartesian coordinate line elements.

The path independence of the J-integral has made it an attractive parameter for the quantification of the crack-tip plasticity. Its use is not restricted by the small scale yielding limitation. However, when small scale yielding conditions prevail, it is uniquely related to the L.E.F.M. stress intensity factor. Paralleling the development of K, critical J-integral has been defined. It is called J_c. And it has been found necessary to extend it to the case of cyclic loading, ΔJ.

The direct evaluation of J is not easy. In many applications, the indirect interpolation proposed by Shih [3], Shih and Hutchinson [4] has become popular. The challenges for the ΔJ are even greater. To begin with, there is no natural extension of Eq. 1.2 for the J-integral. It depends, in general, as will be shown later, not only on the range of loading, (as ΔK does), but also on the loading states. Moreover, when there is reversed loading, it is not always clear how much of the strain energy density range should be used under the integral in Eq. 1.3 [5].

1.3 Damage Accumulation

The growth of a fatigue crack is intuitively perceived as the accumulation of damage in the material. Fatigue crack growth theories have been based on incremental growth due to a critical amount of damage piled up at the crack-tip. The major ingredients of a successful crack growth by damage accumulation theory are the specification of a measure of the damage functions, the failure criterion and the crack advance. One major group of such theories is based on the low cycle fatigue experiments of Miner [6]. In this work, uniaxial fatigue elements are subject to successive different levels of cyclic loading. The cycle ratio is defined as

$$\phi_i = \frac{N_i}{N_{fi}} \qquad 1.4$$

where N_i is the number of applied cycles and N_{fi} is the number of cycles to failure for a virgin specimen maintained at the loading i.

It was found that, the sum $\Sigma\phi_i$ was approximately unity for a large number of loading ranges i. If the elements at the crack-tip are treated as a succession of uniaxial fatigue elements, the crack growth itself can be seen as the successive failure of these elements. The cycle ratio for the loading level, determined by stress/strain range prevailing on each fatigue element can be taken as the damage function. The addition of these cycle ratios to unity is the failure criterion while the breadth of the fatigue element is the extent of crack extension. Some other authors have used this same principle, however, they substituted the fatigue ductility, for the cycle ratio [7]. Others have based the damage criterion on the crack-tip stress and, more recently, damage accumulation criteria based on the strain energy density has been suggested [8].

In general, most of the damage accumulation theories make use of parameters derivable from low cycle fatigue analysis, either as a damage function, or as a failure or crack advance criterion. These theories can be divided

into two classes. In the one, the damage history of each fatigue element is fully accounted for. The crack advance criterion is such that the element reaches the crack-tip at the exact time it has just exhausted its "fatigue damage resistance", and therefore "fails" in the next cycle. Crack growth, by such theories, occurs in every cycle, as there can be no further damage to the crack-tip element. On the other hand are theories that treat the crack-tip elements as basically virgin. The crack advances when the damage accumulated on an element is equal to its damage resistance.

1.4 Probabilistic Considerations

The need for a statistical approach to the problem of crack propagation cannot be over-emphasized. Bolotin [9] has advocated the construction of a statistical theory of the deformation and fracture of solids. Such a theory, it has been argued, would permit the description of plastic deformation, creep and relaxation, brittle fracture and damage accumulation under cyclic loading, all from a single viewpoint. "By utilizing statistical theories, it would be possible to obtain, in a natural way, all the fundamental relationships for the phenomenological theories of plasticity, creep and fatigue, about which much is presently surmised on the basis of a more or less experimental data" [9]. The general idea behind this viewpoint is supported by Griffith's theory, [10], in

which it was proposed that the difference between the calculated strengths of materials (based on microscopic analyses), and those actually observed resides in the fact that there are randomly sized and oriented flaws which weaken it. Accepting this viewpoint is equivalent to assuming that there will be a distribution of strengths in a given specimen in the sense that a different amount of loading will be needed to fracture it at one or another point.

Existing crack propagation laws (e.g. Paris Law [11]), can, in principle, be integrated to give the expected life of a cyclically loaded structure if the initial crack length as well as the amount of fatigue loading are given. In practice, these two are usually known only in probabilistic terms. Even this deterministic law has statistical boundary conditions in practise. In the ideal situation where the inputs are deterministic, there is often the need to quantify the probability of failure as a function of time, in order to assess the risk involved in not carrying out the due maintenance [12]. In such a situation, the probability distribution of the failure time is as important as the deterministically calculated time to failure itself.

The recognition of this need has led the analysts to use some *a posteriori* probabilistic distributions on the deterministically calculated growth path. Such a method requires extensive fracture data for the estimation of the

distribution parameters. A good probabilistic theory would reduce the data dependency in two ways. Firstly, it will be possible to choose the family of distribution functions relevant to the situation at hand, and secondly, it may be possible to obtain a functional correspondence between the probability distribution parameters and growth rate parameters.

A major success of the statistical approach has been recorded in the analyses of brittle fracture. The skewness in the probabilistic distribution of breaking strengths of supposedly identical samples, as well as the dependence of strength on specimen size has been modelled successfully using the Weibull weakest-link concept and extreme value statistics [13,14]. The former has also been modified and applied to the study of composites. In this case, the material is considered to be a chain of bundles, each element of which fails using the weakest-link principle, but the failure of the whole material may not occur until two or more components of the bundle have failed [15].

This success with brittle materials has not been experienced in the application of probability to ductile materials and slow stable cyclic crack propagation. The relative ease in modelling the former stems from the fact that the failure of brittle materials is not preceded (or accompanied) by significant changes in material properties: plasticity, work-hardening, creep and subcritical crack growth. Void interference and

coalescence to form larger cracks and the blunting of the crack-tip are some other complications that are encountered in ductile materials.

Some attempts have been made recently to relate the observed variability in the crack growth parameters to the growth phenomenon using probability theory and damage accumulation. Bogdanoff [16] has described the growth of fatigue cracks as the passage through a sequence of Markovian states from a given initial (virgin) state to an absorbing (fracture) state. The number of cycles to failure can then be stated (stochastically) in terms of first passage probabilities. In this way, one of the major goals of a probabilistic treatment (to have a distribution function around the mean failure time) can be achieved. However, the transition matrix in this model has to be derived from experimental data. This is no easy task. This model is therefore basically descriptive.

1.5 Scope

In this work, a model of fatigue crack growth is described based on probabilistic considerations and damage accumulation. The weakest-link hypothesis is modified in a way to incorporate some of the realities in the growth of a fatigue crack in a ductile situation. The material ahead of the crack-tip is treated as composed of uniaxial elements subjected to the stress/displacement fields in their locations as determined for each configuration using

a continuum law. Rice's hypothesis as described in chapter 2 is used to obtain the cyclic equivalent of this stress/displacement field. The reinitiation of voids as well as crack advance from one configuration to the next is determined by the weakest-link in the chain. From a linearly accumulated damage point of view, this growth sequence is shown to be derivable from a failure criterion approximated by the statistical Miner's law. A simulation procedure quantifies the damage in the highly strained region ahead of the crack-tip resulting from the slow stable crack growth. This leads to a failure criterion in terms of the remaining strength of the predamaged elements in the region. The historical damage in the material elements at the crack-tip vicinity, neglected in previous analyses is quantified, and shown to be significant. The model includes a prediction of the threshold stress intensity factor range, and a comparison with the published growth data for some structural materials.

An alternative method to determine the unloading and the cyclic loadings stress/displacement fields based on dislocation theory is presented. The starting point for this is the non-linear work hardening generalization of the Bilby, Cottrell and Swinden, BCS, [17] model. This is a continuous dislocation model of the modified Ramberg-Osgood stress/strain law. By suitable choice of parameters, it specializes to the elastic-perfectly plastic BCS model, and the elastic-linear hardening model

of Bilby and Swinden [18]. The unloading stress/displacement field is found by solving two non-linear integral equations with singular kernels. A description of the numerical procedure used in solving these equations is outlined. The inversion theorem of Muskhelishvili is used in the derivation of the equations. The criterion for the validity of this procedure is outlined. The singularity removal method to facilitate the use of standard quadrature methods in evaluating the singular integrals is also described.

The cyclic J-integral is evaluated for the non-linear work hardening material, using the stress/displacement fields generated. The effect of hardening is demonstrated by varying the hardening exponent in the integral equations. For small scale yielding, it is shown that in the absence of work-hardening, the J-integral bears the same proportionality relationship with the applied far field strain energy density range as previously used in the literature. For higher amount of the cyclic loading range, and/or when there is considerable work hardening, the relationship is, in general, of a power law type, with the coefficient and exponent depending on the applied loading and the hardening exponent.

1.6 Organization of this Work

In the next chapter, a survey of some selected work related to the analyses here is presented. It begins with a description of the hypothesis by Rice [19] used in deriving a cyclic stress/strain field from fields derived for monotonic loading considerations. The works of Majumdar and Morrow [20] and Glinka [21] are presented to show the two approaches to the damage accumulations modelling of the fatigue crack growth process. The application of the weakest-link statistical theory to ductile materials is described using Oh's combinatorial model. The works of Shih and Hutchinson [4] in the derivation of the J-integral using interpolation method is briefly described with Dowling's extension of these principles to cyclic loading.

Chapter three begins with the damage accumulation modelling of the fatigue crack growth. A stochastic Miner's law [6] is used as the damage failure criterion. Historical damage is incorporated in the simulation process. This is shown to lead to a probabilistic crack growth law. The probability distribution obtained is compared, using probability plots, to several of the commonly used distributions in the literature.

In chapter four, the BCS dislocation model is generalized using a non-linear "friction stress". The resulting singular integral equation is inverted using standard procedure. The condition of validity of this

procedure for the non-linear functions involved is demonstrated. The resulting equation with singular kernel is solved for the monotonic field. This procedure is extended to the unloading and cyclic cases in chapter five. The cyclic J-integral is evaluated.

In chapter six, several of the results obtained in the earlier chapters are discussed. There is also a brief description of the areas of recommended research.

Chapter 2

SELECTED WORK RELATED TO DAMAGE ACCUMULATION MODELLING

The discussion in this chapter includes a description of some of the methods and models existing in the literature on damage accumulation and fatigue crack propagation. Most of the work on fatigue crack growth usually begin with the stress/strain distribution field ahead of a monotonically loaded crack. The latter is usually based on continuum analysis even though some other methods (e.g. dislocation theory) are also becoming increasingly popular. A state of the art survey of these methods is not attempted here. There has been several detailed surveys of the field in recent times, e.g. [1, 19, 22]. The works discussed in this chapter contain some of the materials later improved upon in this dissertation. It also includes certain mathematical techniques which are used later. The other materials appear here basically to show the historical development that culminates in the modelling presented. Several important works are mentioned only in passing, while some are not mentioned at all. The ultimate goal here is to give a more or less detailed description of the most relevant work rather than have a comprehensive review of the field.

2.1 The Plastic Superposition Method

The origin of the plastic superposition method has been traced to Hult and McClintock [23] and Rice [24]. The use of this method to model the response to unloading, reloading and cyclic loading, based on the results of a monotonically loaded crack has been expanded by Rice in [19]. The fundamental assumption is that the components of the plastic strain tensor (or displacement discontinuity components where discrete surfaces of slip or yielding are involved) remain in constant proportion to one another at each point in the plastic region. It is to be noted from start that in most applications of this method, the stringent conditions of proportional plasticity cannot be expected to be satisfied. However, it may be taken as a first approximation in the absence of a better theory to model unloading or cyclic loading.

For a cracked body loaded by a system of stresses proportional to some parameter L, let the loading be reduced by a given amount ΔL, resulting in a final loading of $L - \Delta L$. It is assumed that if the crack-tip rounding is neglected, the infinite stress concentration at the crack-tip results in the formation of a reversed plastic zone, embedded in the original plastic zone however small ΔL may have been. From the proportional flow assumptions, the effect of unloading is to reverse the direction of the stresses in the reversed flow direction, without otherwise affecting their magnitude and distribution. The changes in

stresses, strains, and displacements due to load reductions are then given by a solution identical to the original monotonic loading with the following modifications: the loading parameter is replaced by the load reduction, ΔL, the yield stresses and strains by twice their value for original loading. This gives the change in the respective stress and strain fields (see Fig. 2.1). In order now to obtain the final stress/strain field, there is a superposition of the latter with the original monotonic loading field.

The doubling of the yield stresses and strains for the unloading presumes here that we are considering an elastic-perfectly plastic material. Bauschinger effects are ignored, so that the negative yield stress remains the same in magnitude as the initial value. In this case, a stress/strain field in a monotonically loaded material of the form:

$$\sigma_{ij} = \sigma_{ij}(r/a, \theta, \sigma^{\infty}/\sigma_0)$$

$$\varepsilon_{ij} = \varepsilon_{ij}(r/a, \theta, \sigma^{\infty}/\sigma_0) \qquad 2.1$$

$$u_i = u_i(r/a, \theta, \sigma^{\infty}/\sigma_0)$$

and $\omega = \omega(\theta, \sigma^{\infty}/\sigma_0)$

where,

r = distance from crack-tip, (see Fig 1.1)

a = half crack length

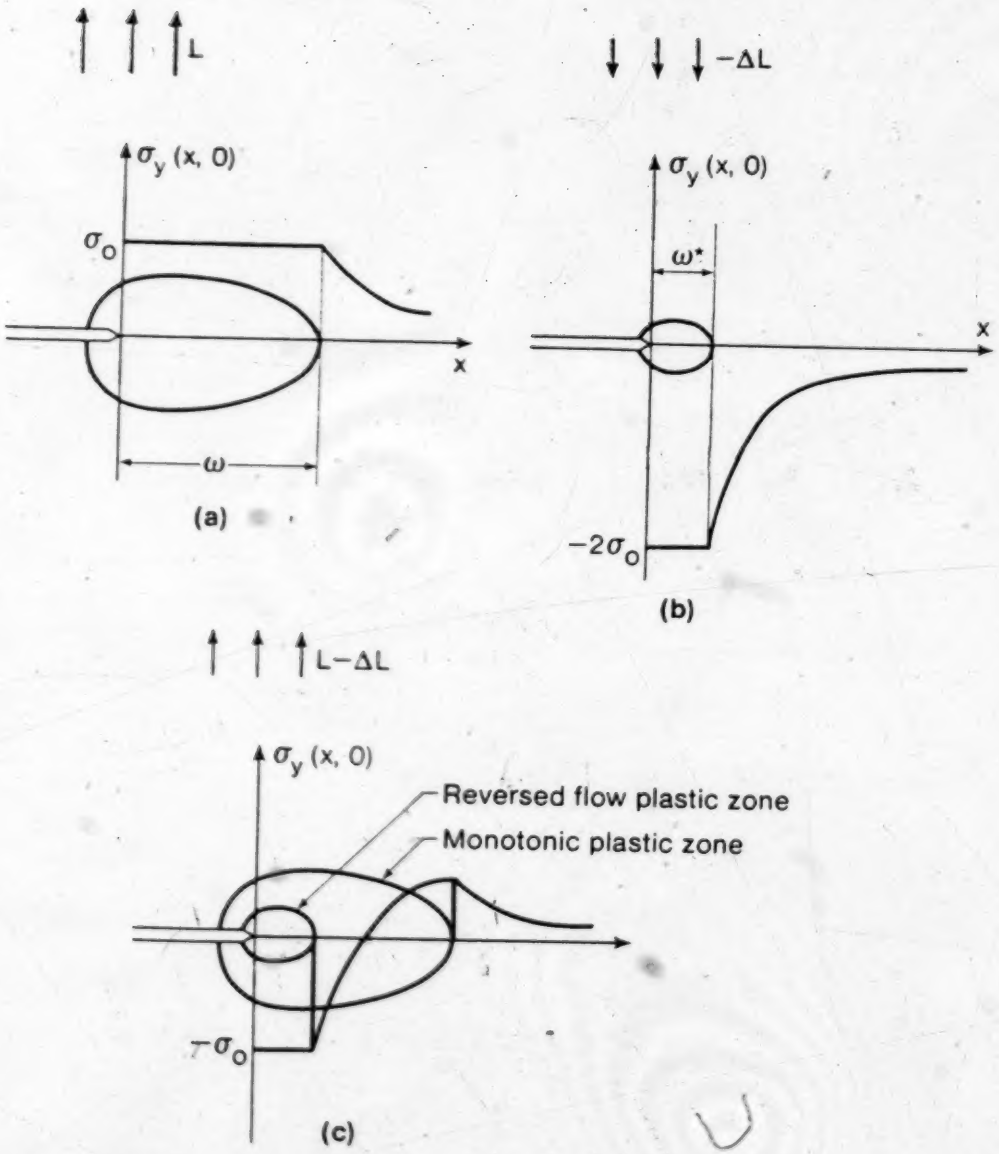

Figure 2.1 Derivation of cyclic distribution from monotonic field

θ = angular distance

σ_o = yield stress

σ^∞ = far field applied stress

ω = plastic zone size,

would become, for a loading reduction of $\Delta\sigma^\infty$,

$$\Delta\sigma_{ij} = \Delta\sigma_{ij}(r/a, \theta, \Delta\sigma^\infty/2\sigma_o),$$

$$\Delta\varepsilon_{ij} = \Delta\varepsilon_{ij}(r/a, \theta, \Delta\sigma^\infty/2\sigma_o).$$

$$u_i = u_i(r/a, \theta, \Delta\sigma^\infty/2\sigma_o), \qquad 2.2$$

and, $\omega = \omega(\theta, \Delta\sigma^\infty/2\sigma_o)$

Complete load removal, ($\Delta\sigma^\infty = \sigma^\infty$) leaves residual stresses and displacements. In this case the reversed plastic zone is half the original plastic zone size. When the loading is completely reversed, the reversed plastic zone becomes equal in size to the original monotonic plastic zone. For any unloading greater than this, the plastic superposition cannot be applied.

In reality, however, the range of validity of this method does not go even that far. Crack closure usually intervenes before complete load reversal, and the stress level at which this closure takes place delimits the range of applicability of the plastic superposition method.

This method was further extended to the situation where there is work-hardening. The assumption here is that the stress/strain relations in the cyclic plasticity zone

may be described as the traversal of stable hysteresis loops. The stress and strain variations following a load reversal are considered related by a law independent of the maximum amplitudes of the loops. In such a case, the unloading stress-strain relationship is the same as the loading case if the latter is referred to a set of reversed axis (Fig. 2.2). The solution for stress and strain variation is thus identical to that of monotonic loading when the following transformations are made.

(1) yield stress, $\tau_0 \rightarrow \tau_0^*$

(2) yield strain, $\gamma_0 \rightarrow \gamma_0^*$

where τ_0^* and γ_0^* are as described in Fig. 2.2.

2.2 Deterministic Cumulative Damage Models

The models in Ref. [25-28] all reflect an attempt to correlate the fatigue crack growth and low cycle fatigue properties. They all basically involve the treatment of the crack-tip vicinity in terms of uniaxial fatigue elements contained in an elastic matrix as described by Head [29]. From this viewpoint, the propagation of the crack is seen as successive failures of the fatigue elements. In order to calculate the time of failure of a fatigue element from a low cycle fatigue perspective it is necessary to know the stress/strain ranges to which it has been subjected. The damage history to failure could then be found. Lehr and Liu [25] and several later succeeding authors used the square root singularity at the crack-tip

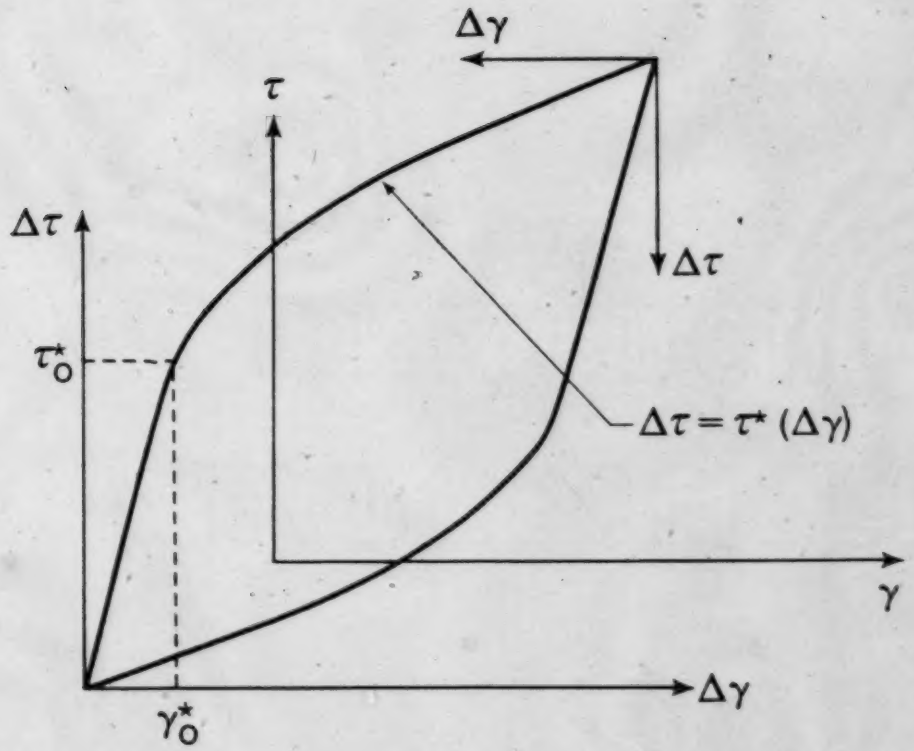

Figure 2.2 Stress-strain relationship in reversed axes

(based on elastic analysis) in order to obtain the strain on each fatigue element. This monotonic strain distribution was taken to represent the level of fatigue cycling for each element.

Later models, notably by Majumdar and Morrow [20], and Glinka [21] have made use of the plastic superposition method described earlier to obtain the cyclic loading field applicable to each fatigue element. These two are described here to show the different aspects of the fatigue crack growth modelling they portray.

(a) Majumdar and Morrow [20]

The reversed plastic zone, obtained from the plastic superposition method is the relevant "damage zone" of interest. The "damage history" of each fatigue element begins when its distance from the crack-tip is equal to or less than the damage zone. It is assumed that, as the crack-tip moves towards a particular element, the stress intensity factor range, ΔK is held constant. Since ΔK is proportional to the square root of the crack size, the only way this can happen is when the far field applied stress is reduced by the right amount with each increase in the crack length. In this case, the damage experienced in each cycle is dependent only on the distance from the crack-tip. The number of cycles to failure of a fatigue element subject to the stress/strain level at a distance x from the crack-tip, $N_f(x)$ is thus independent of crack length. It is assumed also that there is a crack advance

of equal magnitude in each cycle, so that the cumulative damage required to cause fatigue or an element is the sum of the damage experienced during one cycle by each element lying within the damage zone. Using linear damage criterion, this means,

$$1 = \sum_{i=0}^{k} \frac{1}{N_f(x_i)} \qquad 2.3$$

The summation is over all the elements in the damage zone.

The crack advance per cycle, $\Delta x = da/dN$, multiplying the LHS and RHS of Eq. 2.3 respectively by this leads to:

$$\frac{da}{dN} = \sum_{i=0}^{k} \frac{(\Delta x_i)}{N_f(x_i)}$$

which can be approximated by an integral to obtain,

$$da/dN = \int_{0}^{r_p} \frac{1}{N_f(x)}\, dx \qquad 2.4$$

Since the stress/strain range at each point x is known from the plastic superposition, $N_f(x)$ is easily evaluated. However, the integrand in Eq. 2.4 is divergent at the origin. To avoid this divergence, the initial point of the integration is changed to a value equal to half of the crack opening displacement, COD, at the crack-tip.

In an effort to account for the effects of microstructure of a metal, the initial assumptions are modified. It was taken that the element adjacent to the

crack-tip is subject to a stress/strain range equal to the value at a distance 2ρ from the crack-tip. The width 2ρ was determined from the size of the micro-structural element.

It should be noted that in this model, the fatigue elements fail in sequence as each "reaches" the crack-tip. The fatigue element size is also the amount of crack advance per cycle of loading (ie crack growth rate). Therefore, this cannot be linked to any material property since it is completely determined by the loading considerations.

(b) Glinka's model [21]

Glinka's model also belongs to the general class of models that relate crack growth properties to fatigue properties. The same plastic superposition method used above is also used to obtain the cyclic stress/strain field even though the initial monotonic field is obtained from the Hutchinson, Rice and Rosengren, HRR, [30,31] field. Even though the monotonic fields give singular values at the crack-tip, x=0, this model, based on experimental observation presumes that the stress/strain gradient near the crack-tip, (for a distance x^* to be defined) is actually very low. The distribution in this region is approximately constant. This distance is considered a material property, and its value is therefore derivable experimentally.

In order to obtain x^*, it is considered that, since ΔK_{TH} represents a value of ΔK for which cracks do not propagate, it must mean that the maximum value of the strain range on each fatigue element must be lower than the threshold value of the strain range obtained in low cycle fatigue experiments. When these two quantities are known, $(\Delta K_{TH}, \Delta\varepsilon_{TH})$, x^* can be obtained by finding the distance ahead of the crack-tip at which,

$$\Delta\varepsilon = \Delta\varepsilon_{TH} \qquad 2.5$$

when the applied stress intensity factor range is ΔK_{TH}. For any other ΔK, the characteristic distance x^* is fixed at this value, and the strain range in the region $x=0$ to x^* is found as the value at $x = x^*$. The number of cycles required to propagate the crack for a distance x^* is the same as that required for a fatigue element, cycled at the strain range at x^*. Let this number of cycles to failure be $N_f(x^*)$. Fatigue crack growth rate is thus given by,

$$da/dN = x^*/N_f(x^*). \qquad 2.6$$

It is interesting to note that, while the Majumdar and Morrow model considered the damage history up to the point $x = COD/2$ as the amount needed for the failure criterion, and ignores the damage accumulated at the crack-tip, Glinka's model is a complete reversal of this

idea. The damage history up to point x^*, which incidentally is of the same order of magnitude as COD/2, is ignored. The failure criterion is entirely based on the region $x = 0$ to x^*. It is therefore surprising to discover that both models give similar results when applied to experimental results. This paradox is examined and explained later in this work.

2.3 Weakest-Link Modelling of Fatigue Crack Growth

As briefly mentioned in the introduction, the application of probability theory in solid mechanics has been more successful in the modelling of brittle materials compared to ductile materials. Beginning with Weibull's [32] pioneering work, the weakest-link theory has been applied to the former by several investigators. The relative success in brittle fracture modelling is due in part to the fact that, unlike their ductile counterparts, brittle materials do not "flow locally to forgive errors of stress analysis" [13]. This makes it easier to formulate a failure criterion since there is no need to account for changes in local material properties like flow and creep. In this section, we describe Oh's model that uses the weakest-link theory in a way that is not restricted to brittle fracture.

(a) Oh's model [7]

As in previous models, the materials at the crack-tip are assumed to consist of a chain of materials as uniaxial

fatigue elements. Fatigue cycling leads to the accumulation of cyclic damage on each element at each cycle. The amount of damage on a given element in a particular cycle depends only on the relative position of the element. Oh further assumes that the strength of these elements differ from one another. They are, however, pictured as independent observations from the same population, ie, identically distributed. This difference in fatigue strengths (or ductility, in Oh's terminology) implies that the element that has the greatest amount of fatigue damage accumulation is not necessarily the first element to fail. Rather, the damage accumulated on a material must first exceed its damage resistance before it fails in a way that would initiate crack advance. When this is the case, the weakest-link postulate is that, the material element that has exceeded its fatigue damage resistance would fail, creating a void in its location. The material elements between this void and the crack-tip will then disintegrate with none or little additional cycling. This means, in effect, that the crack advances to the position in question.

It is now possible to determine the probability, ϕ, that, the void formation occurs at a time $\eta \leq N$, and at a location $x \leq X$, in the limit as the number of material elements goes to infinity. Such an asymptotic distribution will exist if the initial distribution tends to zero like a power function, that is, if

$$F_j \equiv F(\varepsilon_j) \to \frac{1}{k}\left(\frac{\varepsilon_j - \varepsilon_u}{\varepsilon_0}\right)^m \text{ as } \varepsilon_j \to \varepsilon_u,\ k \to \infty \qquad 2.7$$

where k = number of fatigue elements, and ε_u, ε_0 and m are called location, shape and scale factors, respectively.

The function assumed for the ductility distribution is

$$F_j = \begin{cases} \frac{1}{k}\left(\frac{\varepsilon_j - \varepsilon_u}{\varepsilon_0}\right)^{m_\omega} & \varepsilon \geq \varepsilon_u \\ 0 & \text{elsewhere} \end{cases}$$

where ω is the plastic zone size.

In a random sample of elements, the conditions for a particular element, say, the one between x and x + Δx, to fail at the cycle between N and ΔN are:

(1) all elements survive up to N load cycles and,

(2) the element between x, and x + Δx fail between N and N + ΔN. The small probability associated with these two events is:

$$\Delta\phi = \Pr\,[d(N,x) \leq \xi \leq d(N+\Delta N,x)] \times \Pr\,[\text{all other elements have ductility} \geq d(N,x)] \qquad 2.8$$

where d(N,x) = cumulative damage at x after load cycle N, and ξ = ductility of the material between x, x + Δx. Therefore,

$$\Delta\phi = \frac{\partial F}{\partial N} \Delta N \prod_{i=1}^{k} (1 - F_i) \qquad 2.9$$

$$= \frac{\partial}{\partial N} \{ \left(\frac{d(N,x) - \varepsilon_u}{\varepsilon_0} \right)^m \Delta x \} \Delta N \prod_{i=1}^{k} (1 - F_i) \qquad 2.10$$

where $\Delta x_i = \Delta x = \omega/k$, (as $k \to \infty$, $\Delta x \to 0$) so that,

$$\lim_{\substack{\Delta x \to 0 \\ \Delta N \to 0}} \frac{\Delta\phi}{\Delta x \Delta N} = \frac{\partial}{\partial N} \left[\left(\frac{d(N,x) - \varepsilon_u}{\varepsilon_0} \right)^m \right] \lim_{\substack{\Delta x \to 0 \\ \Delta N \to 0}} \prod_{i=1}^{k} (1 - F_i) \qquad 2.11$$

Let $y = \prod_{i=1}^{k} (1 - F_i)$, then, $\log y = \sum_{i=1}^{k} \log (1 - F_i)$, which for small values of F_i, neglecting product terms, it follows that,

$$y = -\sum_{i=1}^{k} F_i \qquad 2.12$$

Using this in (Eq. 2.10), it becomes clear that when the two limits are applied, the density function is given by,

$$\phi(x,N) = \frac{\partial}{\partial N} \left[\left(\frac{d(N,x) - \varepsilon_u}{\varepsilon_0} \right)^m \right] \exp - \left\{ \int_0^{\omega} \left(\frac{d(N,x) - \varepsilon_u}{\varepsilon_0} \right)^m dx \right\} \qquad 2.13$$

The mean, variance and other moments of the crack growth rate are derivable from this density. For instance, the mean,

$$E[x/N] = \iint \frac{x}{N} \phi(x,N)\, dx dN$$

$$= \frac{\omega^{1+1/m}}{\epsilon_0} \int_{u_L}^{\infty} \exp(-uI_0)\, I_1 u^{-1/m}\, du \qquad 2.14$$

where $u = \omega N^m / \epsilon_0 m$,

$$I_0 = \int_0^1 \left[\Delta\epsilon(x') - \frac{\epsilon_u}{\epsilon_0}\left(\frac{\omega}{u}\right)^{1/m}\right]^m dx' \qquad 2.15$$

and,

$$I_1 = \int_0^1 x' \left[\Delta\epsilon(x') - \frac{\epsilon_u}{\epsilon_0}\left(\frac{\omega}{u}\right)^{1/m}\right]^{m-1} \Delta\epsilon(x')\, dx' \qquad 2.16$$

The integral in (Eq. 2.14) is independent of the stress intensity range, ΔK, and, since the latter is proportional to the square root of the plastic zone size, it follows that,

$$E(X/n) \sim (\Delta K)^{2 + 2/m} \qquad 2.17$$

In which case, the mean growth rate is proportional to ΔK raised to a power greater than two. This exponent is a function of the distribution of the fatigue elements

ductility.

The factor $u_L = \omega N_L^m/\varepsilon_0^m$ introduced, instead of zero as the lower limit of equation 2.14 is needed, as in 2. 4 to remove the singularity in the integrand.

This divergence problem has been addressed by Tsurui and Igarashi [33] who basically repeated the above model but from a discrete statistical viewpoint. Another important deficiency (at which an attempt was made to rectify) is in the fact the historical damage in the material prior to any given configuration is ignored. The weakest-link process is assumed to "reset" the system so that the growth process does not have any "memory" of previous crack growth. Unfortunately, no quantifications of the historical damage was possible with the Tsurui model. Rather, some arbitrary monotonic function of position was used instead.

While it is desirable to have a closed form for the probability density functions to describe the growth rate, the function in Eq. 2.13 is rather too complicated to be useful in crack modelling. It will be helpful to find what simple distributions can approximate the crack growth density function. Such a knowledge will be of great advantage in reliability and risk analysis of structures in which there is crack propagation. In the probabilistic model considered later, a comparison is made between the resulting crack growth distributions and some commonly used probability functions.

2.4 Dislocation Model of the Stress/Strain Field

The damage accumulation treatment of the crack-tip, whether deterministic or probabilistic, requires a knowledge of the cyclic stress or strain field in the damage zone. In all the modelling described earlier, the plastic superposition method has been used to derive the cyclic distribution from any given monotonic stress/strain field. The latter is usually obtained through continuum based analyses. Examples of the most commonly used equations are by Hult and McClintock [23], Hutchinson [31], Rice and Rosengren [30]. The latter two are jointly called the HRR equations. Another method, which can be used to find the cyclic field, as will be shown later, is the method based on dislocation theory. This highly idealized method considers the plastic zones as made up of a line ahead of the crack-tip similar to the Dugdale model [34]. Moreover, there is close agreement between the prediction of this model and the continuum based method in [24]. The discussion here presents the basic model as applied to the monotonic and cyclic loading of an elastic-perfectly plastic crack. This will be extended later to the work-hardening case for both types of loading. In the dislocation model, the plastic superposition method is not needed to extend the monotonic equations to cyclic loading as will be shown.

(a) The Bilby, Cottrell and Swinden, BCS model [17]

Consider a plane crack occupying the region $y = 0$, $|x| < c$, $|z| \leq \infty$ in an isotropic elastic medium (see Fig. 2.3). The medium is considered to deform in plane strain under the application of shear stress $\sigma_{12} = \tau^{\infty}$ as shown. This leads to plastic flow in the regions $|x| > c$ just beyond the tips of the crack, which is supposed to be principally explainable in terms of a row or edge dislocations, coplanar with the crack-tip and occupying the region $c < |x| < a$. As σ_{12} is increased from zero to τ^{∞}, these dislocations glide out from the crack-tip into the medium driven by the external forces, the mutual repulsions etc. and are opposed by a frictional resistance τ_0. By considering the dislocations as a continuum such that the number of dislocations in the interval x, and x + dx is given by $f_1(x)dx$, the equilibrium requirements at a point x demand that,

$$\int_{-a}^{a} \frac{f_1(x')dx'}{x-x'} + \frac{P(x)}{A} = 0 \qquad 2.18$$

where $P(x) = \begin{cases} \tau, & |x| < c \\ \tau - \tau_0, & c < |x| < a \end{cases}$

$A = \mu b/2\pi(1 - \upsilon)$

μ = rigidity modulus

υ = Poisson ratio

c = crack length

b = Burger's vector

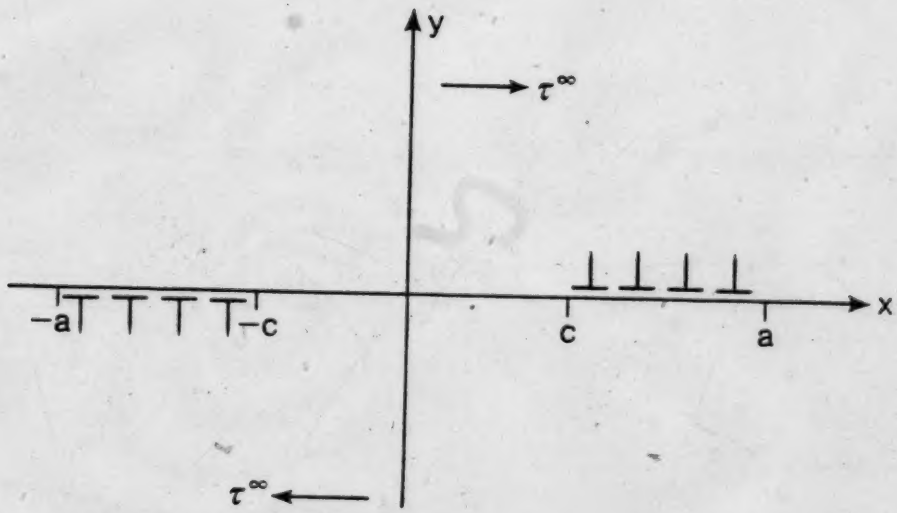

Figure 2.3 Edge dislocations ahead of a loaded crack

Since there are no barriers at x = a, it is required that the function $f_1(x)$ be bounded there. This condition leads to

$$\int_{-c}^{c} \frac{\tau^{\infty} dx}{(a^2-x^2)^{\frac{1}{2}}} + \left(\int_{-a}^{-c} + \int_{c}^{a} \right) \frac{(\tau^{\infty} - \tau_0)dx}{(a^2-x^2)^{\frac{1}{2}}} = 0, \qquad 2.19$$

The above integral can be evaluated to give,

$$c/a = \cos\left(\frac{\pi\tau^{\infty}}{2\tau_0}\right) \qquad 2.20$$

from which the plastic zone size, a - c, can be obtained in terms of the crack length, applied stress and the friction stress, τ_0. The inversion of singular equations of the type in 2.18 exists if $f_1(x)$ and P satisfy some conditions related to the Holder's inequality, (see chapter 4 for details), the density function can be shown to satisfy,

$$bf(x) = B\left\{\cosh^{-1}\left|\frac{a^2-x^2}{a(c-x)} + \frac{x}{a}\right| - \cosh^{-1}\left|\frac{a^2-x^2}{a(x+c)} + \frac{x}{a}\right|\right\} \qquad 2.21$$

where $B = 2(1-\upsilon)\tau_0 / \pi\mu$.

The plastic displacement at each point is defined as:

$$\phi(x) = \int_x^a bf(x)dx$$

$$= B\left\{(x+c)\cosh^{-1}\left|\frac{a^2-x^2}{a(x+c)} + \frac{x}{a}\right| - (c-x)\cosh^{-1}\left|\frac{a^2-x^2}{a(c-x)} + \frac{x}{a}\right|\right\} \qquad 2.22$$

(b) Unloading and cyclic loading

Suppose now that the shear stress is reduced to $\tau^\infty - \tau$. Those dislocations nearest to the crack-tips will suffer a large reversal of stress, due to the stress concentration effect, and will be driven back into the crack, while those near $x = \pm a$ will experience a reduction in stress less than $2\tau_0$ required to move them [35]. If the new dislocation density is $g(x)$, the new equilibrium condition is,

$$\int_{-a}^{a} \frac{g(x')dx'}{x-x'} + \frac{Q(x)}{A} = 0 \qquad 2.23$$

where $Q(x) = \begin{cases} \tau^\infty - \tau, & |x| < c \\ \tau^\infty - \tau + \tau_0, & c < |x| < \delta \end{cases}$

here, δ is the extent of reversed motion of the dislocation, it is identified with the reversed plastic zone. In the region $\delta < |x| < a$, the function Q is unknown. This, as will soon be apparent, does not constitute any problem.

The subtraction of Eq. 2.23 from 2.18 leads to,

$$\int_{-\delta}^{\delta} \frac{f(x') - g(x')}{x-x'}\, dx' + \frac{R(x)}{A} \qquad 2.24$$

where $$R(x) = \begin{cases} \tau & |x| < c \\ \tau - 2\tau_0 & \delta < |x| < a \end{cases}$$

which has the same form as equation 2.18.

If, in the latter, $\tau_0 \to 2\tau_0$, and $a \to \delta$, the function $P(x)$ in 2.18 becomes identical to $R(x)$ in Eq. 2.24. The similarity between these results and the plastic superposition method is immediately apparent. The solution for the monotonic loading can be extended to cyclic loading when the friction stress is replaced by twice its value, and the applied stress replaced by the amount of unloading. Using this in 2.20, we obtain,

$$c/\delta = \cos\left(\pi\tau/4\tau_0\right) \qquad 2.25$$

Weertman [36] had earlier obtained this equation by a slightly different approach.

2.5 Unloading and Cyclic J-Integral

The path independent J-integral has been evaluated for the entire elastic-plastic range by Shih [3], Shih and Hutchinson [4], by interpolating between the small scale yielding and the fully plastic solutions of Goldman and

Hutchinson [37]. For an infinite strip of height 2h, with a semi-infinite slit, it was earlier shown by Rice [2] that the J-integral is:

$$J = W^{\infty} h \qquad 2.26$$

where W^{∞} is the strain energy density.

In the case of a material whose properties are governed by the Ramberg Osgood law,

$$\gamma/\gamma_0 = \tau/\tau_0 + \alpha(\tau/\tau_0)^{n'}, \qquad 2.27$$

Eq. 2.26 becomes,

$$J/(2h\,\tau_0\,\gamma_0) = \tfrac{1}{2}(\tau^{\infty}/\tau_0)^2 + \alpha\,(n'/n'+1)(\tau^{\infty}/\tau_0)^{n+1} \qquad 2.28$$

($n' = 1/n$ where n is the hardening exponent).
Guided by the form of Eq. 2.28, it has been proposed (Shih[3]) that the value of J for a finite slab in the elastic plastic range can be written as:

$$\frac{J}{\tau_0 \gamma_0\, a\,(b-a)/b} = \left(\frac{P}{P_\ell}\right)^2 \chi\, f_1(a_{eff}/b\,,\, n=1) + \left(\frac{P}{P_\ell}\right)^{n+1} f_1(a/b,\, n) \qquad 2.29$$

where a_{eff} = effective crack length = $a + r_y$,

$$\chi = (a_{eff}/a)\left(\frac{b-a}{b-a_{eff}}\right),$$

r_y is an adjustment to the crack length for the strain hardening material, $r_y = \frac{1}{2\pi}\left(\frac{n'-1}{n'+1}\right)\ (K_{III}/\tau_0)^2$

The function $f_1(a/b,n)$ determined using finite element analysis, has a closed form value as $b \to \infty$,

$f_1(n') = n'/n'+1$, P = applied load, P_ℓ = limit load.

The quantities $(P/P_\ell)^2$ and $(P/P_\ell)^{n'+1}$ are proportional to the elastic and plastic strain energy densities respectively. Equation 2.29 is thus an interpolation between the elastic and cyclic J-integrals. The parameter χ as well as the function $f_1(a/b,n)$, the weighting functions can be obtained using finite elements method for the monotonic loading case. Similar equations have been used by Dowling [5] and Mowbray [38] for the cyclic loading case. In the absence of a suitable method to determine the equivalent weighting factors for the interpolation, the cyclic J-integral was estimated by a simple addition of the elastic and plastic components, implicitly taking $\chi = 1$.

Tanaka [39] has proposed the evaluation of the J-integral from a totally different viewpoint. By defining the cyclic J-integral and showing it to be independent of path in a way similar to its monotonic counterpart, it was possible to evaluate the former directly, using dislocation theory. Unfortunately, the procedure used is

valid only for the elastic-perfectly plastic case. In this work, Tanaka's model will be extended to account for work-hardening.

2.6 Numerical Solutions of Integral Equations

In some later analyses, it will be necessary to solve certain singular integral equations. The method that will be used is a generalization [40] of the quadrature method which is first described here. Suppose an approximate solution of the Fredholm equation,

$$\int_0^1 K(x,y)\, f(y)\, dy + g(x) = f(x) \qquad 2.30$$

is desired. The application of Simpson's rule, neglecting the remainder term leads to

$$1/6\{K(x,0)\tilde{f}(0) + 4K(x,\tfrac{1}{2})\tilde{f}(\tfrac{1}{2}) + K(x,1)\tilde{f}(1) + g(x)\} = \tilde{f}(x) \qquad 2.31$$

By selecting points x = 0, 1/2, and 1, it is possible to obtain three equations in terms of the three unknowns f(0), f(1/2) and f(1). This leads to the matrix equation,

$$\underline{M}\,\underline{\tilde{f}} + \underline{g} = \underline{\tilde{f}} \qquad 2.32$$

where M is a 3 x 3 matrix, all of whose elements are specific values of the kernel function K(x,y). A solution for 2.32 thus gives approximate values of the unknown

function f(x) in the locations specified. This simple approach can be refined by using more accurate quadrature formulae. This can also be extended to deal with nonlinear equations in the same way. Only that in the latter case, Eq. 2.32 becomes non-linear. In order to find the values at the intermediate points, the same approximations of the integral can be used to write,

$$\tilde{f}(x) = g(x) + \sum_{j=1}^{n} w_j K(x,y_j)\tilde{f}(y_j) \qquad 2.33$$

where w_j is the weighting function, and y_j's are the collocation points.

The above process in effect implies expressing the unknown function as a combination of some values of the kernel function. In later chapters (e.g. chapter 4) it will be necessary to find approximate solutions to some non-linear integral equations. The expansion method we shall use can be considered a generalization of the above method. The unknown function is expressed at the outset as a combination of functions, which may, or may not involve the kernel function. The coefficients and some other parameters of this formulation will be evaluated in order to obtain the required estimation. This approach is very useful especially in situations where there is a known function with values close to the function to be

estimated. Another advantage is that there is no restriction in this case to the number of equations that can be generated. When it is found necessary to choose a given number of points so as to generate more equations than unknowns, the resulting overdetermined system will be solved by optimization methods. Otherwise, if there are just as many equations as unknowns, the method reduces to a collocation method similar to the one in the quadrature method approach, only that, in this case, the equations involved are non-linear.

Chapter 3

DAMAGE ACCUMULATION AND STOCHASTIC MODELLING OF CRACK GROWTH

In this chapter, the growth of a fatigue crack is modelled from a damage accumulation standpoint. This modelling is later extended using probabilistic simulation to incorporate the statistical aspects of the crack growth process. The damage accumulation rule used in the latter part is a form of the statistical Miner's law. The results include a prediction of the fatigue threshold stress intensity factor range, and a comparison between the expectation of the probabilistic growth law and some published data.

3.1 Crack-Tip Modelling

The material ahead of the crack-tip is considered to be made up of uniaxial fatigue elements. A particular configuration of the crack includes all the fatigue elements in the "damage zone" at any given cycle. The damage zone considered here consists of the extent of the reversed plastic zone ahead of the crack-tip. Fatigue damage leads to failure when the total amount of damage accumulated on it reaches a critical value. Now, each fatigue element is subjected to increasing levels of stress and strain as the crack-tip moves towards it. Each fatigue element is thus viewed as a uniaxial material subjected to several levels of loading. The linear damage

accumulation method proposed by Miner is thus applicable. In the deterministic model, the failure of an element indicates a void initiation at its position. As each void coalesces with the crack, the sequence of initiations is perceived as stable crack growth on the macroscopic scale.

As the general equations for the stress/strain fields ahead of a fatigue crack are not known, approximations are made using the plastic superposition method described in section 2.1. While this procedure may be tenable for a large portion of the damage zone, it has been widely recognized (Majumdar and Morrow [20], Glinka [21], Shih el al. [41], Kujawski and Ellyin [42]) that a region exists ahead of the crack-tip where, due to non-proportional plasticity, the stress and strain field cannot be found in this way. This region, (depicted as region I), is treated differently from the rest of the damage zone (region II). In the latter, the proportional plasticity conditions required for the plastic superposition is assumed. In the former, since the deformation is highly non-proportional, the fatigue fields have to be found in another way. In region II, (Figure 3.1) the stationary singularity solution of Hutchinson [31] is adopted using plastic superposition. For a material modelled by the generalized Ramberg-Osgood stress-strain relationship.

$$\frac{\varepsilon_{ij}}{\varepsilon_0} = \frac{(1+\nu)}{\sigma_0} S_{ij} + \frac{1-2\nu}{3\sigma_0}\sigma_{pp}\,\delta_{ij} + \frac{3}{2}\alpha\left(\frac{\sigma e}{\sigma_0}\right)^{n-1} S_{ij/\sigma_0} \qquad 3.1$$

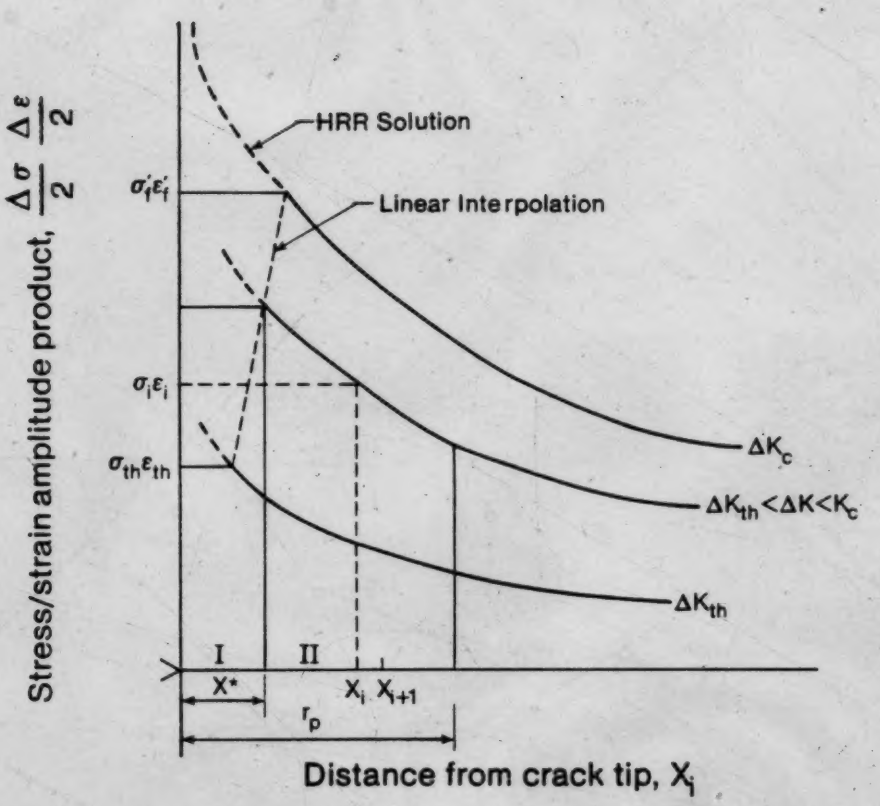

Figure 3.1 Stress-strain field in the plastic zone

where, S_{ij} = deviatoric stress,

σ = equivalent stress, $\sqrt{(3/2)S_{ij}S_{ij}}$

σ_o = yield stress

ϵ_o = yield strain, and

υ, n and α are material constants.

The monotonic solution for the elastic-plastic field [21,31] is:

$$\epsilon_{ij} = \frac{\sigma_o}{E}\left\{\left(\frac{EJ}{\sigma_o^2 I_n r}\right)^{n/n+1} \tilde{\epsilon}_{ij}(n,\theta) + \left(\frac{EJ}{\sigma_o^2 I_n r}\right)^{1/n+1} \tilde{e}_{ij}(n,\theta)\right\}$$

$$\sigma_{ij} = \sigma_o \left(\frac{EJ}{\sigma_o^2 I_n r}\right)^{1/n+1} \tilde{\sigma}_{ij}(n,\theta) \qquad 3.2$$

where E = elasticity modulus,

r,θ = polar coordinates

$\sigma_{ij}, e_{ij}, \epsilon_{ij}$ = known dimensionless function of n, θ,

and I_n = function of n only.

Using plastic superposition for cyclic loading, this equation can be expressed in terms of ΔK, the stress intensity factor range [42],

$$\Delta\epsilon = \frac{\sigma_o}{E}\left[(B-\nu A)\left(\frac{\Delta K^2}{\alpha I \sigma_o{}^2{}_x}\right)^{1/(n+1)}\right.$$

$$\left. + (B - \frac{A}{2})\alpha^{1/(n+1)}\left(\frac{\Delta K^2}{I\sigma_o{}^2{}_x}\right)^{n/(n+1)}\right]$$

and,

$$\Delta\sigma = \sigma_o' \left[B \left(\frac{\Delta K^2}{\alpha I \sigma_o'^2 x} \right)^{1/(n+1)} \right] \qquad 3.3$$

where A and B are constants obtainable from the loading condition. In Fig. 3.1, as the crack-tip moves toward the element between x_i and x_{i+1}, the rate of damage accumulation increases. The time interval spent under the conditions of this configuration is:

$$\frac{x_{i+1} - x_i}{(da/dN)_i} \equiv \frac{\Delta x_i}{(da/dN)_i} \qquad 3.4$$

where (da/dN) is the mean growth rate at the interval in question. If N_{fi} is the number of cycles to failure under the combined effect of the stress and strain ranges, $\Delta\sigma_i$, $\Delta\varepsilon_i$, the cycle ratio,

$$\frac{\Delta x_i / \left(\frac{da}{dN}\right)_i}{N_{fi}} \qquad 3.5$$

is the ratio of damage accumulated in the range x_i, x_{i+1} to the total damage if the material had remained under these conditions from zero damage to failure. Hence,

$$\sum_{\text{region II}} \frac{\Delta x_i / \left(\frac{da}{dN}\right)_i}{N_{fi}} = p \qquad 3.6$$

where $0 < p < 1$, is the proportion of the total damage to failure incurred in region II. Equation 3.6 expresses the fact that the fatigue element does not fail in region II, but rather, it is weakened by the amount of damage undergone there. If region II is small compared to crack length, $(da/dN)_i$ is independent of i, so that Eq. 3.6 becomes

$$p \frac{da}{dN} = \sum_{II} \frac{x_i}{N_{fi}} \qquad 3.7$$

Thus, if N_{fi} can be found for all x_i in this region, the knowledge of the "damage ratio", p is all that is needed to find the crack growth rate.

However, the damage ratio is difficult to determine. Its value depends on the size ratio of the two regions as well as the cyclic stress/strain distributions. It therefore may not be constant. An indirect approach will be used to find the growth rate. This is achieved by examining the damage due to region I.

The premise here is that, for stable crack growth, the maximum cyclic stress/strain sustainable by the fatigue elements cannot exceed the fatigue strength and ductility limits, σ_f', ε_f', of the material. Values of stress/strain higher than these, when they exist, would lead to an increasing sequence of finite crack advance up

to the fatigue element where the stress/strain value is lower than σ_f'/ε_f'. Such finite growths occurring a number of times in less than one cycle, is evidence of instability. Sufficient time is not allowed for the stable translation of the stress/strain front with the crack. An upper bound for the stress/strain field in region I is thus given by the strength and ductility coefficients. This bound is evidently attainable only at the transition value of the applied stress intensity factor range, ΔK_c. In this case, neglecting elastic terms, the maximum extent of region I is given by:

$$x^* = C \left(\frac{\Delta K_c^2}{4\pi \sigma_o'^2 \varepsilon_f' \sigma_f'} \right) \qquad 3.8$$

where C is a constant that can be evaluated from the other material parameters in Eq. 3.3. The stress/strain field in region I can be approximated by the values obtained from Eq. 3.3 for point x^*, provided that x^* is small. Using 3.5 in this region,

$$\frac{x^*/\frac{da}{dN}}{N_f(x^*)} = 1 - p \qquad 3.9$$

and combining it with Eq. 3.7 leads to,

$$\frac{da}{dN} = \frac{x^*}{N_f(x^*)} + \sum_{II} \frac{\Delta x_i}{N_{fi}} \qquad 3.10$$

The sum in the last equation can be approximated by an integral, so that,

$$\frac{da}{dN} = \frac{x^*}{N_f(x^*)} + \int_{x^*}^{r_p} \frac{1}{N_f(x)}\, dx \qquad 3.11$$

is the proposed crack propagation rate law.

It is noted here that the two extreme values of p(0,1) specialize Eq. 3.9 to that of Glinka [21] and Majumdar and Morrow [20]. The upper limit r_p, is the extent of the reversed plastic zone.

The expressions relating stress/strain ranges to the number of cycles to failure in a strain controlled experiment are [43,44],

$$\frac{\Delta\varepsilon}{2} = \frac{\sigma_f'}{E} N_f^{\,b} + \varepsilon_f' N_f^{\,c}$$

and,

$$\frac{\Delta\sigma}{2} = \sigma_f' N_f^{\,b} \qquad 3.12$$

where b and c are material constants. It has been shown [43] that the above relationship is valid even when the loading in not fully reversed provided steady state is reached in each loading level. Either of the equations in 3.12 can be inverted (numerically at least), to obtain the quantity N_f whenever either the stress or strain range is given. For reasons that will become apparent in chapter 5, for the purpose of the damage failure criterion used in determining Eq. 3.11, it is found better to use a product;

$$\Delta\sigma\Delta\varepsilon = \frac{4\sigma_f'^2}{E} N_f^{2b} + 4\varepsilon_f'\sigma_f' N_f^{b+c} \qquad 3.13$$

This is inverted by a numerical procedure to give the number of cycles to failure in a fatigue element at any given values of the stress/strain range.

In estimating the size of x*, a corollary of the arguments leading to equation 3.8 was used by Glinka. In this case, if the values σ_{TH} and ε_{TH} of the fatigue threshold stress and strain ranges are known for the material in question, using the threshold stress intensity range, it was argued that x* is the distance at which these values of stress and strain range can be achieved. Otherwise, the crack would still propagate. This argument leads to

$$x^* = C \frac{\Delta K_{TH}}{4\pi\sigma_o^2 \varepsilon_{TH}\sigma_{TH}} \qquad 3.14$$

If x^* is a material property as has been previously assumed, the values calculated in eqs. 3.8 and 3.14 should be equal. In practise, we find that this is not so (see fig. 3.1). When they are of the same order of magnitude, an interpolation method can be used to find x^* in the intermediate range.

For a constant value of x^*, Eq. 3.9 is similar to the growth rate law derived by Glinka [21]. The main difference is the occurrence of 1 - p on the RHS instead of unity. This shows that when a damage failure criterion is to be applied to the zone adjacent to the crack-tip, one has to consider the historical damage due to the rest of the damage zone. The material at the crack-tip at each configuration is not "virgin", but predamaged, and p is a measure of this amount of fatigue predamage.

The latter will be called "historical damage", and its significance will be investigated in the next section.

3.2 Probabilistic Growth Rate Law

(a) Physical considerations and assumptions.

Chakrabotty [28] has described the crack-tip region in terms of layers of randomly dimensioned "microstructural deformation zones", MDZ which depict the major deformation barriers in the reversed plastic zone, Fig. 3.2. The effect of strain cycling is to tend to equalize the plastic strain distributions in this region, so that a continuum field will be averaged out as shown.

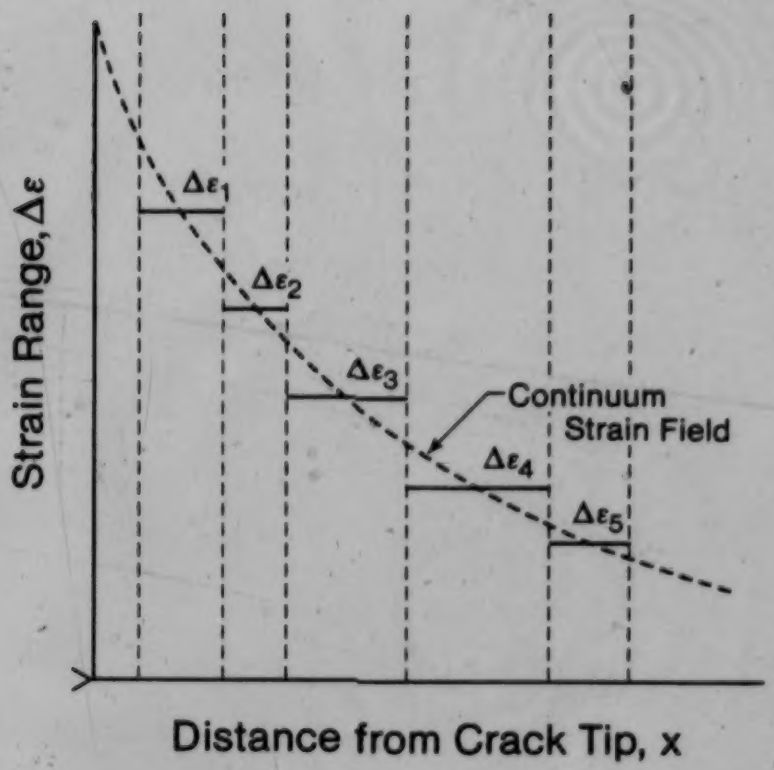

Figure 3.2 Random microstructural deformation zones

These deformation barriers, (e.g. grain boundaries, inclusions, voids etc.) are also crack growth barriers. The material properties in the bulk can be applied to these microstructural deformation zones as an average measure [9]. In a probabilistic modelling of the crack-tip, an attempt will be made to take these physical considerations into account. The following assumptions, similar to Oh's [7] weakest link model are made:

(i) A damage zone, DZ, exists ahead of the crack-tip beyond which the accumulated damage in fatigue cycling is insignificant.

(ii) The materials in the DZ (defined, as before as the reversed plastic zone) are uniaxial fatigue elements, with fatigue damage resistance, FDR, that are random observations from the same probability distribution.

(iii) Damage is accumulated linearly on each element due to the stress/strain level at its position. When an element exceeds its FDR, a void is created, and the material between the crack-tip and the void disintegrates after a few cycles , so that the crack advances to its position.

Additional assumptions are:

(iv) The elements are finitely dimensioned, so that macroscopic laws and properties are applicable.

(v) For each element in the DZ , the fatigue damage incurred throughout the number of cycles they remained in the DZ (prior to the configuration where

the crack advances through their positions), is defined as "historical damage". It is subtracted from the initial strength of the material so that the fatigue criterion applies to the remaining (residual) strength of the predamaged elements.

Assumption (iv) shows that, unlike Oh [7], the fatigue elements cannot be allowed to have "zero" dimensions (e.g. taking the limit as the element size tends to zero). McClintock [46] has pointed out that the use of macroscopic laws implies a lower bound on the size of elements to which a failure criterioncan be applied. Assumption (v) is an attempt to include the entire damage history of each fatigue element in the determination of the crack advance. This is a major departure from the memoriless process described in [7], where the system is "reset" after each crack advance, and the fatigue elements somehow "forget" the previous damage due to the history in the damage zone. This assumption is illustrated in Fig. 3.3.

In the four cases shown, let the appplied ΔK (or ΔJ) be kept constant. Let the damage zone consist of ten fatigue elements, ahead of the crack-tip. At the beginning of a simulation run, the crack-tip is assumed to be completely without any damage. The single circle on the DZ elements in I, illustrates that each accumulates one level of damage (depending on its distance from the crack-tip) at this state. Due to the satisfaction of some failure

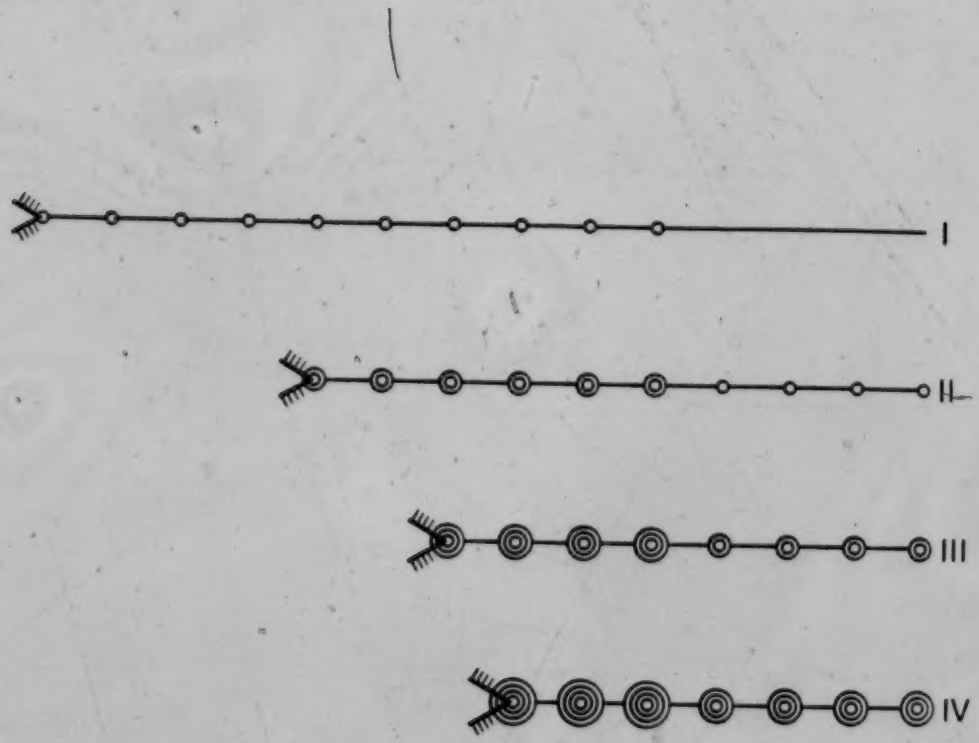

Schematic of "Historical Damage" pile up due to previous crack advances each circle denotes a higher level of damage accumulation

Figure 3.3 Stages of damage accumulation

criterion and crack advance in assumption (iii), the crack state in II is attained. The damage zone now consists of predamaged elements (shown by double circle) and new elements accumulating damage for the first time. By III, the crack has moved again, and each additional circle shown depicts another level of damage accumulation on each element. The total fatigue damage on an element prior to a given crack state is what we have termed historical damage. The representation of the historical damage by circles does not totally quantify this portion of fatigue damage. The fact that two locations, for instance, are shown to have two circles does not mean they have equal amounts of historical damage. Rather, it means that the two fatigue elements have gone through the same number of crack configurations. The exact amount of historical damage is calculated numerically as will be shown.

In general, the historical damage is a random, decreasing function of the distance from the crack-tip. The value at a given position (constant distance from the crack-tip) is shown in Fig. 3.4, plotted against the number of crack advance states. Starting with a value of zero (undamaged element) the historical damage changes randomly until a statistical equilibrium is attained. This is defined as the existence of a stable mean (Fig. 3.4) which is the mean historical damage at the point in question. Fig. 3.5 shows the two kinds of damage accumulated on fatigue elements in a given configuration.

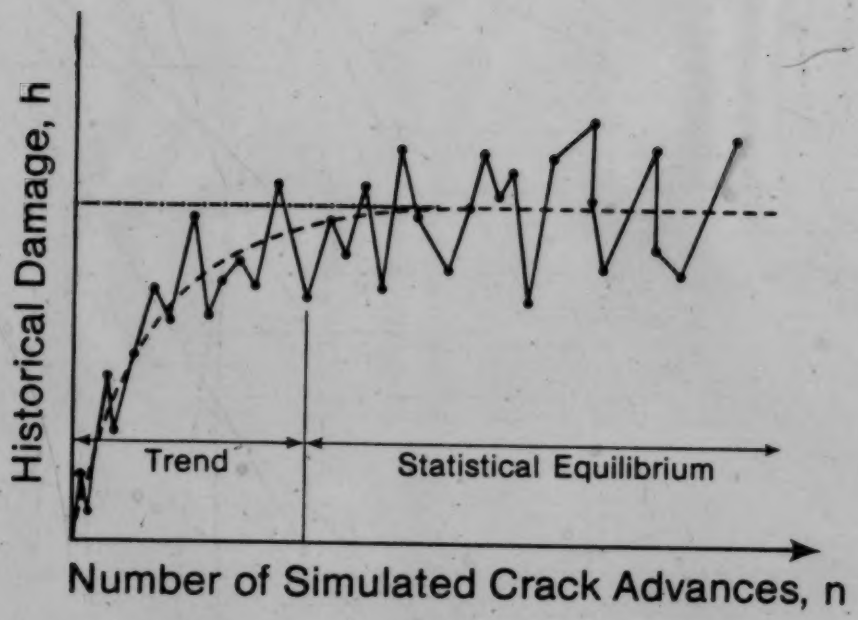

Figure 3.4 Trend and statistical equilibrium

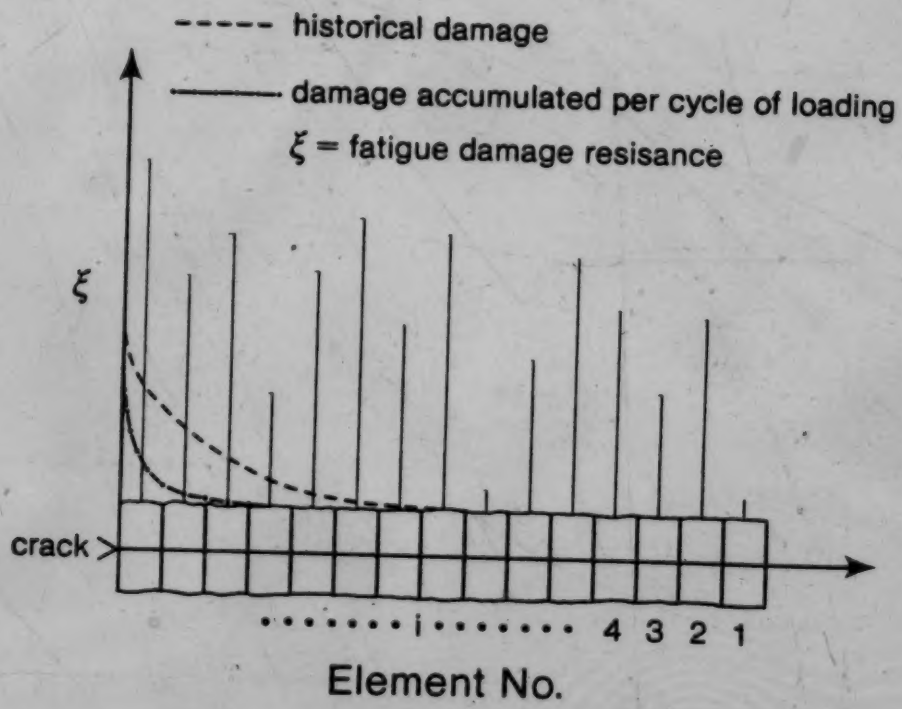

Figure 3.5 Cumulative damage and fatigue damage resistance

(b) Damage Criterion

As in section 3.1, for a given value of the stress/strain range, $\Delta\sigma_i$, $\Delta\varepsilon_i$, the number of cycles to failure, N_{fi}, is calculated from a numerical inversion of Eq. 3.13.

Let n_i be the number of cycles actually spent under the influence of these stress/strain levels by the fatigue elements at position i. The cycle ratio for this element is:

$$\phi_i = n_i/N_{fi} \qquad 3.15$$

Now, let k be the number of crack advances from the first time the particular fatigue element in question entered the damage zone until the time it actually fractures, then the total damage to failure (using a linear damage law) is:

$$\sum_{j=1}^{k} \alpha_j n_j = \phi_1 + \phi_2 + \ldots + \phi_j + \ldots + \phi_k \qquad 3.16$$

where $\alpha_j \equiv 1/N_{fj}$.

For a constant applied stress intensity factor range, ΔK, it is reasonable to assume that the n_j's are independent, identically distributed random variables. Note however, that the ϕ_j's cannot be identically distributed, since the stress/strain distributions is known to be a decreasing function of position. In which

case, even though they are random, the following inequalities hold,

$$N_{f1} > N_{f2} > \ldots > N_{fi} > N_{fi+1} > \ldots$$

$$\alpha_1 < \alpha_2 < \ldots < \alpha_i < \alpha_{i+1} < \ldots \qquad 3.17$$

(Both the N_{fi}'s and the α_i's are ordered random variables).

Therefore, in order to find the probability distribution of the random sum in Eq. 3.16, it will be necessary to be able to specify the individual distribution of the elements. To illustrate the problem involved in establishing the distribution function for the sum $\Sigma\phi_i$, consider that, when all the elements ϕ_i are identically distributed, the random sum is a compound distribution,

$$\sum_{n=0}^{\infty} g_n\{f_i\}^{n*} \qquad 3.18$$

where g_n is the distribution function of k, and
f_i is the distribution function of each ϕ_i,
n* shows that the n-fold convolution of the bracketed term is taken with itself (see Appendix)

In situations where the ϕ_i's are not identically distributed, like the present one, the compound distribution will involve the convolution of all the

individual distributions.

It is convenient to seek the asymptotic behaviour of the sum $\Sigma\phi_i$. In this case, the exact distribution of the ϕ_i's will not be required, and it will closely approximate the distribution of the random sum in question for large k.

For the constant values of α_i's related by the inequality in 3.17, Eq. 3.16 can be shown to be asymptotically normal from physical considerations:

(i) Independence of the n_j's imply independence of the ϕ_j's.

(ii) In the damage zone, defined in this work as the RPZ, the stress/strain range on each fatigue element is always greater than the endurance values. It follows that the number of cycles for a fatigue failure in any element is finite, i.e., $\phi_j = n_j/N_{fj}$ is finite for all j, i.e., $0 < \phi_j < \Phi$ where Φ is some large number.

The distribution of each ϕ_j is thus carried over a finite interval, $(0, \Phi)$. The random sum of such variables defined only in finite domains are asymptotically normal if the sum of individual variances diverge in the limit (Linderberg's condition [47]). And, in this case,

$$\sum_{j=1}^{k} \mathrm{Var}(\phi_j) = \sum_{j=1}^{k} \mathrm{Var}\,(\alpha_j\, n_j)$$

$$= \sum_{j=1}^{k} \alpha_j^2\, \mathrm{Var}(n_j) \qquad 3.19$$

Now, since the n_j's are identically distributed,

$$\mathrm{Var}(n_j) = \text{const} = V(\text{say}) \tag{3.20}$$

$$\lim_{k\to\infty} \sum_{j=1}^{k} \mathrm{Var}(\phi_j) = V \lim_{k\to\infty} \sum_{j=1}^{k} \alpha_j^2 \tag{3.21}$$

But from 3.17, the RHS in Eq. 3.21 is an increasing sequence. It follows immediately, that Eq. 3.21 diverges.

The fatigue damage resistance of each element can thus be defined as approximately normally distributed for large k, i.e.

$$\sum_{j=1}^{k} \phi_j \sim N(\mu,\sigma^2) \tag{3.22}$$

If $\mu = 1$, Eq. 3.22 becomes a form of the statistical Miner's law (Shimokawa and Tanaka [48]).

(c) Stress/strain field.

Using the plastic superposition principle, equation 3.2 for cyclic loading can be written,

$$\Delta\varepsilon_{ij} = \frac{\sigma_o'}{E} \{(\frac{E(\Delta J)}{\sigma_o'^2 I_n r})^{n/n+1} \tilde{\varepsilon}_{ij}(n,\theta) + (\frac{E(\Delta J)}{\sigma_o'^2 I_n r})^{1/n+1} \tilde{e}_{ij}(n,\theta)\}$$

$$\Delta\sigma_{ij} = \sigma_o' \{(\frac{E(\Delta J)}{\sigma_o'^2 I_n r})^{1/n+1}\} \tilde{\sigma}_{ij}(n,\theta) \tag{3.23}$$

Equation 3.23 obviously gives infinite values at r = 0. This singularity can be avoided by arguments similar to that in section 3.1. We consider the quantity x^*, determined previously as the minimum distance to which the above continuum equations can be applied. The stress/strain amplitude to this distance is assumed constant in a way similar to the Irwin's plastic correction factor [49].

3.3 Simulation Process

For each given loading, characterized by the applied ΔK (or ΔJ), the number of fatigue elements in the damage zone is determined by dividing the RPZ by the parameter x^*. The fatigue damage resistance on each element is generated from a standard normal variate generator, displaced rightwards so that the mean value, $\mu = 1$. Since this distribution goes to infinity on both ends, it was necessary to truncate the density function at the origin so that negative values of fatigue damage resistance are avoided. Fig. 3.5 depicts the random fatigue damage resistance generated in this way by the vertical lines on each element. The stress/strain range on the first element is the value at x^* [1] (Fig. 3.6), while for other locations, midpoint values are used. The historical damage on each

---

[1]Here, we have followed Glinka [21] in assuming that the strain gradient in this small region ahead of the crack-tip is negligibly small. Experimental and analytical results discussed later (chapter 4) justifies this assumption.

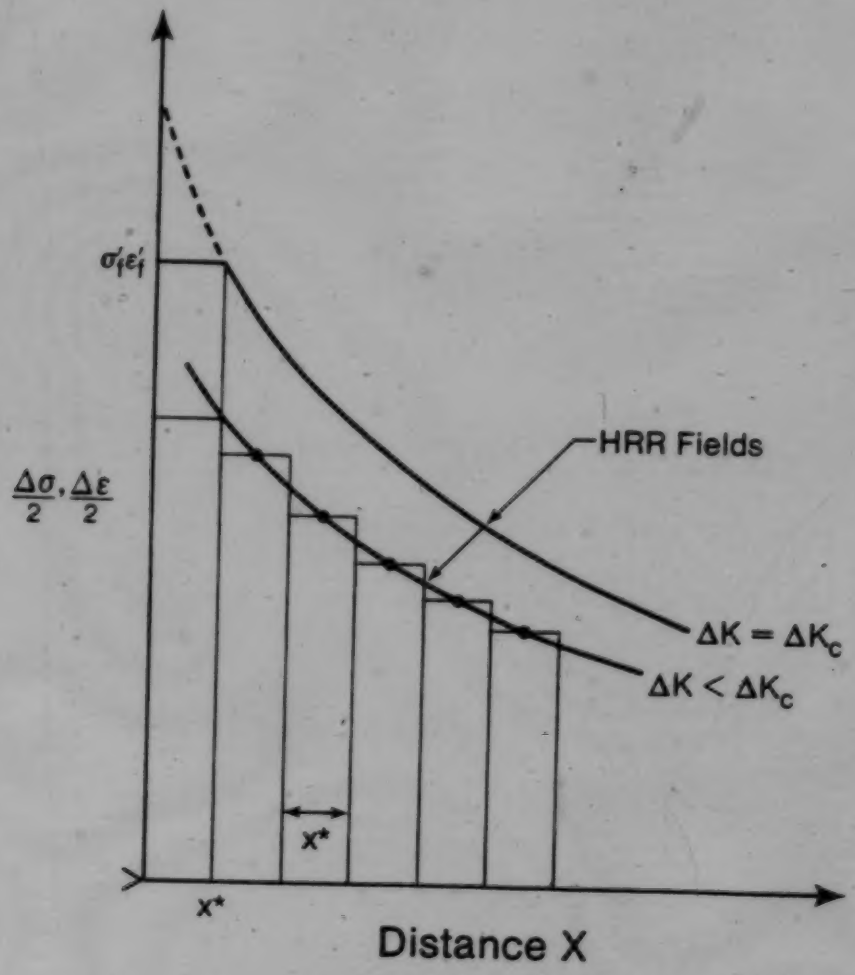

Figure 3.6 Modified continuum stress-strain ranges

element is initially set to zero. For the first simulated crack advance, the damage accumulation was due to the value of stress/strain range applied in that configuration. The crack advances to the position of the first fatigue element fracture, which is the first element to exceed its fatigue damage resistance. The damage zone "moves" with the crack front to a new configuration, as explained before (see Fig. 3.3). Some new (undamaged) fatigue elements are now in the damage zone in addition to the remaining elements from the previous configuration. The total damage history on an element prior to the configuration in question is stored as "historical damage" and it is subtracted from the fatigue damage resistance before the application of any failure criterion. This procedure is repeated until the statistical equilibrium described in Fig. 3.4 is attained. The applied stress intensity range is kept constant (this in reality means that the applied stress range is reduced to complement the increase in the crack length due to crack growth). After a crack advance, the random growth rate is recorded:

$$\left\langle \frac{da}{dN} \right\rangle = \frac{ix^*}{n} \qquad 3.24$$

where i = element number to which there was crack advance,

n = number of cycles spent in the configuration.

About twenty simulation steps were used for each applied stress intensity factor range.

3.4 Results

(a) Historical Damage

Figures 3.7 to 3.9 show the distribution of the mean historical damage on the elements ahead of the crack-tip. For each applied ΔK, the distance from the crack-tip is normalized against x^*. This quantifies the amount of predamage at each position ahead of the crack-tip of a growing crack. It can be seen that in all cases, the historical damage is significant at least on the first few elements ahead of the crack-tip. It is of the same order of magnitude as the mean damage to failure. A fracture criterion should be specified in terms of the residual strength rather than the undamaged strength of the material. The amount of predamage at each location is dependent on both the distance from the crack-tip and the applied stress intensity factor range. Figures 3.10 to 3.12 are plots of the mean historical damage against the applied stress intensity factor range, for four element positions: (1) crack-tip element, (2) one quarter, (3) one half and (4) three quarters of the reversed plastic zones respectively. For each of the metals modelled, the element at the crack-tip has a significant amount of historical damage which is practically independent of the applied stress intensity factor range. For the other three element

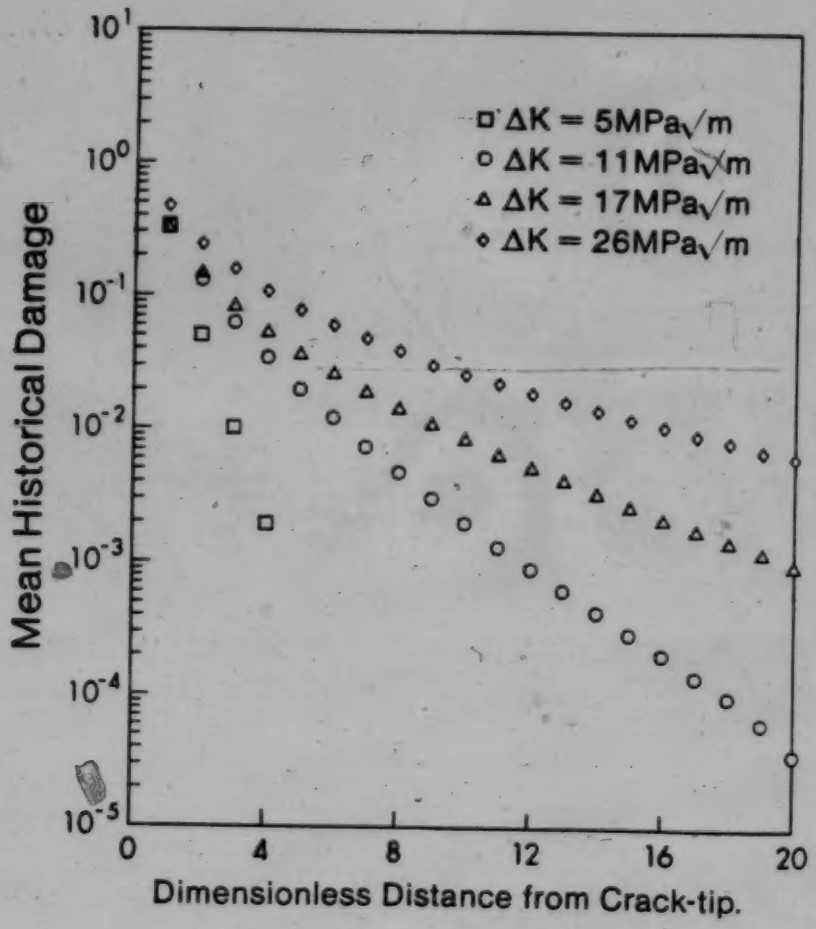

Figure 3.7 Historical damage vs distance for 2219-T851-Aluminium

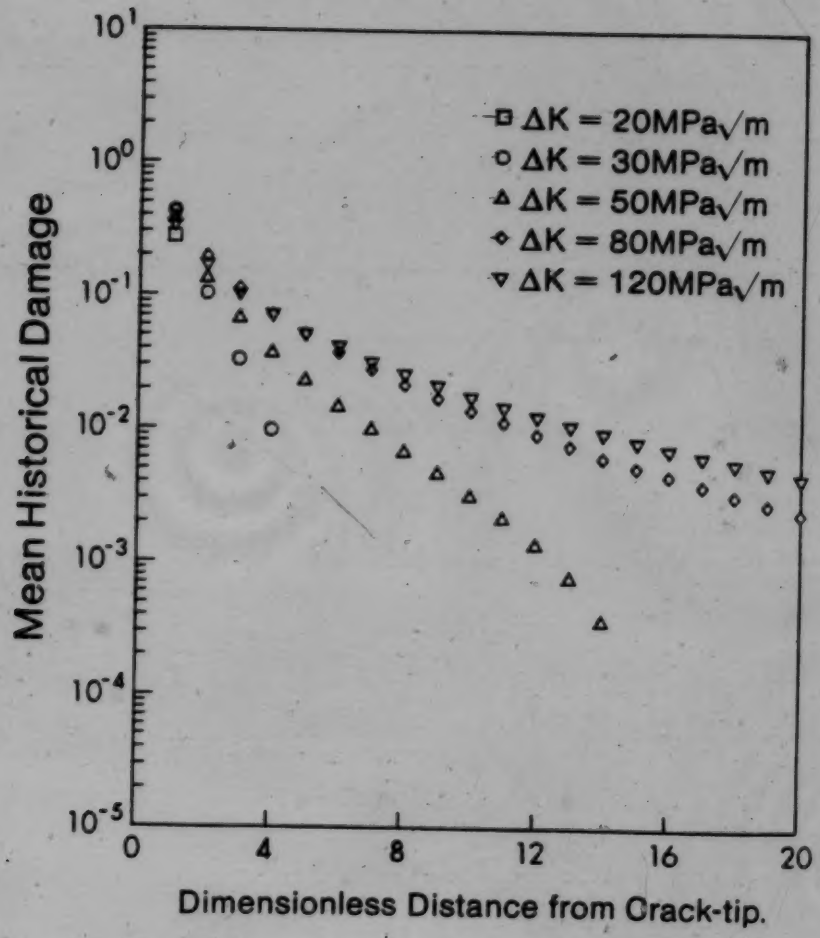

Figure 3.8 Historical damage vs distance for A516-Gr 70Steel

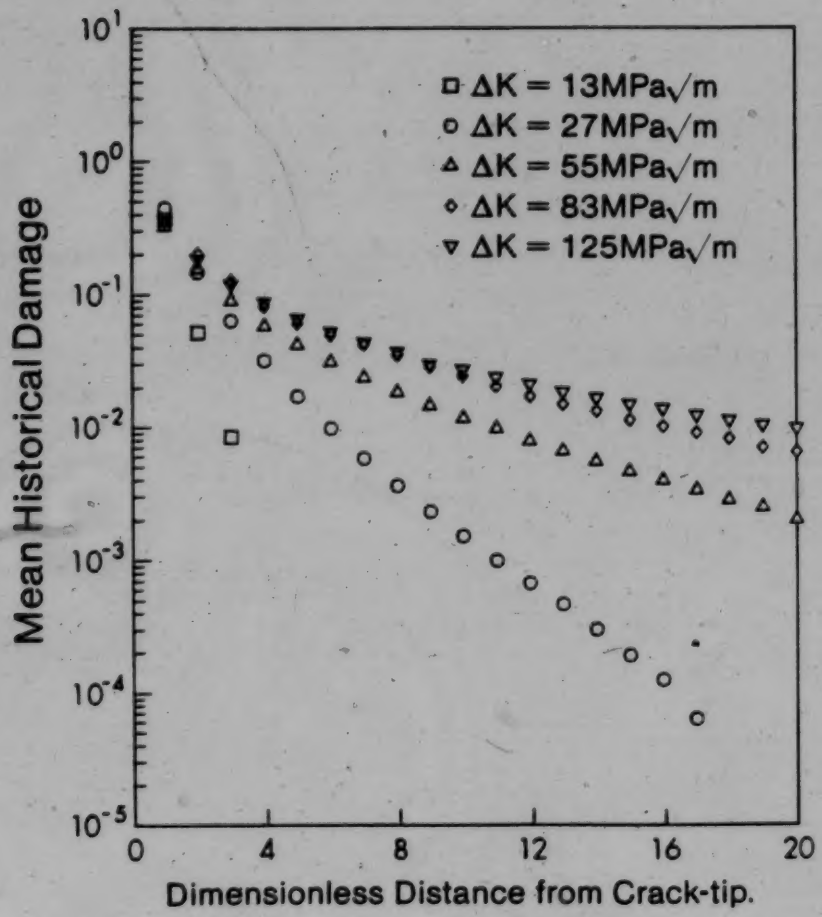

Figure 3.9 Historical damage vs distance for A533B Steel

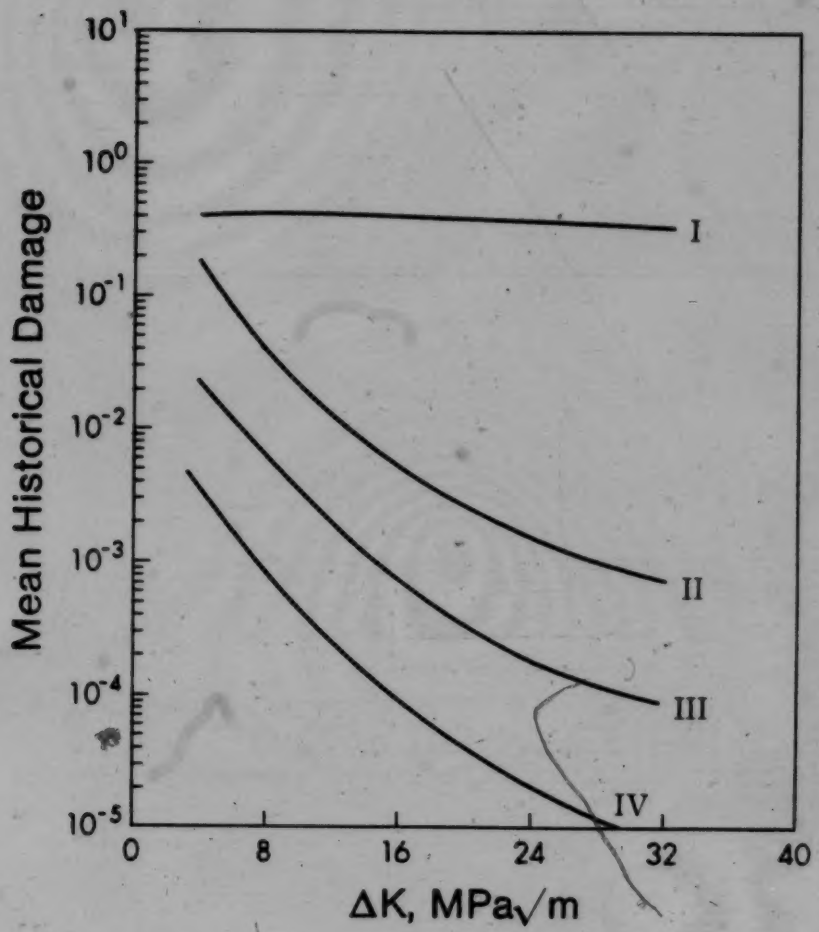

I, adjacent to the crack-tip; II, one quarter; III, one half; and IV, three quarters of the damage zone.

Figure 3.10 Historical damage vs ΔK for 2219-T851-Aluminium

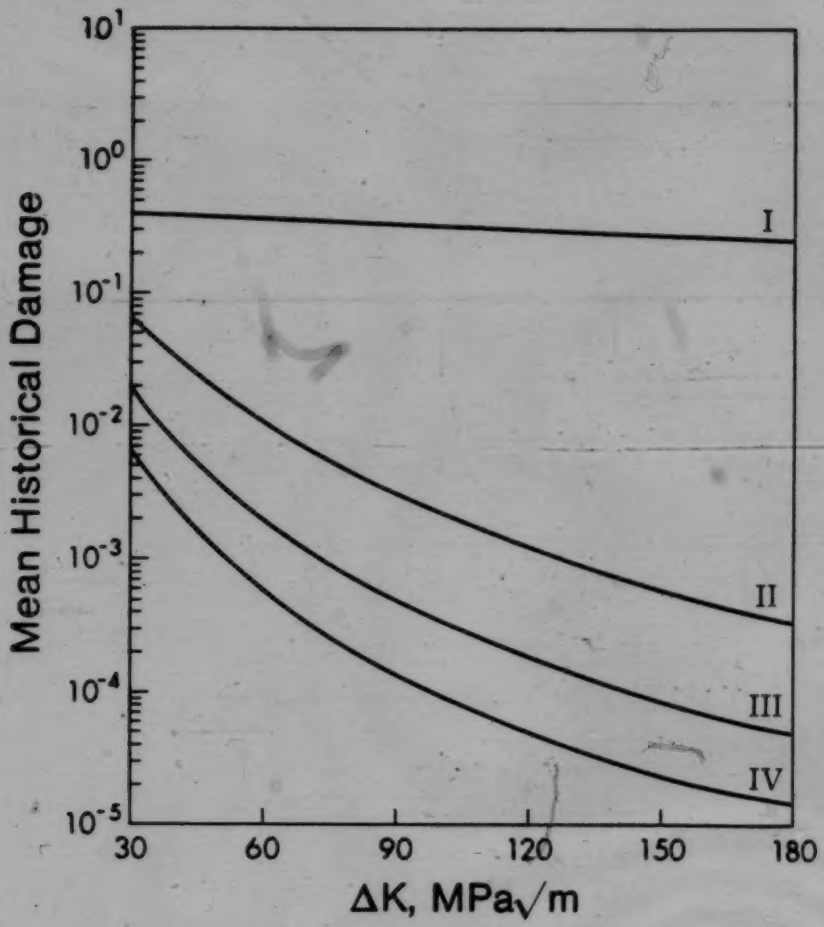

I, adjacent to the crack-tip; II, one quarter; III, one half; and IV, three quarters of the damage zone.

Figure 3.11 Historical damage vs ΔK for A516-Gr 70-Steel

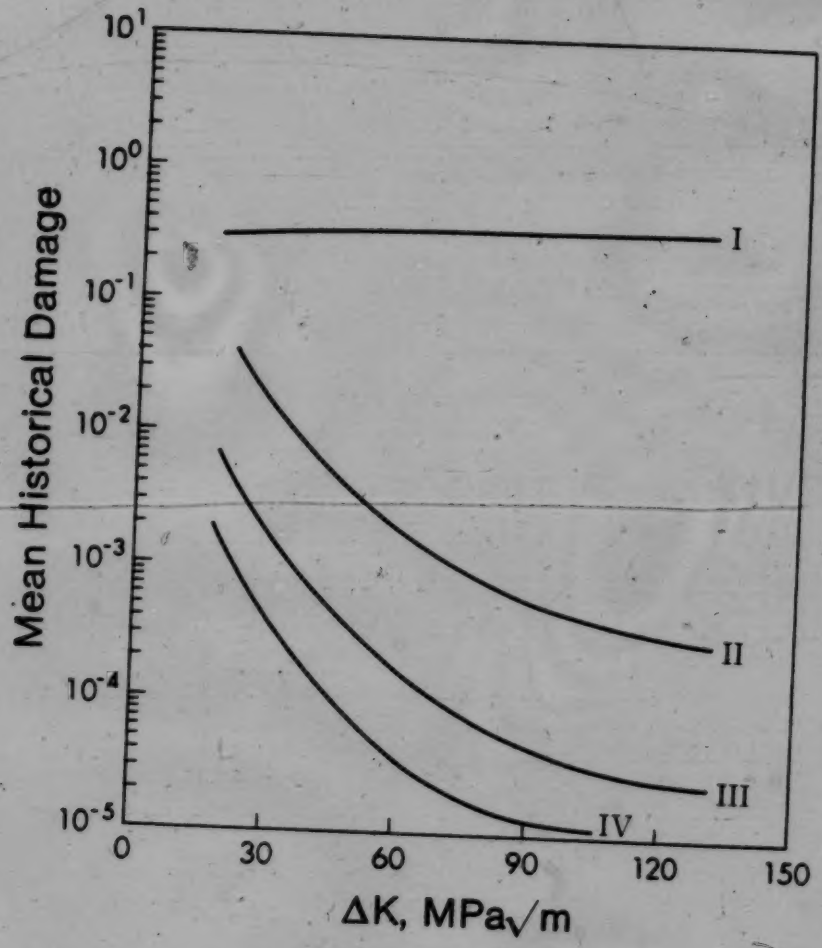

I, adjacent to the crack-tip; II, one quarter; III, one half; and IV, three quarters of the damage zone.

Figure 3.12 Historical damage vs ΔK for A533B Steel

positions, there is a strong dependence on the applied stress intensity factor range, but the amount of historical damage is not significant (i.e. it is of a lower order of magnitude than the damage to failure) from a linear damage accumulation standpoint.

(b) Probability distribution

While it is important to have the mean value of the growth rate law to be close to experimental observation, the main contribution of a probabilistic model is what information it provides on the scatter around this mean. The amount of scatter in any experiment depends on how much experimental values are used - the larger the number of observations, the larger the scatter. It is thus difficult to measure the success of probabilistic model in terms of the predicted second central moments. In this work, the probability distribution of the crack growth rate is not given in closed form. Even if a closed form were to exist, experience (with Oh's model, and the discussion in section 3.2) shows that it may be too complicated to serve any useful purpose. It was thus considered best in this work to compare the resulting probability density function of the crack growth rates to some of the most frequently assumed densities in the literature. These densities are:

1. Weibull,

$$f(x) = \frac{x_3}{x_2} \left(\frac{x - x_1}{x_2} \right)^{x_3 - 1} \exp \left\{ - \left(\frac{x - x_1}{x_2} \right)^{x_3} \right\} \qquad 3.25$$

x_1, x_2 and x_3 are the location, scale and shape factors respectively, satisfying: $x_1 < x$, $-\infty < x_2 < \infty$, and $0 < x_2, x_3$.

2. Extreme value distribution

$$f(x) = \frac{1}{x_2 \Gamma(x_3)} \left(\frac{x - x_1}{x_2} \right)^{x_3 - 1} \exp \left\{ - \left(\frac{x - x_1}{x_2} \right) \right\} \qquad 3.26$$

where, $-\infty < x_1 < \infty$, $0 < x_2 < \infty$, and $0 < x_3 < \infty$.

3. Log-normal distribution

$$f(x) = \frac{1}{(x - x_3)\, x_2 \sqrt{2\pi}} \exp \left\{ - \tfrac{1}{2} \left(\frac{\ln(x - x_3) - x_1}{x_2} \right)^2 \right\} \qquad 3.27$$

$x_3 < x$, $0 < x_2$, and $-\infty < x_1, x_3 < \infty$

Figs. 3.13 to 3.15 show probability plots of typical distribution from this simulation process, with respect to these three distributions. A linear plot indicates a measure of correlation with the underlying distribution for each probability plot [50]. As can be seen from these plots, the log normal distribution gives the closest approximation to the distribution of the simulated results. A Shapiro-Wilk normality test was performed on the logarithm of the simulated data. Acceptance of a lognormal distribution was indicated at 5% level of

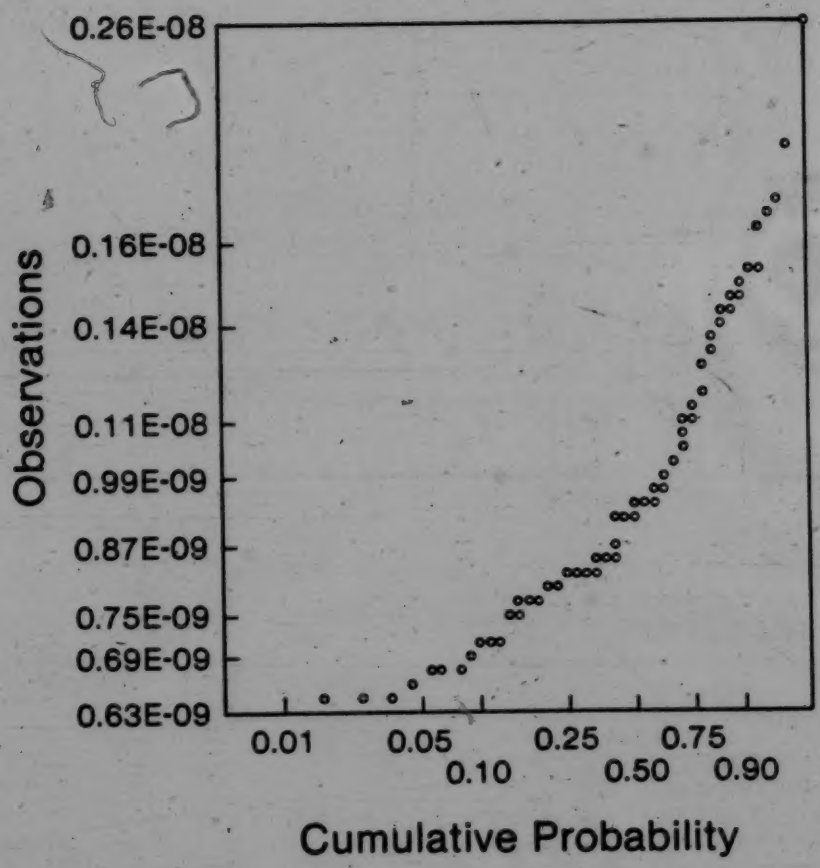

Figure 3.13 Weibull probability plot

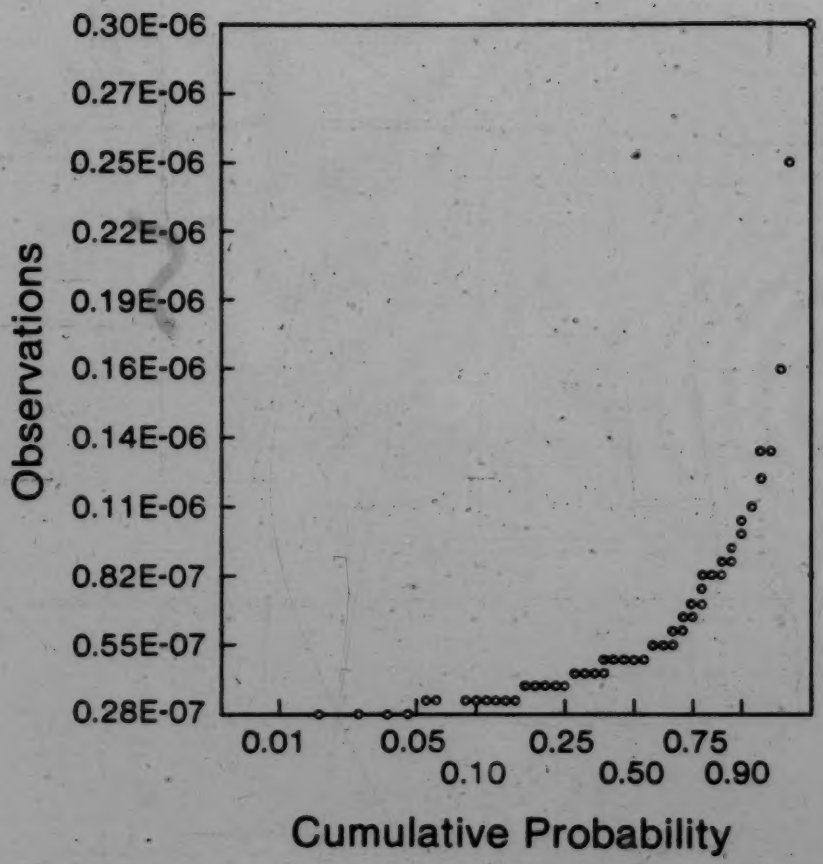

Figure 3.14 Extreme value probability plot

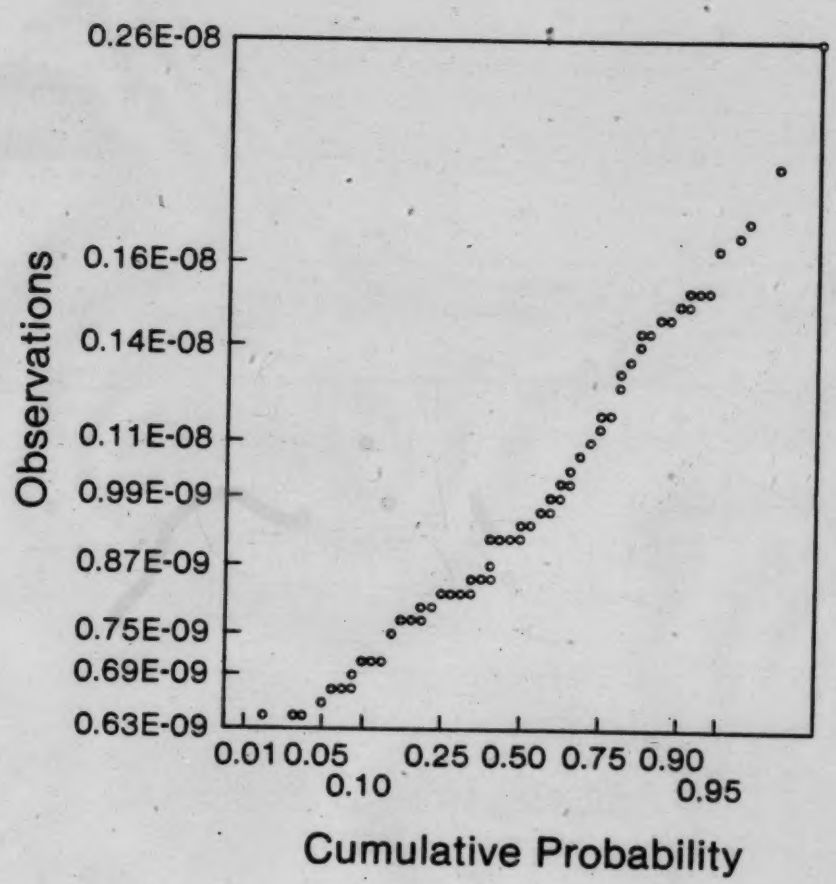

Figure 3.15 Log-normal probability plot

significance in most cases. Experimental results reported in ref. [51] confirm this trend.

(c) Fatigue threshold and comparison with experimental data.

Table 3.1 shows the material properties of the three metals used for comparison. One feature of the model is that it allows the estimation of the threshold stress intensity factor range. The number of fatigue elements in the damage zone depends on the applied stress intensity factor range. This is because the reversed plastic zone increases with the latter. If the applied stress intensity factor range is decreased, a stage is reached when the damage zone consists of only one fatigue element. At lower values of stress intensity factor range than this, the growth rate is insignificant since the damage accumulation outside the RPZ is negligible. This value of ΔK thus defines the threshold level of the stress intensity factor range, ΔKth. Table 3.2 shows the values of ΔK_{TH} determined this way compared to experimental data.

Figures 3.16 and 3.17 are the plots of the median growth rate from the simulation compared with published data, for 2219-T851-Aluminium alloy [21] and A516-Gr 70-Steel [45]. These results show good agreement with experimental data. In Fig. 3.18, the growth rate curve was plotted against ΔJ for both linear elastic tests and elastic-plastic tests for A533 B steel [5]. The linear elastic tests were in good agreement with the

Table 3.1 Material properties

Material Properties	2219 T851 Al	A516 Gr 70 Steel	A533 B Steel
b	-0.0756	-0.108	-0.085
c	-0.55	-0.506	-0.516
n'	0.121	0.19	0.165
σ_o' (MPa)	334.0	310.0	345.0
ε_f'	0.35	0.26	0.32
σ_f' (MPa)	613.0	900.0	869.0
E (GPa)	71.0	200.0	200.0
Δk_c (MPa $\sqrt{m}$)	30.0	200.0	140.0

Table 3.2 Threshold stress intensity factor range

MATERIAL	ΔK_{TH} (MPa $\sqrt{m}$)	
	PREDICTED	EXPERIMENT
1. 2219 T851 Al	3.0	3.0
2. A516 Gr 70 Steel	10.0	
3. A533 B Steel	7.0	8.0

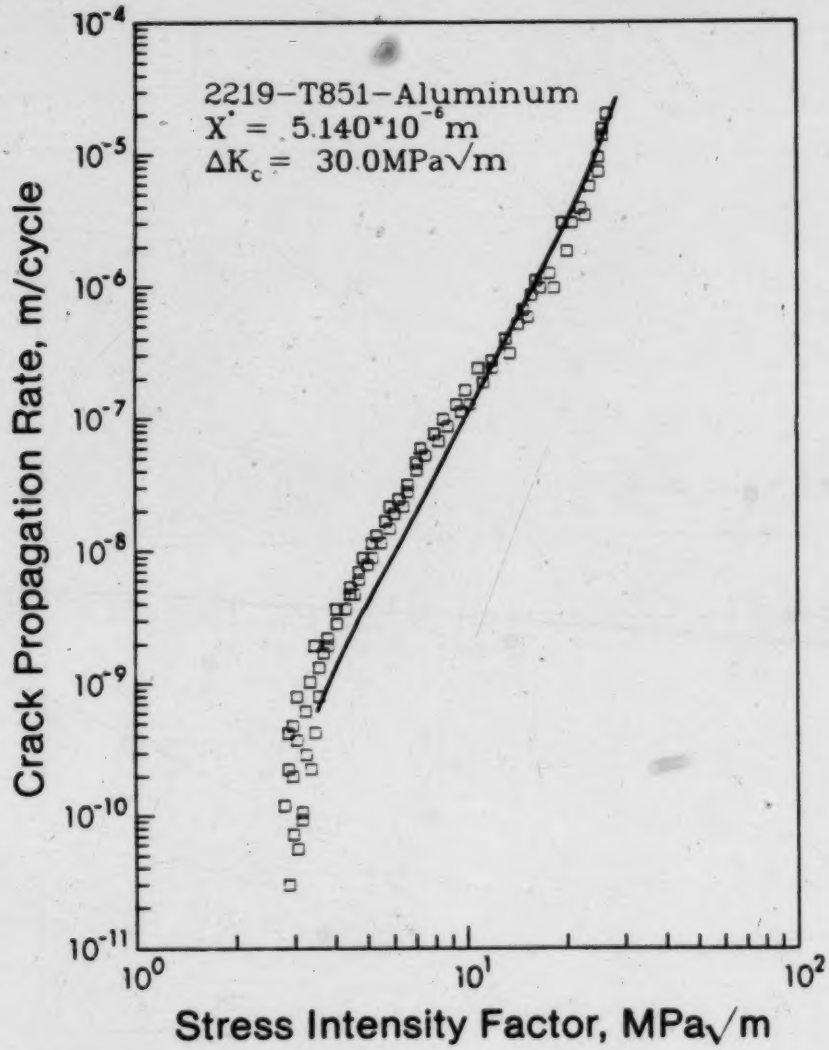

Figure 3.16 Comparison of experimental and predicted crack propagation rate vs stress intensity factor range

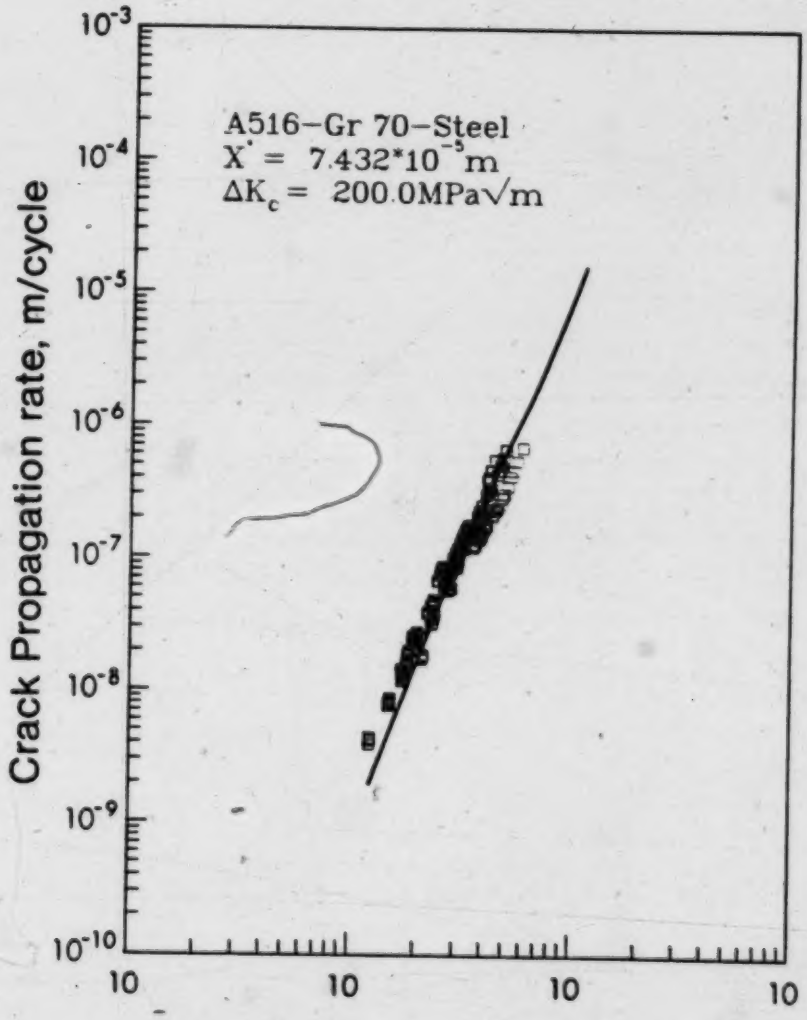

Figure 3.17 Comparison of experimental and predicted crack propagation rate vs stress intensity factor range

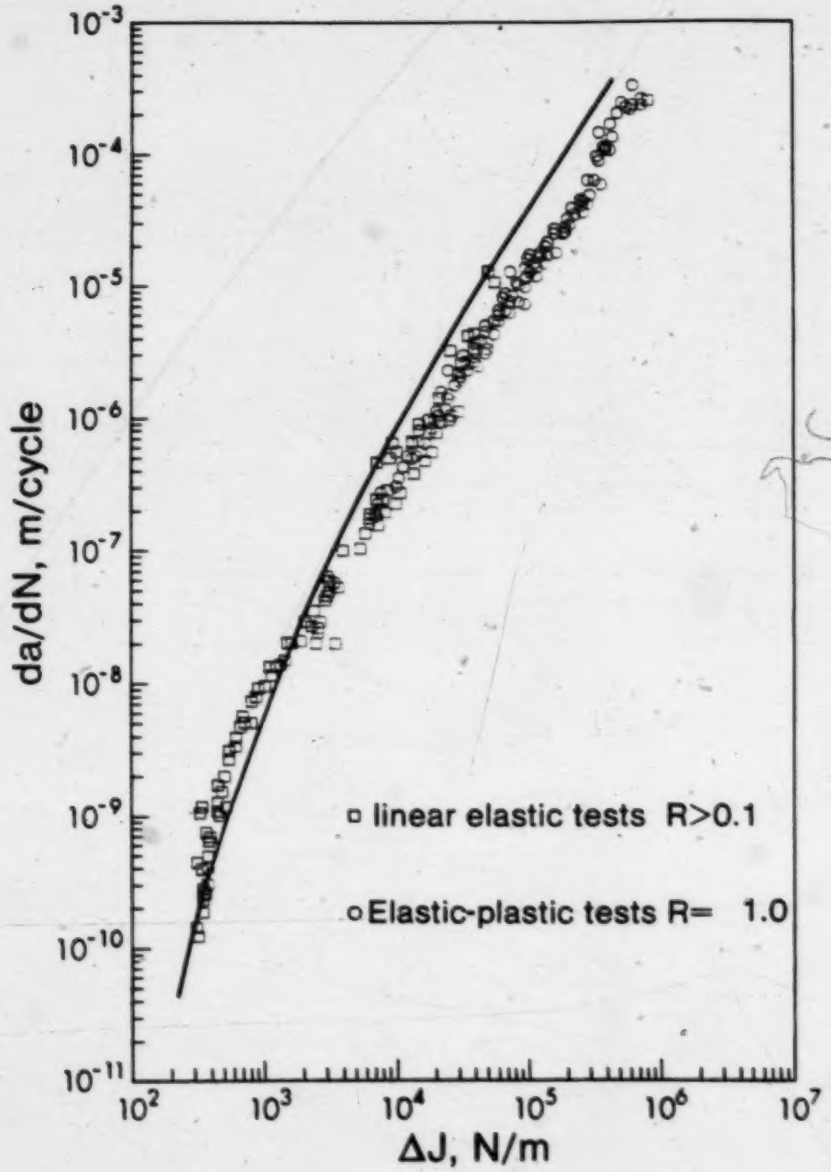

Figure 3.18 Comparison of experimental and predicted crack propagation rate vs cyclic J-integral (A533 B Steel)

model. However, the elastic-plastic tests deviated from the model by a factor of nearly two. This disparity is partly attributed to the definition of ΔJ used in plotting the experimental results, which were conducted at a different stress ratio from the linear elastic tests. ($R = -1$ for elastic-plastic, $R > 0.1$ for linear elastic). The definition of ΔJ in the elastic-plastic test is sensitive to the assumptions made on the stress ratio used.

For monotonic loading, see Dowling [5],

$$J = Je + Jp$$

$$= (\alpha W_e + \beta W_p)a \qquad 3.28$$

where J_e is the elastic J integral,

J_p is the plastic J integral,

a = half crack length,

$\alpha;\beta$ = constants derived in [3,4]

W_e = elastic work

W_p = plastic work

Dowling modified Eq. 3.28 in the following form:

$$\Delta J = (\alpha \Delta W_e + \beta \Delta W_p)a$$

The data in Fig. 3.18 are based on taking ΔW_e and ΔW_p as the full range of work done (Fig. 3.19). For fully reversed loading ($R = -1$), Mowbray [38] suggested a truncation of the applied ΔW_e and ΔW_p as shown to account for crack closure. Since crack closure was assumed to come

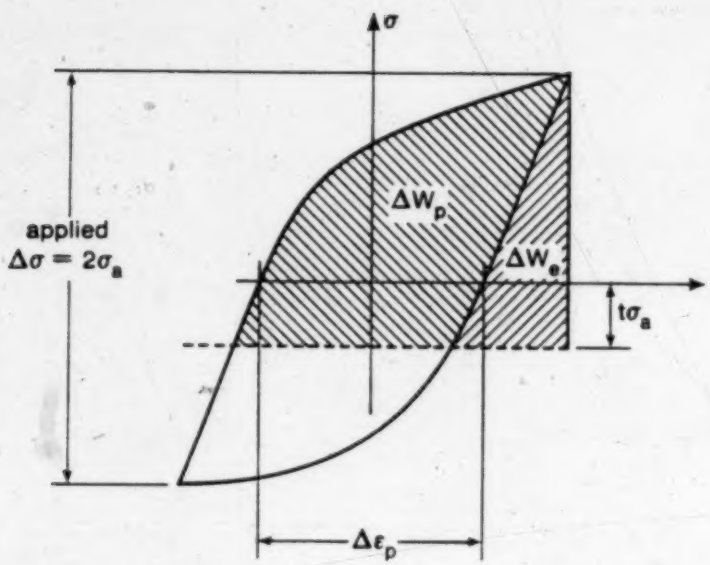

Estimation of crack ΔJ from stress strain hysteresis loops.

Figure 3.19 Estimation of crack ΔJ from stress-strain hysteresis loops

at a lower value of applied loading than the zero level, it was suggested in [38] that some (but not all) of the compressive portion should be included in the calculations of ΔW. The fraction suggested is $t = 1/3$. The works of Hudson [52] and Newman [53] suggest that only the positive part of the respective work done ($t=0$) should be applied. In the latter case, the value of the calculated ΔJ would be reduced by about half. This leads to the shifting of the elastic-plastic data (Fig. 3.18) to the left by a factor of 2.

(d)Concluding Remarks

Apart from the ability to predict the mean or median crack growth rate, this probabilistic simulation of fatigue crack growth leads to several fresh insights on the crack propagation phenomenon. Within the limits of the assumptions of the model, the simulation leads to a prediction of the threshold stress intensity range, below which the crack is not expected to grow. The simulation process also facilitates the consideration of the total damage history of the crack-tip elements. This way, the the historical damage is quantified. It is demonstrated that this quantity, often neglected by previous investigators, is of considerable significance. A Markovian treatment of probabilistic crack growth is thus inadequate unless a relationship can be found between the historical damage and the position of each fatigue element. Figures 3.7 to 3.12 show that such a relationship

in general depends on several factors. These include the applied loading, crack length and intrinsic material properties. This will be further complicated in the case of the elastic-plastic crack growth (large scale yielding) by the effects of plastic unloading discussed in the last section. The probabilistic distribution resulting from this model has been compared to three of the commonly used probability densities in the literature. No conclusive results can be drawn from probability plots alone. However the tendency toward the lognormal function in the Figs 3.13 to 3.15 cannot be ignored.

Chapter 4

DISLOCATION MODEL OF NON-LINEAR HARDENING

4.1 Introduction

In the preceding analysis, it has been necessary to know the distribution of stress and displacement (or strain) in the vicinity of the crack-tip, when the body in question is loaded cyclically. So far, in the literature, there has been no rigorous determination of these field quantities. As a result of this, the plastic superposition rule, extensively outlined by Rice [19] is widely used. This method was used to determine the cyclic fields in chapters 2 and 3. If the size of the crack in relation to the applied loading justifies the assumption of small scale yielding, for cyclic loading between σ_A and σ_B, the cyclic loading can be characterized by, ΔK, defined as:

$$\Delta K = \Delta\sigma\sqrt{\pi a} \qquad 4.1$$

where $\Delta\sigma = \sigma_B - \sigma_A$, so that,

$$\Delta K = K_B - K_A, \qquad 4.2$$

That is, the change in the stress intensity factor within the range.

However, the assumption of small scale yielding is very restrictive. Even with the far field stresses within

the elastic range, it is well known that the ratio of the plastic zone size to the crack length could be large enough to invalidate the results. Usually, in such a case, the J-integral would be a preferred quantity to characterize the crack-tip plasticity. The simple relationship between J-integral and K (or any other loading quantity), holds only in small scale yielding. Even for monotonic loading, analytical expressions for J-integral are difficult to obtain, except for small scale yielding. Goldman and Hutchinson [37] obtained closed form expressions for fully plastic materials and this has been used in conjunction with the small scale yielding results to provide some interpolated estimate for J-integral in the midrange [3,4]. The relevant weighting functions in this interpolation procedure were obtained using finite element methods.

Two problems arise when this interpolation method is applied to cyclic loading. Firstly, there is no equivalent of equation 4.2 for the J-integral. The cyclic J-integral cannot be obtained by simply subtracting the monotonic J-integral of the two levels of loading. Secondly, the weighting functions for the interpolation are available only for monotonic loading. Previous investigators [5, 38] have simply added the small scale yielding and fully plastic components of the J-integral in the midrange. Such a method is of doubtful validity unless the loading conditions are close to either small scale yielding or

full plasticity.

Using an extension of the BCS dislocation model, a method is described in this chapter that facilitates the direct evaluation of the J-integral. The extension involves the incorporation of work-hardening into the classical dislocation model in a more realistic way than previously attempted. We begin with a brief description of the Bilby and Swinden Linear Hardening Model. Then the conditions for the existence of a solution for the nonlinear work-hardening model presented are elucidated. The displacement integral equations are derived. The method of numerical solution is briefly described. Some of the significant results of the analysis are then presented.

(a) The Bilby and Swinden [18] model

This model is based on the dislocation model of BCS [17] already described in chapter 2. The main difference is in the assumption that the "friction stress", $\tau_1(x)$ resisting the motion of the dislocation into the material in question is now a function of position and of the plastic displacement at a given point;

$$\tau_1(x) = \tau_0 + \omega\gamma_p(x) = \tau_0 + \frac{\omega\phi(x)}{\alpha} \,. \qquad 4.3$$

where τ_0 = minimum friction stress

$\gamma_p(x)$ is the plastic strain at distance x from the crack-tip,

$\phi(x)$ is the plastic displacement at the same point,

ω is a constant with the dimension of stress, and

α is a constant with the dimension of length.

Identifying τ_0 (equation 4.3) with the material yield stress implies the modelling of a material, exhibiting a linear Hookean response for the states of stress within the yield point, and a linear hardening plastic behaviour for those outside. The plastic zone is, as in the BCS model, the extent of dislocation motion into the material.

The displacement field in this case was found by evaluating a linear integral equation where the unknown function also occurred inside the integral. The linearity of this problems allows a solution using linear algebra and matrix methods.

Even though the results show quite considerable change in the crack-tip displacement as a result of the incorporation of work-hardening, the plastic zone was not significantly affected. The only major problem observed was the occurrence of negative displacements ahead of the crack-tip when the plastic zone becomes too large.

4.2 A Non-Linear Work-Hardening Model

A bilinear stress-strain law in which the post yield behaviour of a material is considered linear can be considered as a first approximation. Such a choice is

attractive (as in the Bilby and Swinden model discussed earlier) because of the linearity of the resultant integral equations. However, in spite of this simplicity, there was no obvious closed form solution for the relevant plastic displacement field. The need to seek a fully numerical solution removes virtually all the advantages it may have over the more realistic (even though slightly complicated) modelling of the stress-strain law.

In the non-linear work-hardening model considered here, all the assumptions of the BCS model are retained except that the friction stress is considered to be of the form:

$$\tau_1(x) = \tau_0\left(\frac{\gamma(x)}{\gamma_0}\right)^{n'}, \qquad 4.4$$

where, γ_0 is the yield strain, $\gamma(x)$ is the total strain at a distance x from crack centre, and n' is the hardening exponent in the modified Ramberg-Osgood stress-strain law. Since the plastic line represents states of plastic strain, the total strain at each point can be expressed as:

$$\gamma(x) = \gamma_p(x) + \gamma_0, \qquad 4.5$$

where $\gamma_p(x)$ is the plastic strain.

From equations 4.3 and 4.4, we have:

$$\tau_1(x) = \tau_0\left(\frac{\phi(x)}{\alpha\gamma_0} + 1\right)^{n'} = F\left(\phi(x)\right), \qquad 4.6$$

so that the post yield behaviour is non-linear of the Ramberg-Osgood type. Setting n'=0 in equation 4.6, the original BCS model is recovered, while n'=1, with a suitable choice of parameters, become identical with the linear hardening model of Bilby and Swinden.

For an external loading, resulting in a far field stress of magnitude τ^{∞}, equilibrium conditions requires that the sum of all forces (dislocation and external) acting at each location must vanish. Considering a continuous distribution of dislocations with density f(x), and Burger's vector b, this condition leads to:

$$\mathcal{R}\int_{-a}^{a} \frac{f(x')dx'}{x-x'} + \frac{P(x)}{A} = 0 , \qquad 4.7$$

where, $\mathcal{R}$ signifies that only the Cauchy Principal value of the singular integral is considered,

$$P(x) = \begin{cases} \tau^{\infty} & |x| < c \\ \tau^{\infty} - F(\phi(x)) & c \leq |x| \leq a , \end{cases}$$

and $A = \mu b/2\pi(1-\upsilon)$,

μ = rigidity modulus,

υ = poisson ratio,

c = crack length.

The plastic zone size, a, is an unknown in the equation 4.7 above. Its value can be evaluated by imposing a boundedness condition on the dislocation distribution density f(x), as will be discussed later.

In the next section, the conditions for the inversion of equation 4.7 will be described, and the integral equations for the displacement field will be formulated.

4.3 Conditions for Inversion of Equilibrium Equation

The inversion of the equilibrium equation 4.7 depends on the satisfaction of certain conditions related to the Holder inequality. We begin this section by presenting some definitions and lemmas to be invoked later in the inversion procedure.

(a) Holder Condition on a line segment [54,55]

Definitions and Lemmas

(i) Consider a function $\theta(t)$ defined on a line segment L, $\theta(t)$ is said to satisfy the Holder condition, or, equivalently, to belong to the class H, if for two arbitrary points of this line,

$$| \theta(t_2) - \theta(t_1) | < A | t_2 - t_1 |^{\lambda}, \qquad 4.8$$

where A (>0), is called the Holder constant, and, $0 < \lambda < 1$, is the Holder index.

(ii) If $\theta_1(t)$ defined on L, satisfies the Holder condition on every closed part of L not containing the

ends, and if, near any end, t=c, it is of the form,

$$\theta_1(t) = \frac{\theta(t)}{(t-c)^{\alpha}}, \quad 0 < \alpha \leq 1 \qquad 4.9$$

Given that θ belongs to the class H, then, $\theta_1(t)$ belongs to the class H^* on L.

It is convenient at this point to state two lemmas which will be found useful later on:

Lemma 4.1

Consider f(t) defined on the line segment [c,a]. If f(x) is a positive monotonic decreasing function of t, then, the function,

$$\phi(x) \equiv -\int_x^a b\, f(t)dt, \quad c < x \leq a \qquad 4.10$$

belongs to class H, provided f(t) is bounded.

PROOF:

Consider $c < t_1 < t_2 < a$,

$$\phi_1(t_2) - \phi_1(t_1) = -b\int_{t_2}^{t_1} f(x)dx = b\int_{t_1}^{t_2} f(x)dx$$

$$\leq bf(t_1)\,|\,t_2 - t_1\,|\,. \qquad 4.11$$

Hence, $|\,\phi_1(t_2) - \phi_1(t_1)\,| \leq M\,|\,t_2 - t_1\,|^{\lambda}$, $M = bf(t_1)$

So that M is the Holder constant, and the index $\lambda=1$.

A corollary lemma follows immediately for f(t) monotonically increasing.

Lemma 4.2

Given that $\phi_1(t)$ is of class H on the line segment [c,a]. And given that $\phi_1'(t)$ and $\phi_2'(t)$ are both of the same sign (i.e., either both positive or both negative), if,

$$| \phi_2'(t) | < | \phi_1'(t) |, \text{ then}^3$$

$\phi_2(t)$ is also of class H in the same range.

PROOF:

$$| \phi_2(t_2) - \phi_2(t_1) | = \left| \int_{t_1}^{t_2} \phi_2'(t)dt \right|$$

$$= \int_{t_1}^{t_2} | \phi_2'(t) | dt < \int_{t_1}^{t_2} | \phi_1'(t) | dt.$$

$$\text{But } \int_{t_1}^{t_2} | \phi_1'(t) | dt = \left| \int_{t_1}^{t_2} \phi_1'(t)dt \right| = | \phi_1(t_2) - \phi_1(t_1) |. \qquad 4.12$$

Now, M and λ can be found such that,

$$| \phi_1(t_2) - \phi_1(t_1) | < M | t_2 - t_1 |^{\lambda}, \quad M > 0, \ 0 < \lambda \leq 1 \qquad 4.13$$

so that, from the above relationship,

$$| \phi_2(t_2) - \phi_2(t_1) | < M | t_2 - t_1 |^{\lambda}. \qquad 4.14$$

---

[3]The primes on the ϕ_1's here imply differentiation

(b) Inversion of the Equilibrium Equation

In order to obtain the dislocation distribution, the equilibrium equation 4.7 has to be inverted. The general solution of this problem has been given by Muskhelishvili [54,55]. The conditions to be satisfied are that, the dislocation $f(x)$ is of class H^*, and that $P(x)$ is of class H. With these conditions satisfied, if the Cauchy Principal value of the integrals exist at each point, then,

$$f(x) = \frac{2(1-\nu)}{\pi\mu b} \int_{-a}^{a} R(x,y)\, P(y)\, dy \,.$$

$$R(x,y) = \frac{1}{x-y} \sqrt{\frac{a^2-x^2}{a^2-y^2}} \,. \qquad 4.15$$

Guided by the solution of the BCS model (Chapter 2), it is reasonable to make the following assumptions about $f(x)$: Firstly, $f(x)$ is of class H^*, and secondly, $f(x)$ is a monotonic function of position in the two line segments [0,c], and [c,a]. These assumptions are based on the fact that for mild hardening, (moderate values of n') the function $f(x)$ should behave like $f_1(x)$ of chapter 2. Now, $f_1(x)$ is monotonic in the interval [c,a] and it is easily shown to be of class H^* in the vicinity of the crack-tip thus:

For any λ in the range, $0 < \lambda < 1$,

$$\lim_{x \to c^+} (x-c)^{\lambda} f_1(x) = \frac{\sigma_o}{\pi^2 A} \lim_{x \to c^+} (x-c)^{\lambda} \{ \cosh^{-1} \left| \frac{a^2 - c^2}{a(c-x)} + \frac{c}{a} \right| - \cosh^{-1} \left| \frac{a^2 - c^2}{a(c+x)} + \frac{c}{a} \right| \} \qquad 4.16$$

Using L'Hospital's rule, it follow that

$$\lim_{x \to c^+} (x-c)^{\lambda} f_1(x) = \frac{\sigma_o}{\pi^2 A} \lim_{x \to c^+} \left(\frac{2c}{x^2 - c^2} \sqrt{\frac{a^2 - c^2}{a^2 - x^2}} \right) / - \lambda (x-c)^{-\lambda - 1} = 0 \qquad 4.17$$

where c^+ indicates an approach from the positive direction, so that $(x-c)^{\lambda} f_1(x)$ is bounded and continuous in the neighborhood of the crack-tip. Therefore, $f_1(x)$ belongs to the class H^* in this neighborhood.

(c) Holder Condition for P(x)

Now, define,

$$\phi(x) \equiv - \int_x^a b\, f(t)dt, \quad c < x \leq a, \qquad 4.18$$

By Lemma 4.1, $\phi(x)$ belongs to the class H in the open interval, (c,a]. It follows easily that any linear function of $\phi(x)$ also belongs to class H. In particular, the function

$$\phi_1(x) \equiv \frac{\mu\phi(x)}{\alpha} \qquad 4.19$$

where μ and α are constants.

We now proceed to show that non-linear function

$$\phi_2(x) = \tau_o \left\{\left(\frac{\phi(x)}{\alpha\gamma_o} + 1\right)^{n'} - 1\right\} \qquad 4.20$$

satisfies all the conditions of Lemma 4.2. Differentiating Eq. 4.20, we obtain,

$$\frac{d\phi_2(x)}{dx} = \frac{n'\tau_o}{\alpha\gamma_o}\left(\frac{\phi(x)}{\alpha\gamma_o} + 1\right)^{n'-1}\frac{d\phi(x)}{dx} \qquad 4.21$$

From the relationship 4.19 and noting that $\mu = \tau_o/\gamma_o$, the above equation can be used to obtain,

$$\frac{d\phi_2(x)/dx}{d\phi_1(x)/dx} = n'\left(\frac{\phi(x)}{\alpha\gamma_o} + 1\right)^{n'-1} \qquad 4.22$$

By definition, $0 < n' < 1$, and $\phi(x)$ is positive. Therefore, the right hand side of equation 4.22 is always positive. This immediately shows that $\phi_1'(x)$ and $\phi_2'(x)$ are of the same sign.

Rewriting equation 4.22,

$$\frac{\phi_2'(x)}{\phi_1'(x)} = \frac{n'}{\left(\frac{\phi(x)}{\alpha\gamma_0} + 1\right)^{1-n'}} \qquad 4.23$$

The numerator on the right hand side of equation 4.23 is less than unity but the denominator is always greater than unity as long as $\phi(x)/\alpha\gamma_0$ is positive. This is always the case. It therefore follows that,

$$\left| \phi_2'(x) \right| < \left| \phi_1'(x) \right| \qquad 4.24$$

In which case, we have shown that $\phi_2(x)$ is of class H for $|x|$ the interval $(c,a]$.

In the open interval $|x| < c$, $P(x)$ in equation 4.7 meets the Holder condition. In the open interval,

$$c < |x| \leq a,$$

$$P(x) = \tau^{\infty} - \tau_1(x) = \tau^{\infty} + \tau_0 - \phi_2(x), \qquad 4.25$$

using the notation in this section. It is clear that the Holder condition is also satisfied in the open interval $(c,a]$. In order to include the discontinuity at $x=c$, it is convenient to modify the function $P(x)$ slightly by approximating the step at $x=c$ by a linear function in the interval $[c-\delta, c+\delta+\epsilon]$ as shown in Fig. 4.1. In the limit

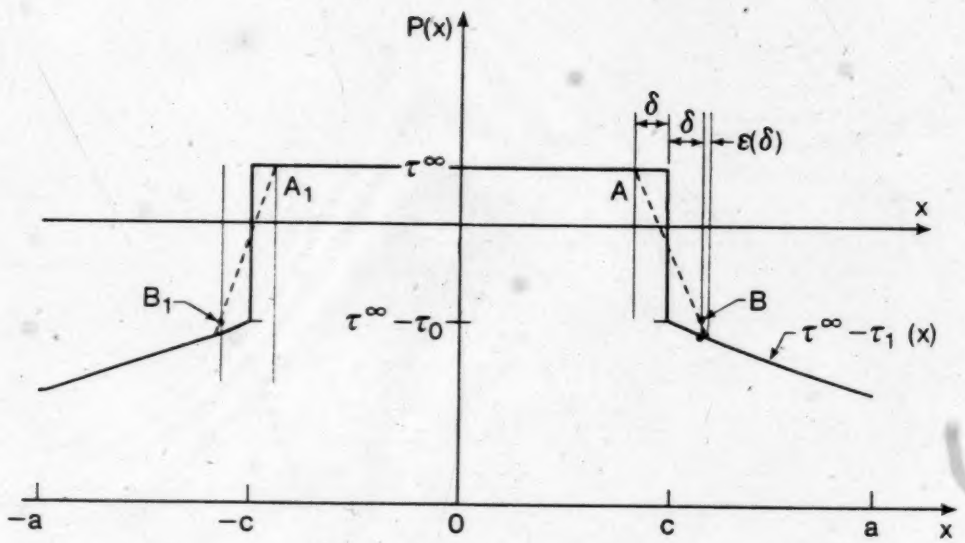

$A = (c-\delta, \tau^{\infty})$, $A_1 = (-c+\delta, \tau^{\infty})$

$B = (c+\delta, \tau^{\infty}-\tau_1)$, $B_1 = (-c-\delta, \tau^{\infty}-\tau_0)$

Figure 4.1 Holder condition for a step function

as $\delta \to 0$, the function $P_2(x)$ becomes identical with the function $P(x)$. Moreover, the inversion problem in question, using $P_2(x)$ converges to a solution equivalent to what would be obtained if $P(x)$ had been used in the first place. A justification for this is discussed in the rest of this section.

Consider the straight line AB (or A'B') in Fig. 4.1. It is convenient to divide the region $|x| \leq a$ into the following sub-intervals

$$
\begin{aligned}
&I_1; \quad |x| \leq c - \delta \\
&I_2; \quad c + \delta + \varepsilon \leq |x| < a \\
&I_3; \quad c - \delta \leq x \leq c + \delta + \varepsilon \\
&I_4; \quad c - \delta - \varepsilon \leq x \leq -\varepsilon - \delta
\end{aligned}
\tag{4.26}
$$

where the parameters δ and ε are as defined in the Figure. As a modification of the function $P(x)$, define $P_2(x)$, as

$$
P_2(x) = \begin{cases} P(x), & x \in I_1, I_2 \\ \tau^{\infty} - (\tau_0/2) - (|x| - c)\,\tau_0/2\delta, & x \in I_3, I_4 \end{cases}
\tag{4.27}
$$

Now, for any finite values of δ, and $\epsilon(\delta,n')$, $P_2(x)$ satisfies Holder condition in the entire range, $|x| < a$. Using $P_2(x)$ instead of $P(x)$ in 4.7, which can be inverted as in 4.23 to give:

$$f(x) = \frac{2(1-\upsilon)}{\pi\mu b} \int_{I_1 U I_2 U I_3 U I_4} R(x,y)\, P_2(y)dy$$

4.28

$$= \frac{2(1-\upsilon)}{\pi\mu b} \left\{ \int_{I_1 U I_2} R(x,y)\, P_2(y)dy + \int_{I_3 U I_4} R(x,y)\, P_2(y)dy \right\}$$

where

$$R(x,y) = \frac{1}{x-y} \sqrt{\frac{a^2 - x^2}{a^2 - y^2}}\,. \qquad 4.29$$

For any point $x \neq c$, however close to the crack-tip c, δ_o can be found satisfying:

$$\left| x-c \right| > 2(\delta_o + \epsilon(\delta_o,n')) > 2(\delta + \epsilon(\delta,n')) \qquad 4.30$$

near the crack-tip closer to the point x in question.

Given that $y \in I_3 U I_4$, then y satisfies,

$$\left| y-c \right| < \delta + \epsilon(\delta,n')\,. \qquad 4.31$$

Using 4.30 and 4.31, therefore, it follows that,

$$| x-y | = | x - c - (y-c) | > | x-c | - | y-c | > \delta + \varepsilon(\delta,n'). \qquad 4.32$$

In which case, the second term on the right hand side of equation 4.28 is free of singularity, for all values of δ satisfying 4.30. Moreover, from the construction in Fig. 4.1, it is clear that if δ approaches zero, $\varepsilon(\delta,n')$ will also approach zero. But the integral of any finite function vanishes as the domain of integration tends to zero. It follows therefore, that,

$$\lim_{\delta \to 0} P_2(x) = P(x) \qquad 4.33$$

and,

$$\lim_{\delta \to 0} \frac{2(1-\upsilon)}{\pi\mu b} \int_{I_1 \cup I_2 \cup I_3 \cup I_4} R(x,y)\, P_2(y)dy$$

$$= \frac{2(1-\upsilon)}{\pi\mu b} \int_{-a}^{a} R(x,y)\, P(y)dy \qquad 4.34$$

So that, even though P(x) does not satisfy the Holder conditions, a supplementary function $P_2(x)$ can be found belonging to the class H, which converges to the function P(x) in the limit as just described.

A similar argument was used by Swinden [55] for the simpler case when the value of P(x) is constant in the whole range with the exception of a step at the point x=c.

4.4 Displacement Integral Equations

Having established the conditions of validity of the inversion of Eq. 4.33, we proceed in this section to generate the integral equations for the plastic displacement function and the relevant boundary condition. The requirement that the dislocation density function f(x) be bounded at the end points ±a, similar to the condition in Eq. 2.19, is:

$$\int_{-a}^{a} \frac{F(x')dx'}{[(x'-a)(x'+a)]^{1/2}} = 0. \qquad 4.35$$

In the case of this non-linear hardening model, the relevant function F(x) is the function P(x) defined in 4.7. In which case, 4.35 becomes,

$$\int_{-a}^{-c} \frac{\tau^{\infty} - \tau_1(x')}{(a^2 - x'^2)^{1/2}} dx' + \int_{-c}^{c} \frac{\tau^{\infty} dx'}{(a^2 - x'^2)^{1/2}} + \int_{c}^{a} \frac{\tau^{\infty} - \tau_1(x')}{(a^2 - x'^2)^{1/2}} dx' = 0 \qquad 4.36$$

which after rearranging, and substituting from 4.6, becomes,

$$\int_{-c}^{c} \frac{\tau^{\infty} dx'}{(a^2 - x'^2)^{1/2}} + \left(\int_{-a}^{-c} + \int_{c}^{a}\right) \frac{\tau^{\infty} - \tau_0\left\{\frac{\phi(x')}{\alpha\gamma_0} + 1\right\}^{n'}}{(a^2 - x'^2)^{1/2}} dx' = 0 \qquad 4.37$$

Unfortunately, 4.37 does not lead to a closed form relationship between the applied loading, τ^{∞} and the extent of plasticity, a, like in 2.20. In the present case, the plastic displacement $\phi(x)$ at each position must be found, by integrating 4.15, before solving 4.37. The plastic displacement at any point x,

$$\phi(x) = b \int_{x}^{a} f(x')\, dx' \qquad 4.38$$

where a is the plastic zone extent closer to the point x. Substituting for f(x) from 4.15, we obtain,

$$\phi(x) = \frac{2(1-\upsilon)}{\pi\mu} \int_{-a}^{a} \int_{x}^{a} b\, R(x',y)\, P(y)\, dy\, dx'. \qquad 4.39$$

From equation 4.7, P(x) can be rewritten,

$$P(x) = \begin{cases} \tau^{\infty} & |x| < c \\ \tau^{\infty} - \tau_0\left\{\left(\frac{\phi(x)}{\alpha\gamma_0} + 1\right)^{n'} - 1\right\} & c < |x| < a \end{cases} \qquad 4.40$$

$$= P'(x) - P''(x) .$$

so that, 4.39 becomes,

$$\phi(x) = \frac{2(1-\nu)}{\pi\mu} \left[\int_{-a}^{a} \int_{x}^{a} bR(x',y)\, P'(y)\, dydx' \right.$$

$$\left. - \int_{-a}^{a} \int_{x}^{a} bR(x',y)\, \tau_o \left[\left(\frac{\phi(y)}{\alpha\gamma_o} + 1 \right)^{n'} - 1 \right] dydx' \right] \quad 4.41$$

Clearly, P' in the above equation is the same function as P(x) in equation 2.18. We can write, therefore,

$$\phi(x) = \phi_o(x) - B \int_{c}^{a} \tau_o \left\{ \left(\frac{\phi(y)}{\alpha\gamma_o} + 1 \right)^{n'} - 1 \right\} dy \int_{x}^{a} [R(x',y) + R(x', -y)]dx' \quad 4.42$$

where $B = 2(1 - \upsilon)\gamma_o/\pi$

Writing,

$$K(x,y) = \int_{x}^{a} [R(x';y) + R(x';-y)]dx', \quad 4.43$$

equation 4.42 becomes,

$$\phi(x) = \phi_o(x) - B \int_c^a \left[\left(\frac{\phi(y)}{\alpha \gamma_o} + 1 \right)^{n'} - 1 \right] K(x,y)\, dy \qquad 4.44$$

It can be shown (see appendix) that,

$$K(x,y) = \cosh^{-1} \left| \frac{a^2-x^2}{a(x-y)} + \frac{x}{a} \right| + \cosh^{-1} \left| \frac{a^2-x^2}{a(x+y)} + \frac{x}{a} \right| - 2 \sqrt{\frac{a^2-x^2}{a^2-y^2}} \qquad 4.45$$

and, $\phi_o(x)$ is given by,

$$\frac{1}{B} \phi_o(x) = (x+c) \cosh^{-1} \left| \frac{a^2-x^2}{a(x+c)} + \frac{x}{a} \right| - (x-c) \cosh^{-1} \left| \frac{a^2-x^2}{a(c-x} + \frac{x}{a} \right|$$

Equations 4.44 and 4.37 can be treated therefore as simultaneous integral equations in the two unknowns, $\phi(x)$, and a. In 4.37 the unknown quantity, a, appears as a limit in one of the integrals, as well as under the integral signs. There is no obvious analytical solution to these equations. The next section of this chapter deals with the procedure used in arriving at an optimal numerical solution.

4.5 Numerical Solution of the Work-Hardening Equations

(a) General Procedure

The displacement function has been expressed in the last subsection in the form of a Fredholm Integral Equation of the second kind (Eq. 4.44) and a boundary condition (also expressed as an integral), Eq. 4.37. The method chosen to solve this problem belongs to the general class called "expansion methods". As already discussed in chapter 2 (section 2.6), a more familiar procedure is the quadrature method, where the integral in the equation in question is changed, using standard quadrature formulae, to an algebraic expression in terms of specific values of the kernel function and the unknown function in question. This is basically an expansion method, but with the basis functions limited to the kernel of the integral equation. Since the kernel function in Eq. 4.44 is singular, it is found desirable that there be freedom to choose basis functions other than the kernel function itself.

In general, we can choose to represent the unknown function $\phi(x)$ in 4.44 as a linear combination of certain prescribed functions, thus:

$$\phi(x) = \sum_{i=0}^{n} \alpha_i \phi_i(x), \qquad 4.46$$

the α_i's are the parameters to be estimated and n is the number of basis functions. It is usual to choose for the α_i's, functions that are independent of any unknown

parameters. Polynomials in x are common examples. If the friction stress is, for instance, as given in Eq. 4.3, then 4.44 will be linear. In this case, the choice of polynomials, or other functions independent of the α_i's in Eq. 4.46 will lead to a set of linear equations, which can be solved by standard matrix methods. However, when the friction stress is non-linear (Eq. 4.6), choice of α_i's independent of unknown parameters will still not give linearity. In this case, the choice of non-linear combinations of functions of the form,

$$\phi(x) = \sum_{i=1}^{n} \alpha_i \phi_i(\underline{\alpha}, x), \qquad 4.47$$

where $\underline{\alpha}$ is the vector $\{\alpha_i\}$, and the ϕ_i's are arbitrary functions, does not necessarily lead to greater complications because the resulting equations will always be non-linear anyway. In the next subsection, methods of singularity removal including the use of the basis functions to eliminate the kernel singularity, will be treated.

(b) Singularity Removal Method

In the case of linear hardening, n'=1 the friction stress has the form of Eq. 4.3. The simplest set of basis functions are polynomials. If the functions ϕ_i's in Eq. 4.46 are polynomials or any elementary functions, we can choose a vector x_j, j = 1, . . ., m, where x_j is any point in the domain [c,a]. A substitution in the equation 4.44

results in the m equations:

$$\eta_j \equiv \eta(x_j) \equiv \phi(x_j) - \phi_o(x_j) + B \int_c^a \frac{\mu\phi(y)}{\alpha} K(x_j,y)dy, \qquad 4.48$$

where $\phi(x_j) = \sum_{i=1}^{n} \alpha_i \phi_i(x_j)$

$$\phi(y)K(x_j,y) = \sum_{i=1}^{n} \alpha_i \phi_i(y)K(x_j,y) \quad , \qquad j=1, \ldots, m \qquad 4.49$$

and, η_j is the residual at the point x.

As long as the function ϕ_i's do not involve the parameters α_i, Eq. 4.48 is linear. The solution method used depends on the choice of the number of points, m. For a unique solution to exist

$$m>n \qquad 4.50$$

When m=n, there is the same number of solutions and unknowns. An attempt can be made to solve the linear algebraic equations,

$$\eta_j = 0, \quad j=1, \ldots, n \qquad 4.51$$

The condition for existence of a solution to Eq. 4.51 is that the matrix whose i,j^{th} term, A_{ij} is defined by,

$$A_{ij} = \phi_i(x_j) + B \int_c^a \frac{\mu}{\alpha} \phi_i(y) K(x_j, y) dy \qquad 4.52$$

has a unique inverse.

Within the range [c,a] of the integral on the RHS of Eq. 4.52, there are singularities at points x=y, and y=a. One method available for removing the latter singularity is to choose the functions ϕ_i's that satisfy:

$$\phi_i(x) = (a^2 - x^2)^t \xi_i(x), \quad t \geq 3/2 \qquad 4.53$$

provided that $\xi_i(x)$ is bounded, and has bounded derivatives in the domain [c,a]. It can be shown then that,

$$\lim_{y \to a} \phi_i(y) K(x_i, y) \qquad 4.54$$

exists. The other kernel singularity, x=y, is an integrable one. The following procedure was used in integrating around it.

Consider the function F(y), and let K(x,y) have a singularity at x=y in the integral,

$$\int_c^a F(y)\,K(x,y)\,dy = \int_c^a \Big[F(y) - F(x)\Big]K(x,y)dy + F(x)\int_c^a K(x,y)dy \qquad 4.55$$

as $x \to y$, $K(x,y) \to \infty$. But the quantity $F(y)-F(x)$ approaches zero. The first term in the expression in 4.55 vanishes in the limit, otherwise, the integral does not exist [56]. At the same time, if $K(x,y)$ has a closed form integral, as it indeed does in this case, then the expression 4.55 can be evaluated by standard procedures. This way, the second kernel singularity can be avoided.

In the general case, $n' \neq 0,1$, in place of Eq. 4.48, we have;

$$\eta_j = \phi(x_j) - \phi_o(x_j) + B\tau_o \int_c^a \{(\frac{\phi(y)}{\alpha\gamma_o} + 1)^{n'} - 1\}K(x_j,y)dy \qquad 4.56$$

that is,

$$\eta_j = \sum_{i=1}^{n} \alpha_i\phi_i(\underline{\alpha},x_j) - \phi_o(x_j) + B\tau_o \int_c^a \{(\frac{\sum_{i=1}^{n} \alpha_i\phi_i(\underline{\alpha},y)}{\alpha\gamma_o} + 1)^{n'} - 1\}\,K(x_j,y)dy \qquad 4.57$$

so that the functions η_j's are non-linear in the unknown parameters. There is, therefore, no obvious advantage in choosing $\varphi(x)$ as a linear combination of functions. We

return to this point later, but now, we can discuss the problem of singularity removal due to the nonlinearity.

The singularity at $x_i=y$ can still be removed as demonstrated in Eq. 4.55. However, functions satisfying the condition in Eq. 4.53 are no longer guaranteed to ameliorate the singularity at y=a. Since the latter is at a fixed point, at the end of the domain of integration, it is found convenient to avoid the point y=a by selecting the points x_j in the open interval [c,a). That is, we go as near to a as we may desire, but avoid using the point $x_j=a$ itself.

(c) Numerical Solution

The following perturbation of the elastic-perfectly plastic solution (Eq. 2.22),

$$\phi(x) = \alpha_1(x+c)\cosh^{-1}\left[(1+|\alpha_2|)\left|\frac{a^2-x^2}{a(c+x)}+\frac{x}{a}\right|\right] - \alpha_3(x-c)\cosh^{-1}\left[(1+|\alpha_4|)\left|\frac{a^2-x^2}{a(c-x)}+\frac{x}{a}\right|\right] + \alpha_5 e^{-\alpha_6(x/a)} + \alpha_7 e^{-\alpha_8(x^2/a^2)} \qquad 4.58$$

with an exponential and Gaussian background (the last two terms respectively) is used as the approximation function. Since there are eight unknown parameters, in principle, only eight equations are needed to evaluate them. However, it was found more accurate to choose more points x_j than

eight, so that the resulting set of equations (of the type of Eq. 4.57) becomes a set of overdetermined non-linear equations. This approach is chosen because, in this way, accuracy of the procedure can be improved by choosing more points provided the point $x_j=a$ and the other singularity ($x_j=y$) in Eq. 4.57 are avoided as already described. In the calculations presented in this chapter, twenty equally spaced points were chosen, and the resulting equations were solved via a non-linear least squares method. The sum of square residuals,

$$\sum_{j=1}^{20} \eta_j^2 \qquad 4.59$$

was minimized using the IMSL [57] subroutine based on a derivative-free optimization method for non-linear least squares. The method used there is based on the Levenberg-Marquardt algorithm. The optimization routine does not require the computation of gradient vector or the Hessian matrix. One only needs to supply an initial estimate of the vector $\{\alpha_i\}$. The initial estimate used was (1,0,1,0,0,1,0,1). Using this vector in Eq. 4.58, the initial estimate corresponds to the elastic-perfectly plastic solution (Eq. 2.22). The boundary conditions 4.37 was included in this way: starting from a reasonable initial estimate a_0 of the parameter a, for any value a_k, the residual at the k^{th} iteration,

$$r_k = \int_{-c}^{c} \frac{\tau^{\infty}\, dx'}{(a_k^2 - x'^2)^{1/2}} + \left(\int_{-a_k}^{-c} + \int_{c}^{a_k} \right) \frac{\tau^{\infty} - \tau_0 \left\{ \frac{\phi(x')}{\alpha \gamma_0} + 1 \right\}^{n'}}{(a_k^2 - x'^2)^{1/2}} \qquad 4.60$$

is found, using the value of the vector $\{\alpha_i\}_k$ corresponding to this optimization. It turns out that the choice of a_0, close to the elastic-perfectly plastic value (Eq. 2.20), gives r_k close to zero. By using different values of a_k in an iterative scheme, the magnitude of r_k can be made as small as possible, giving a good estimate of a. Another way to solve this problem is to solve the integral equation 4.37 directly for each optimal value of the vector $\{\alpha_i\}_k$. However, the computational requirement for this solution make it unattractive.

Apart from converging to an optimal (minimal) value of the sum in 4.59, the final solution is tested at each optimization point. When the residuals, N_j's are of a lower order of magnitude than the function, $\sum_{i=1}^{n} \alpha_i \phi_i(\underline{\alpha}, x_j)$ the vector $\{\alpha_i\}_k$ is taken as a sufficiently close estimate of the unknown parameter vector. Various values of the hardening exponent were considered in the range $0 \leq n' \leq 0.2$. The iterative method described here converged in all cases for applied stress values up to $0.6\tau_0$. For values of the hardening exponent higher than this range, and/or higher values of the applied loading, the convergence rate is slow, and both the sum of squares errors as well as the individual errors become large. In

some cases, the latter has a magnitude comparable to the estimated displacement function.

The optimal vector $\{\alpha_i\}$ obtained by the method described can then be substituted in Eq. 4.58 to obtain the plastic displacement $\phi(x)$ as a function of distance from the crack centre. The stress distribution, $\tau_1(x)$ can be obtained from $\phi(x)$ using Eq. 4.6. Another important quantity to be evaluated is the J-integral. By definition,

$$J = \int_{\Gamma} W dy - T_m \frac{\partial u_m}{\partial x} ds \qquad 4.61$$

where Γ is a suitable integration path around the crack-tip plastic zone, u_m is the displacement vector,

$W = \int_0^{\varepsilon_{k\ell}} \sigma_{k\ell} \, d\varepsilon_{k\ell}$ the strain energy density,

and, T_m is the traction vector.

In the dislocation model, the simplest path of integration is the upper and lower surfaces of the plastic zone. Along the plastic line, dy=0, so that the first term in the integral (Eq. 4.61) vanishes. Also, ds=dx.

Equations 4.6 and 4.61 lead to:

$$J = -\int_c^a \tau_1(x) \frac{d\phi(x)}{dx} dx \qquad 4.62$$

Since $\phi(x)$ is the relative plastic displacement at point x

between the two surfaces constituting the integration path Γ, so that,

$$J = -\tau_0 \int_c^a \left\{\frac{\phi(x)}{\alpha\gamma_0} + 1\right\}^{n'} d\phi(x) \qquad 4.63$$

and, now, $\phi(x)$ can be obtained from Eq. 4.58.

4.6 Results and Discussion

In the range of applied loading $0 \leq \tau^{\infty} \leq 0.6\tau_0$, the plastic displacement $\phi(c)$ at the crack-tip varied widely. In Table 4.1, the spread of values can be seen to span over two orders of magnitude. A linear plot of these values will give the impression that there is no change in displacement over the range of values between $0.0 < \tau^{\infty} < 0.4\tau_0$. These values are therefore plotted on a logarithmic scale as shown in Fig. 4.2. Here, the displacement is made dimensionless by dividing it by the quantity $\alpha\gamma_0$. As expected, the displacement increases rapidly with the applied far field loading. There is a reduction in the crack-tip displacement when the hardening exponent n' is increased. Even though this has been attenuated by the logarithmic plot, the trend is consistent with expectations.

Figure 4.3 depicts the variation in the dimensionless crack-tip stress, $\tau_1(x)/\tau_0$ with the applied loading, for

Table 4.1 Variation in crack-tip displacement due to external loading and hardening

τ/τ_0	n' = 0.0005	0.05	0.10	0.125	0.1667	0.200
.0500	0.13759	0.13751	0.13747	0.13742	0.13738	0.13731
.1000	0.55205	0.55097	0.55041	0.54976	0.54911	0.54794
.1500	1.24862	1.24416	1.24157	1.23849	1.23524	1.22936
.2000	2.23626	2.22460	2.21712	2.20681	2.19688	2.18022
.2500	3.52823	3.50389	3.48509	3.46564	3.44544	3.40970
.3000	5.14275	5.09540	5.06532	5.02979	4.99235	4.92473
.3500	7.10415	7.02624	6.97635	6.91611	6.85170	6.73366
.4000	9.44450	9.32203	9.24248	9.14461	8.98563	8.71281
.4500	12.20600	12.01720	11.85480	11.66790	11.40470	11.03870
.5000	15.44440	15.11890	14.89110	14.59560	14.19540	13.36660
.5500	19.23480	18.72250	18.35800	17.88660	17.33220	16.22549
.6000	23.68040	22.87650	22.30840	21.49730	20.47749	20.37900

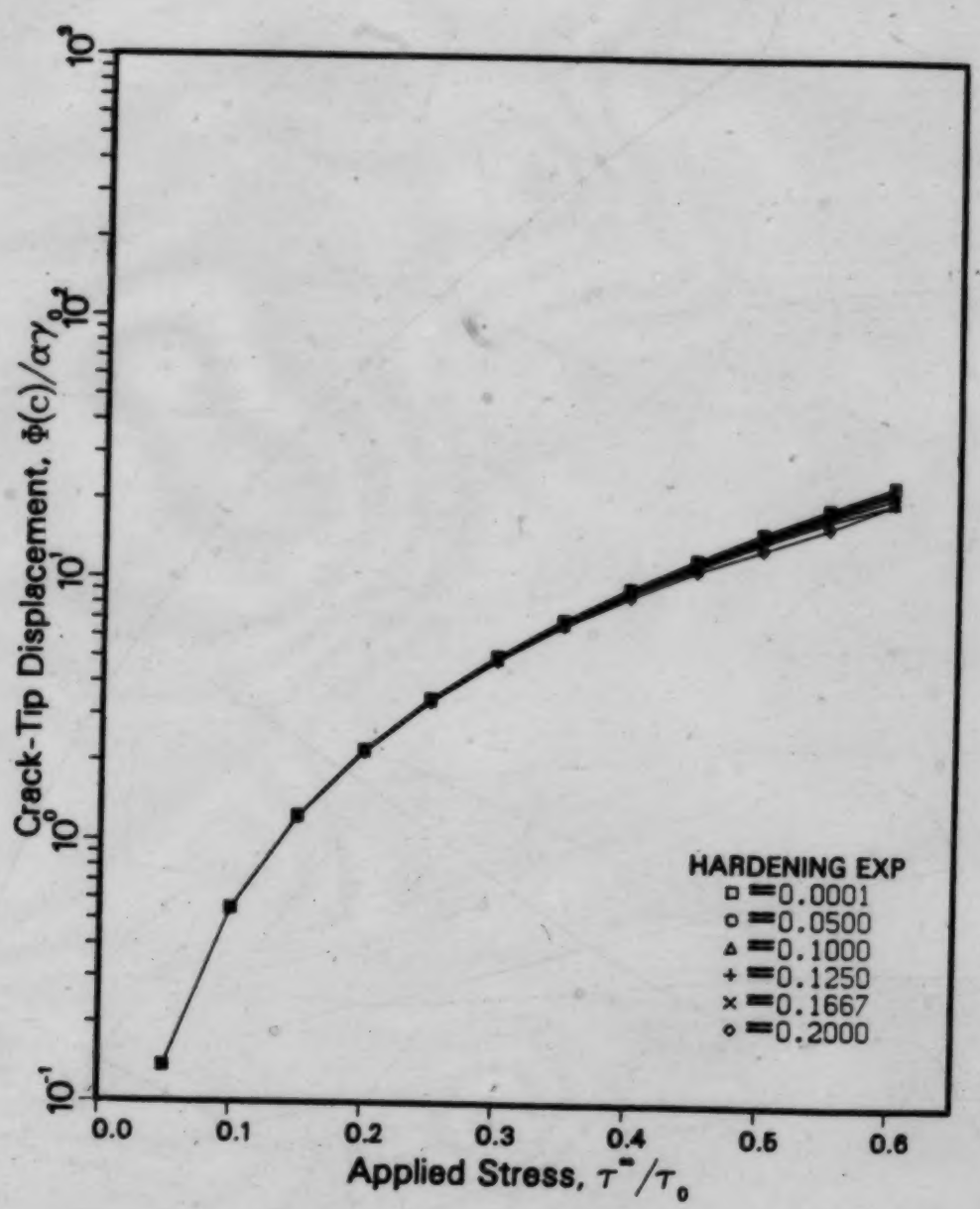

Figure 4.2 The effect of hardening on crack-tip displacement

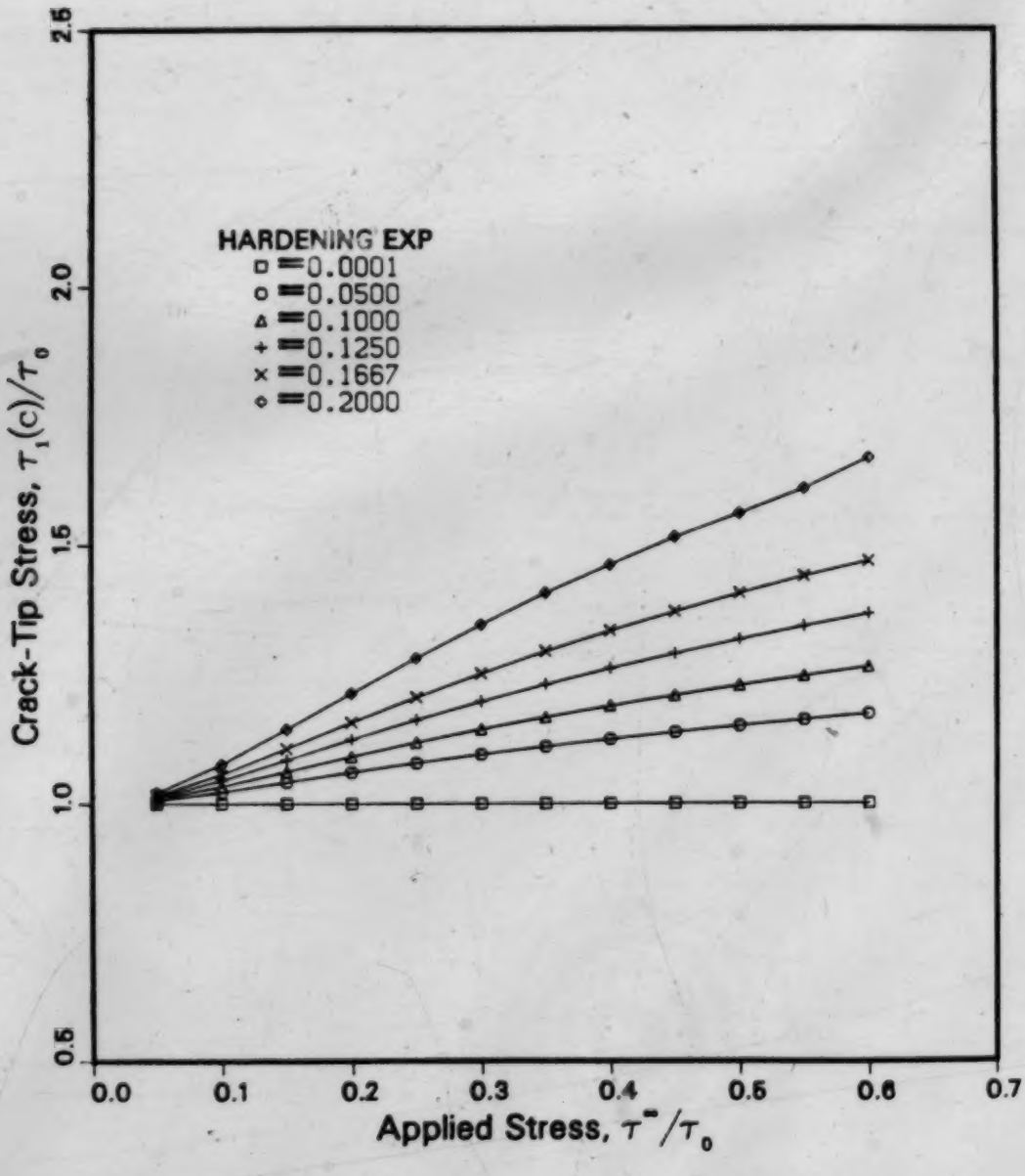

Figure 4.3 The effect of hardening on crack-tip stress

the various values of the hardening exponent. The trend here, as expected, is that the crack-tip stress increases with the applied loading. For a fixed amount of the far-field loading, it is also evident that the crack-tip stress increases with the amount of work-hardening.

Using the crack-tip displacement as a criterion for plastic damage at the crack-tip, the result would indicate that work-hardening reduces the plastic damage. The exactly opposite conclusion might be reached using the crack-tip stress. In Fig. 4.4, another quantity, the strain energy density at the crack-tip, based on both displacement and stresses, is plotted. From this Figure, it is clear that the strain energy density increases with both applied stress and the extent of work-hardening in the material depicted by n'.

In all the quantities considered so far, the value at a given point, (in this case, the crack-tip) was considered. In order to demonstrate the variation in the plastic damage with either applied stress or work-hardening, it is necessary to choose a parameter that is defined for the whole plastic zone. Such a parameter is the J-integral. Earlier investigators have related this to the strain energy density. This can be done here, using Eq. 4.63. In general, there is no closed form solution to the displacement function $\phi(x)$. A numerical integration of Eq. 4.63 enables us to calculate the J-integral for various values of n'. This can also be made dimensionless

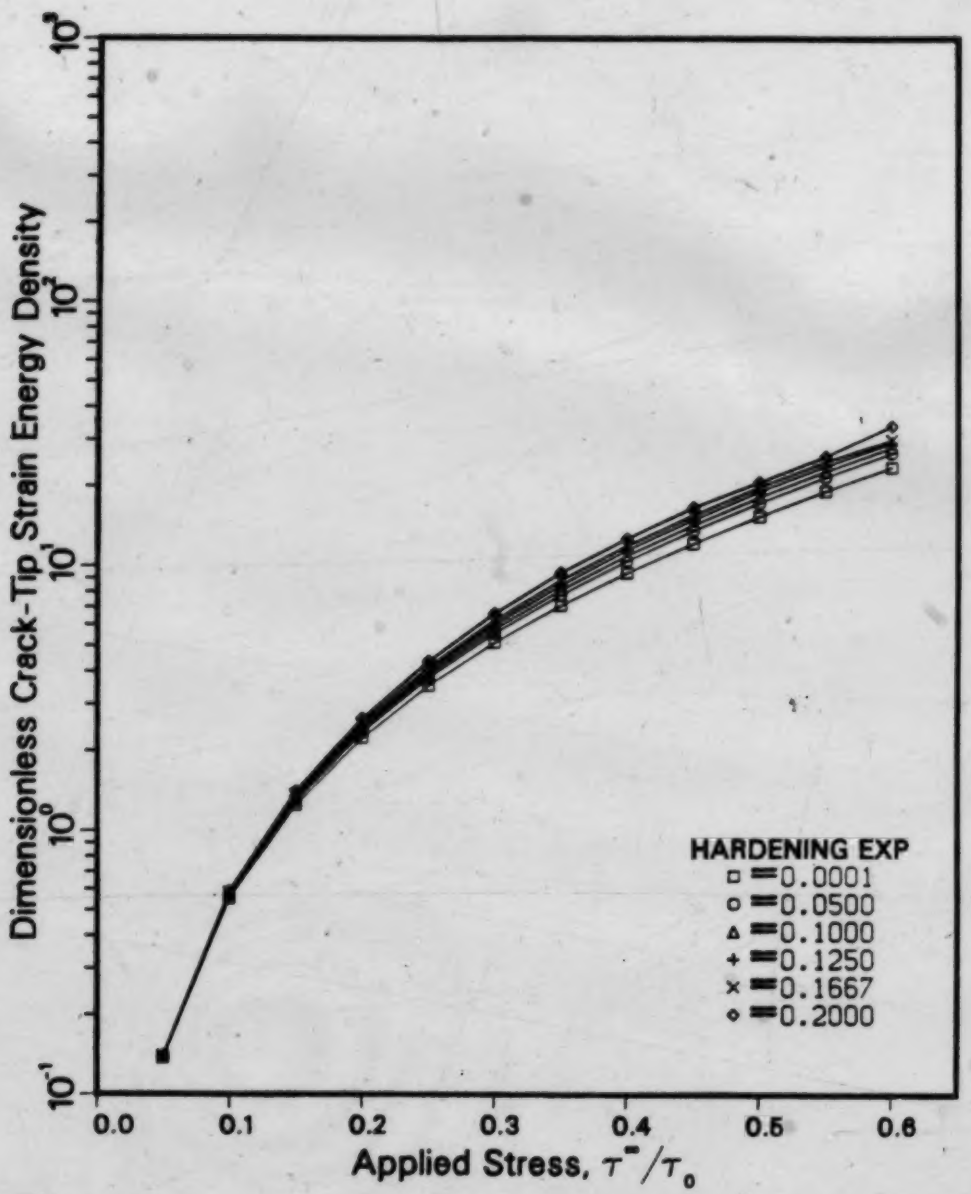

Figure 4.4 The effect of hardening on crack-tip strain energy density

by dividing by the quantity, $\alpha\gamma_0\tau_0$. The dimensionless J-integral is plotted against the applied far field, dimensionless strain energy density as shown in Fig. 4.5. The linearity of the curves shows that there is a power law relationship of the type,

$$J = C(W^{\infty})^m \qquad 4.64$$

where C and m are dependent on both the applied loading, and the hardening exponent.

A special case exists in Eq. 4.64. When n'=0, Eq. 4.63 can be integrated analytically. In this case,

$$J = -\tau_0 \int_c^a d\,\phi(x) = \tau_0\,\phi(c), \qquad 4.65$$

since $\phi(a)=0$.

Using the vector (1,0,1,0,0,1,0,1) for $\{\alpha_i\}$ in Eq. 4.58,

$$\begin{aligned}\phi(c) &= 2Bc\,\ell n(a/c)\\ &= 2Bc\,\ell n\left\{\sec\frac{\pi\tau^{\infty}}{2\tau_0}\right\}\\ &= 2\,Bc\left[\frac{\pi^2}{8}\left(\frac{\tau^{\infty}}{\tau_0}\right)^2\left\{1-\frac{\pi^2}{16}\left(\frac{\tau^{\infty}}{\tau_0}\right)^2\right\}\right]\end{aligned} \qquad 4.66$$

In the last expression, the first two terms of the

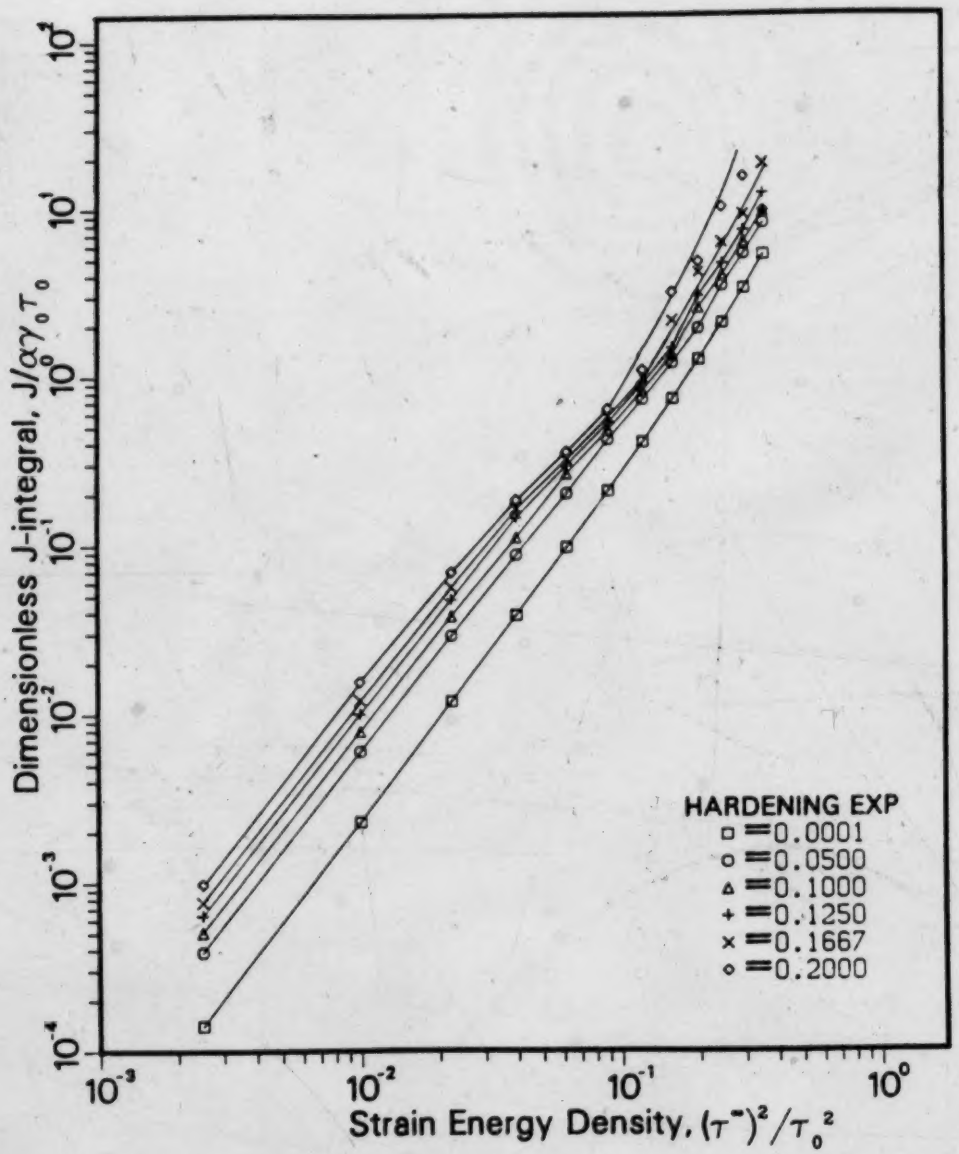

Figure 4.5 The effect of hardening on the J-integral

Taylor's series expansion have been taken.

Substituting Eq. 4.66 in 4.65,

$$J = (1 - \nu)\pi\, c \left[1 - \frac{\pi^2}{16}\left(\frac{\tau^\infty}{\tau_o}\right)^2\right] W^\infty \qquad 4.67$$

where writing $W = (\tau^\infty)^2/2\mu$, is substituted for the far field strain energy density.

Note that, in Eq. 4.67, if $\tau^\infty << \tau_o$, i.e., for small scale yielding,

$$J = (1 - \nu)\pi c\, W^\infty \qquad 4.68$$

In which case, J is linearly related to W^∞.

4.7 Comparison With Continuum Models

The original elastic-perfectly plastic model of BCS has been shown to compare favorably with the continuum based model of Hult and McClintock [17,29]. This comparison was made on the basis of the extent of the plastic zone only. Analytical results [19] and, more recently, experimental results [59,60] are available in the literature for comparison with the elastic-nonlinear hardening model presented here. Figures 4.6 to 4.15 are the comparisons of the predicted crack-line strain, stress and Strain Energy Density compared with the continuuum model of Rice [19]. As these Figures show, there is considerable disparity between the two predictions in the

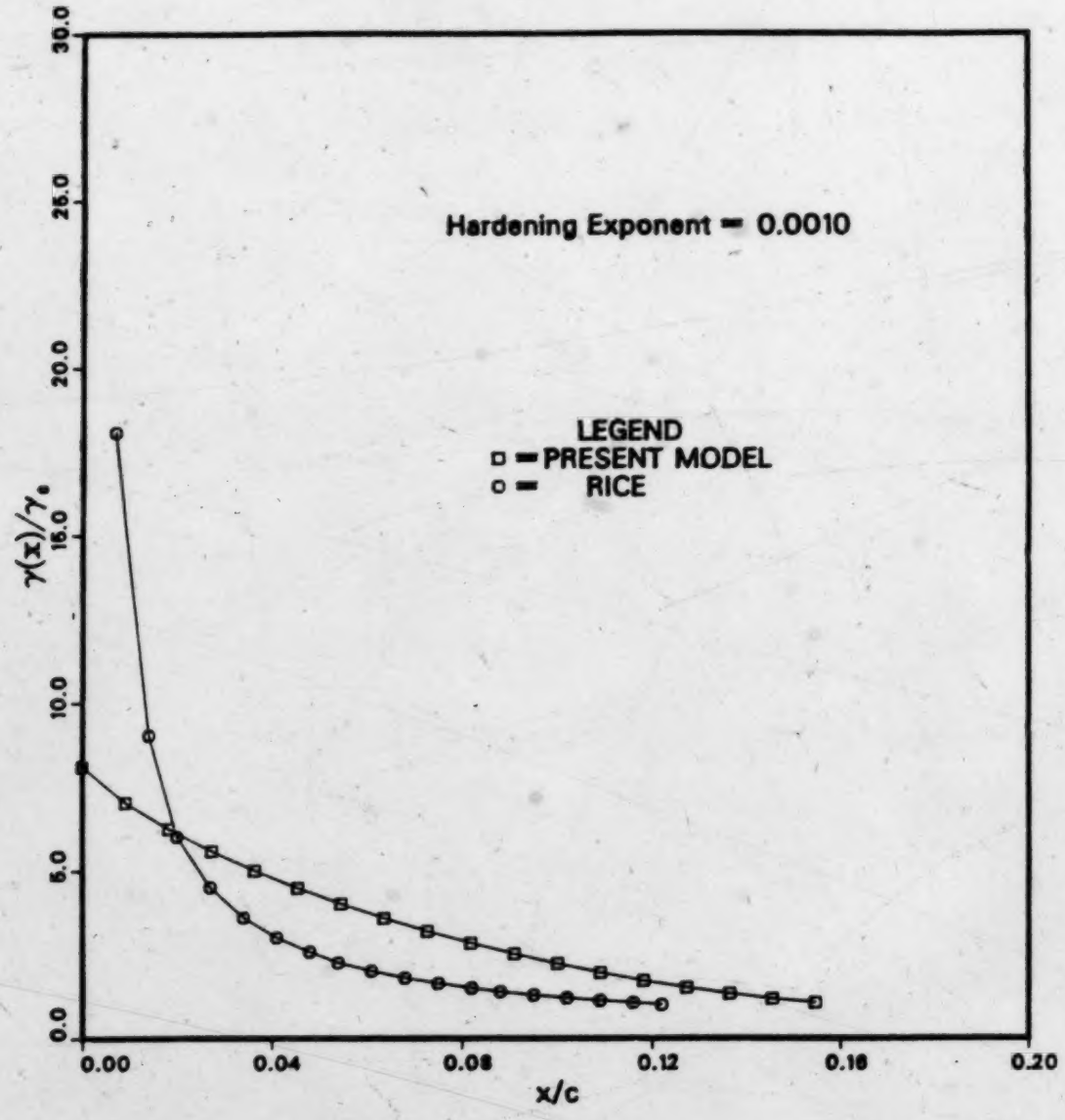

Figure 4.6 Crack-line strain comparison (negligible hardening)

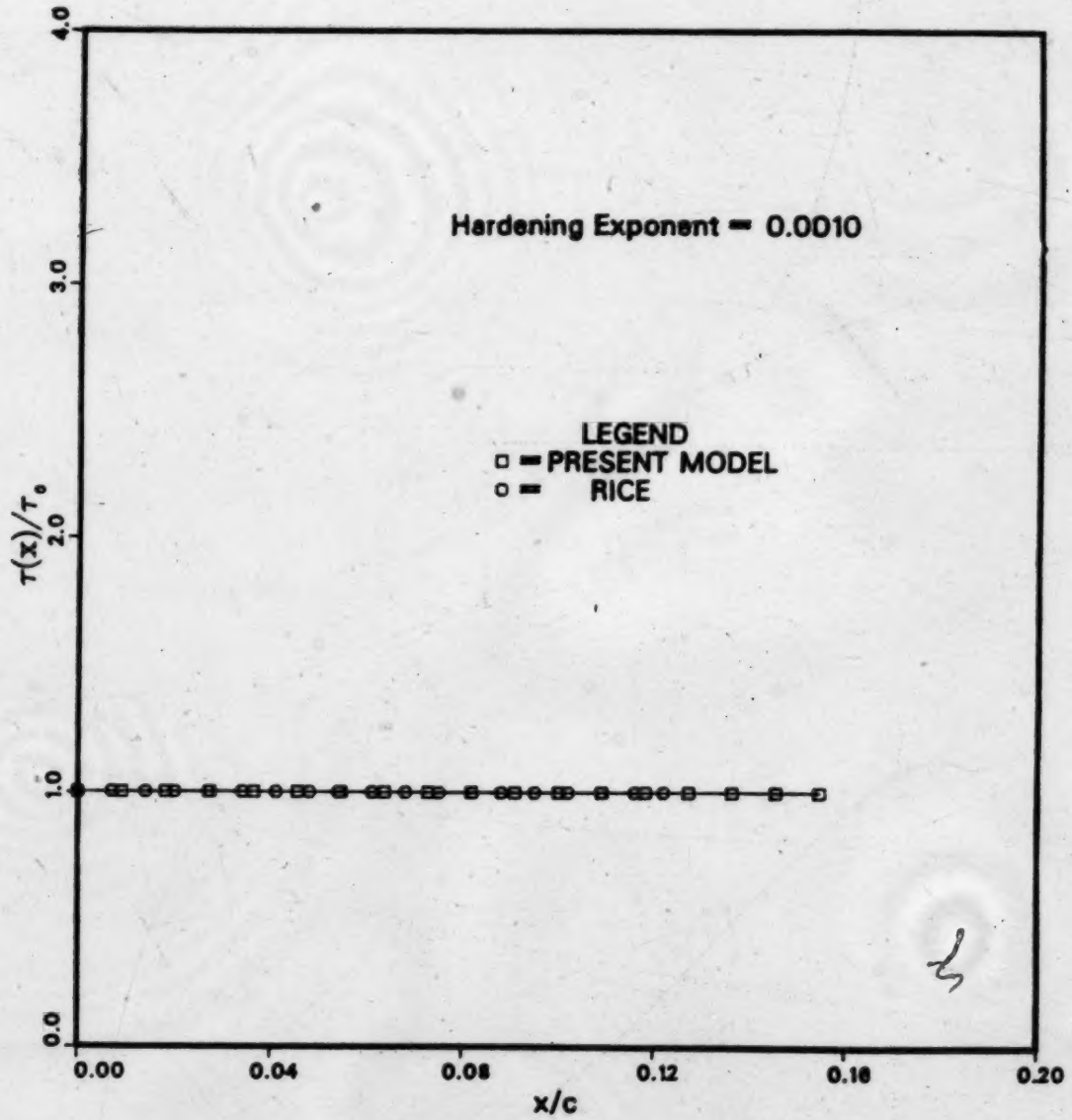

Figure 4.7 Crack-line stress comparison (negligible hardening)

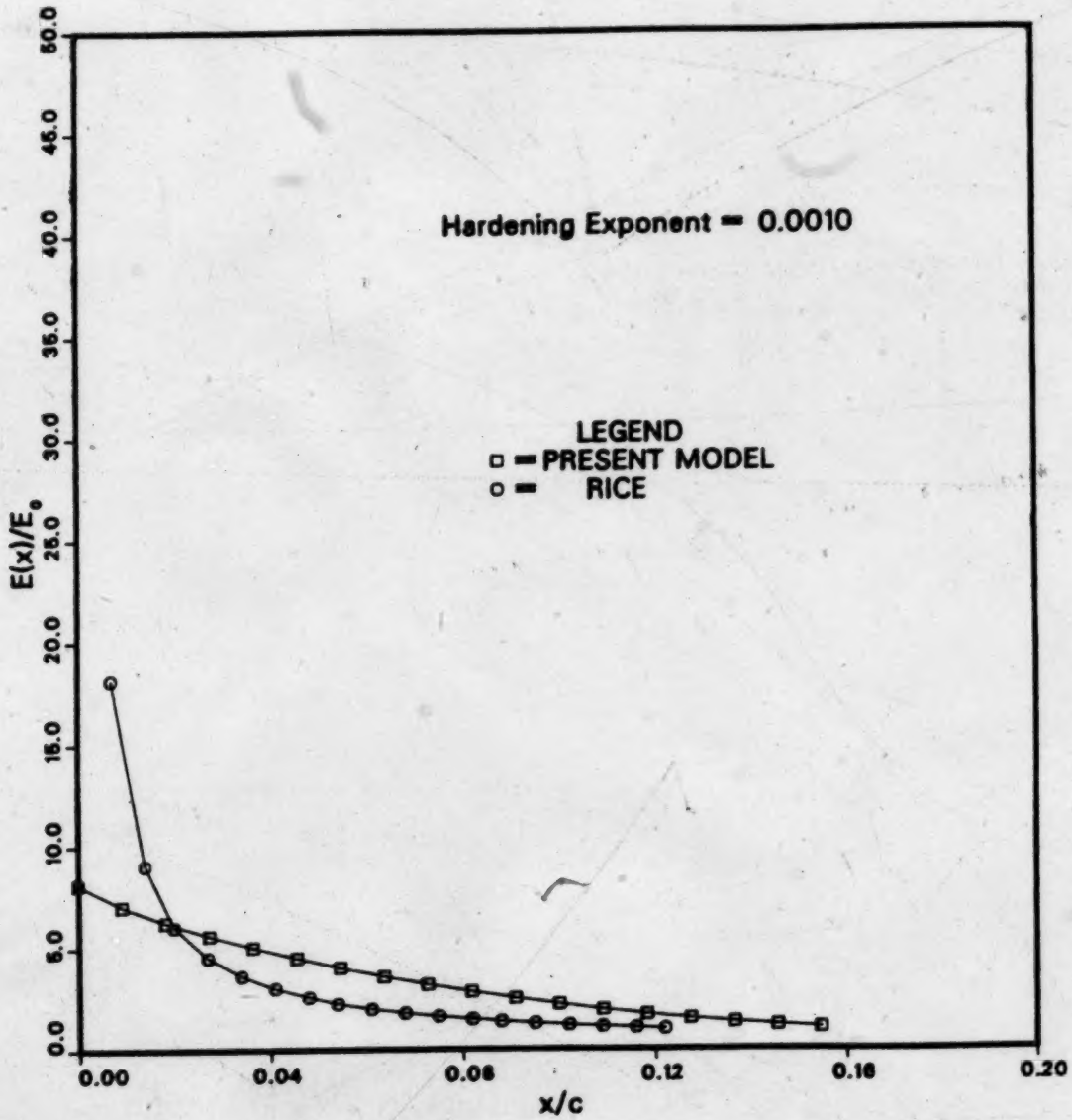

Figure 4.8 Crack-line strain energy density comparison (negligible hardening)

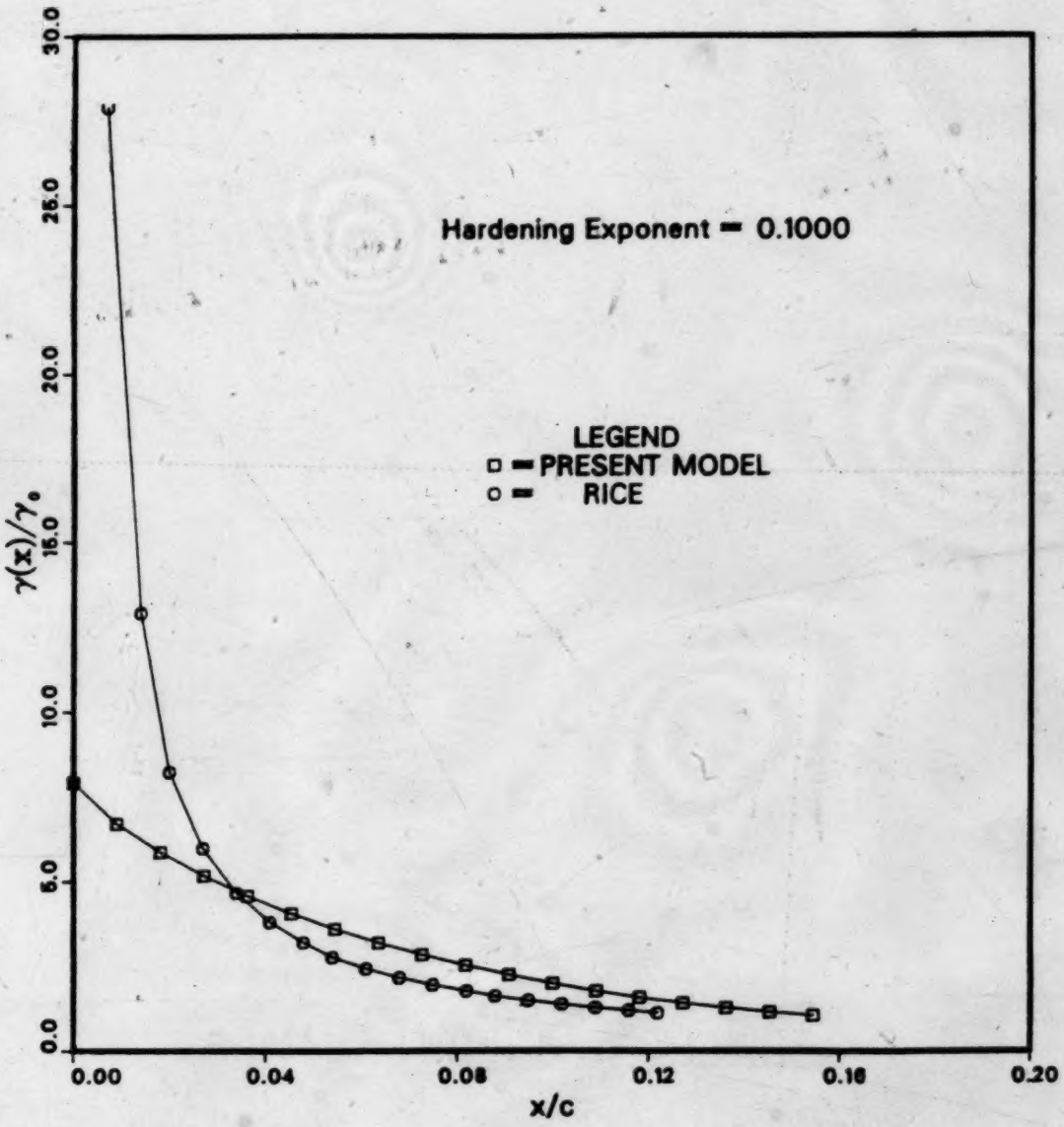

Figure 4.9 Crack-line strain comparison (mild hardening)

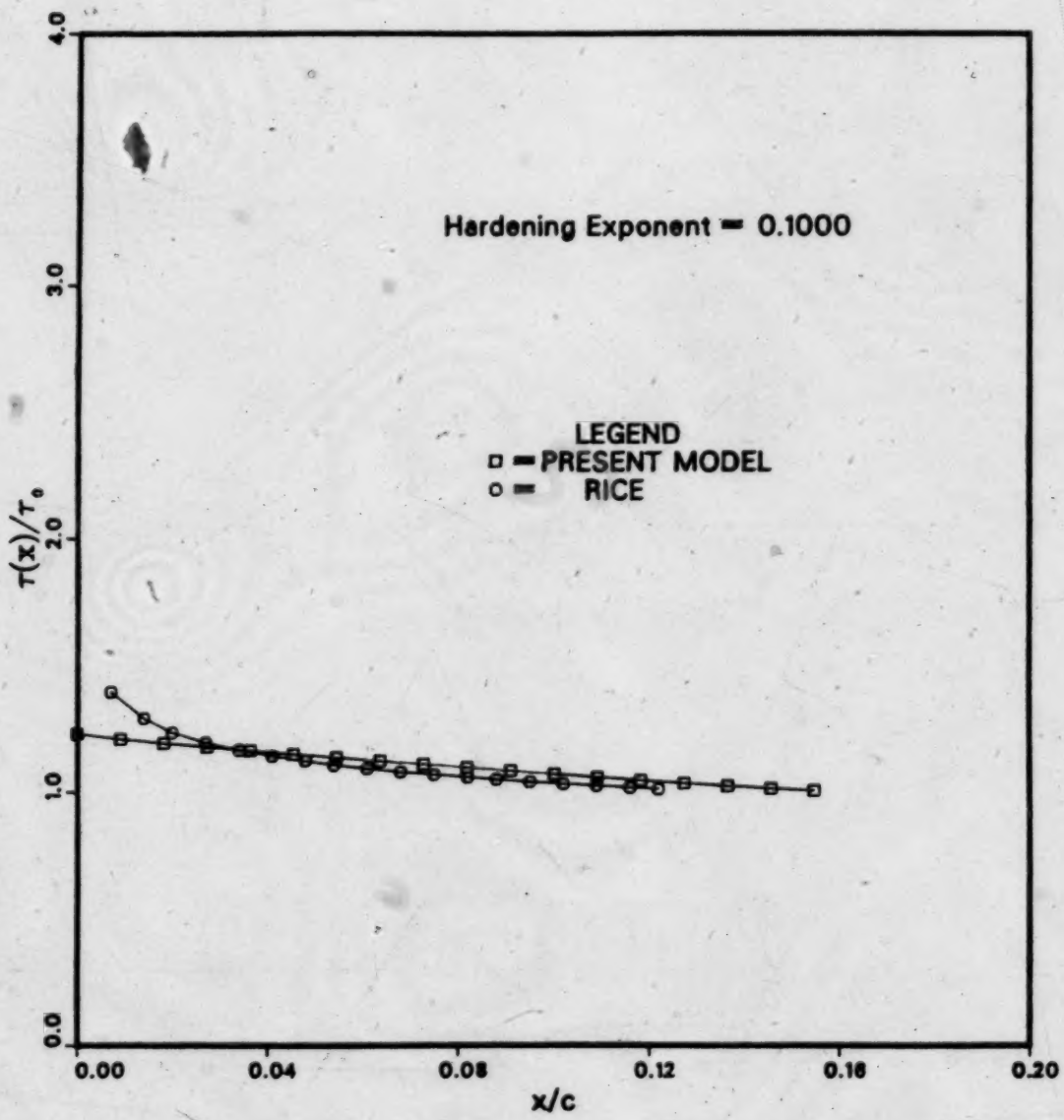

Figure 4.10 Crack-line stress comparison (mild hardening)

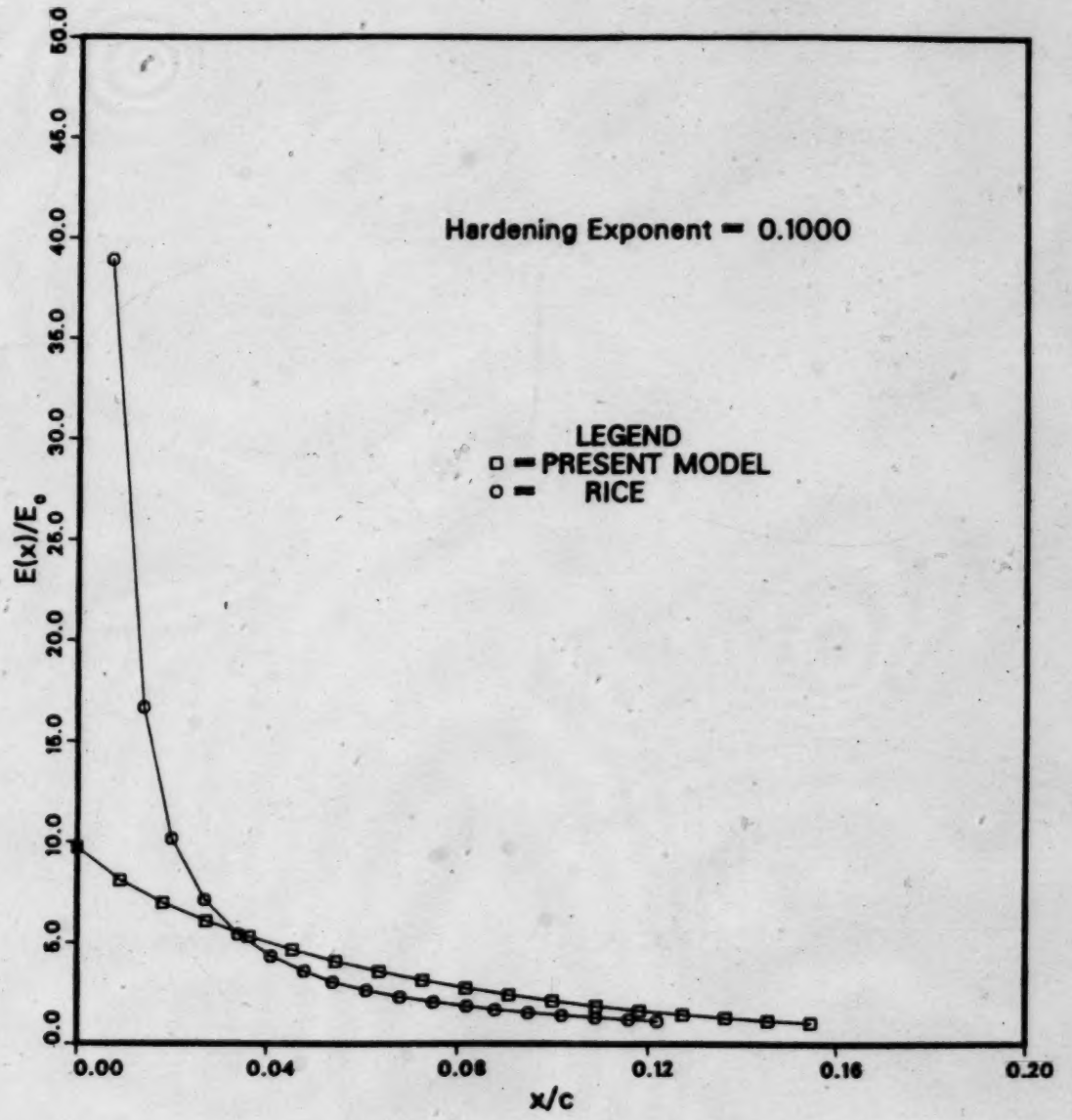

Figure 4.11 Crack-line strain energy density comparison (mild hardening)

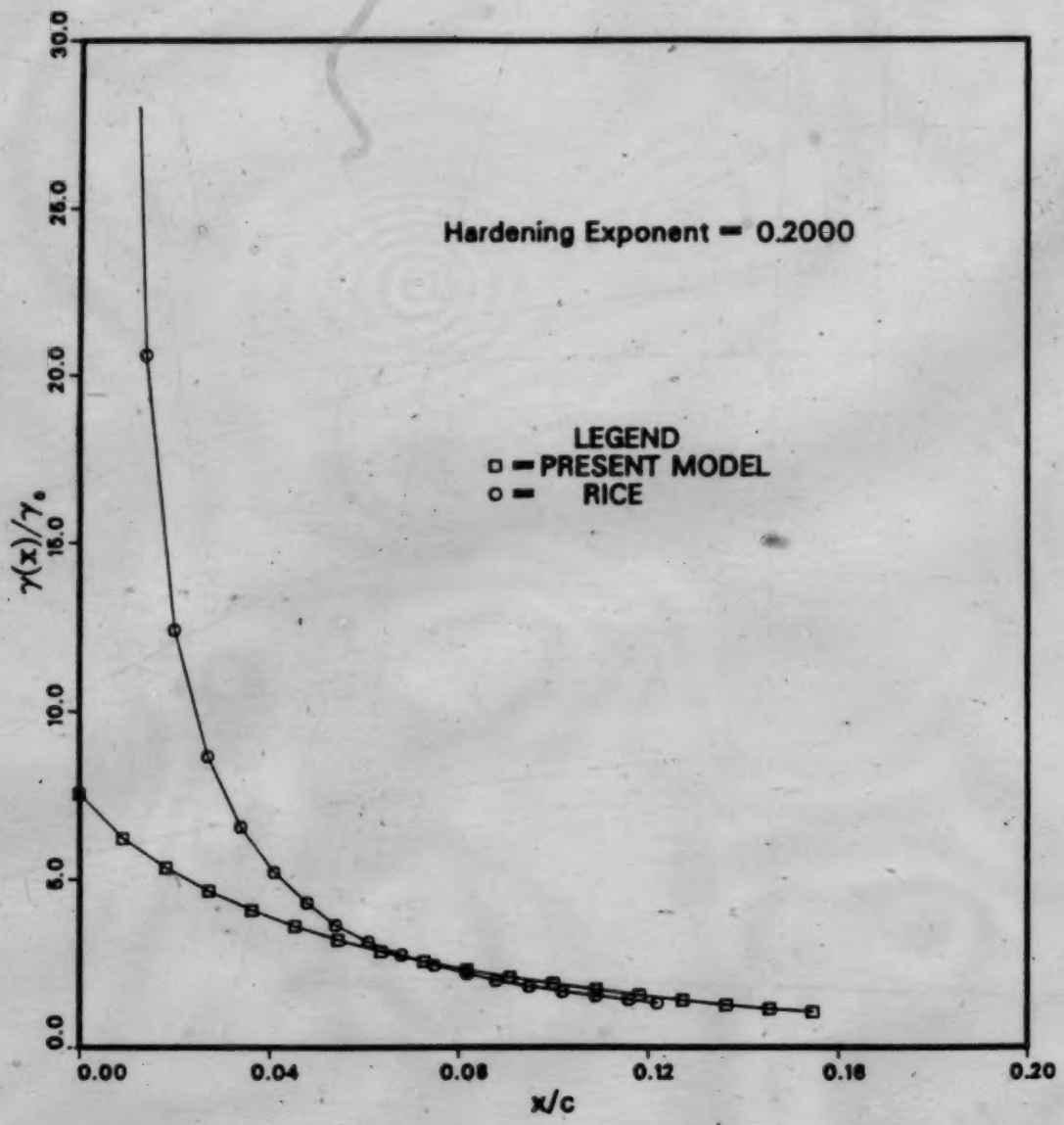

Figure 4.12 Crack-line strain comparison (hign hardening)

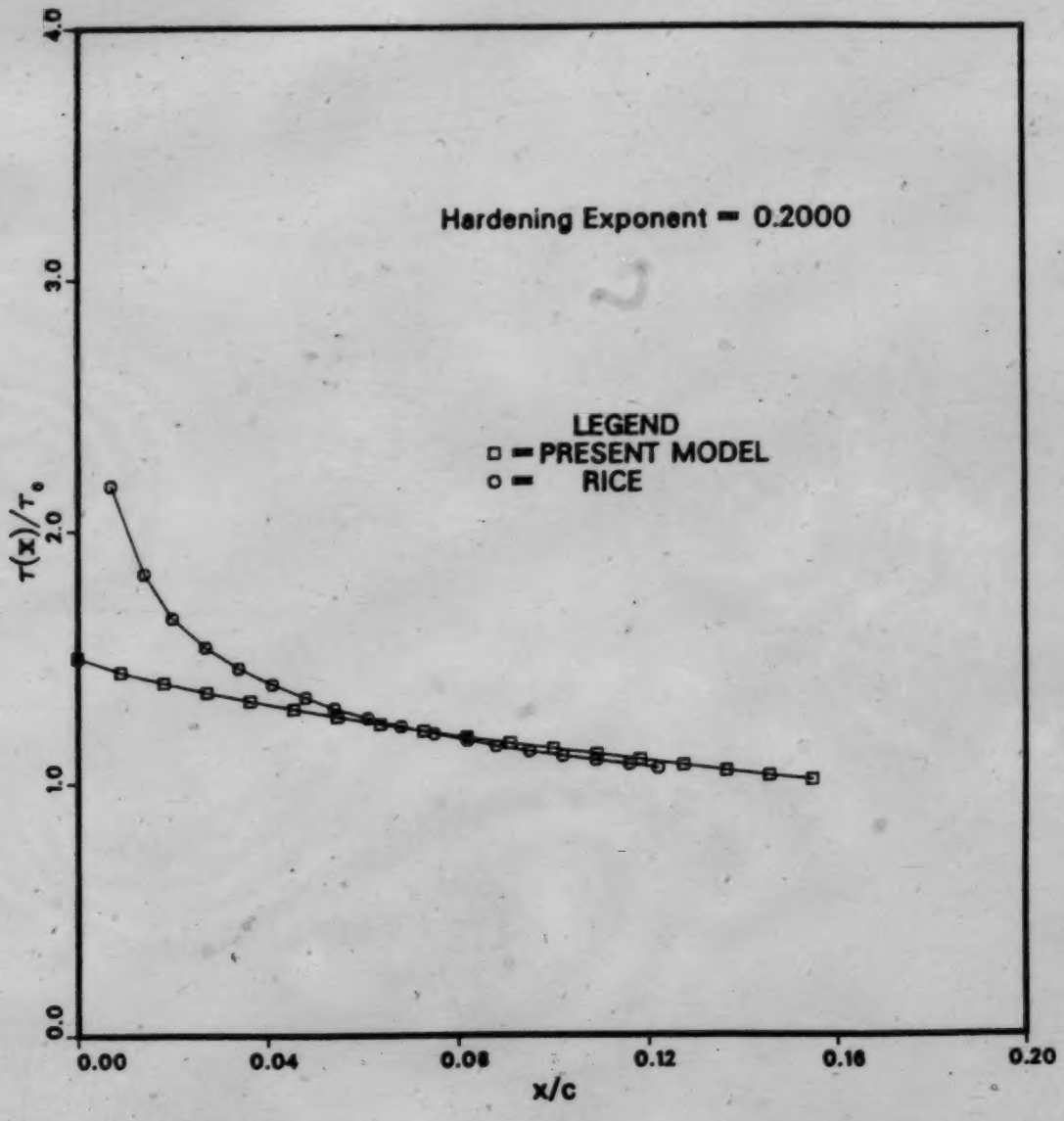

Figure 4.13 Crack-line stress comparison (high hardening)

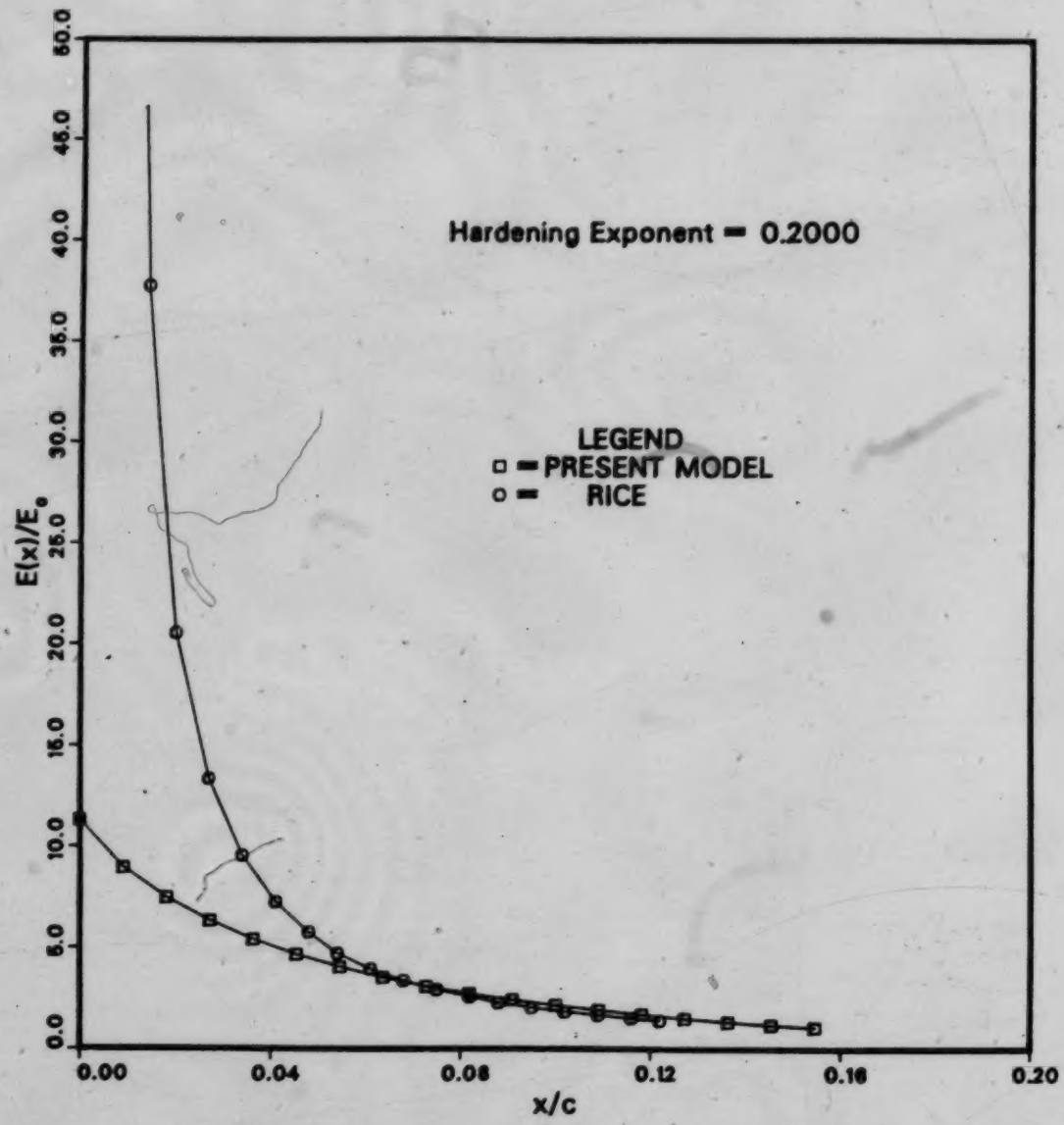

Figure 4.14 Crack-line strain energy density comparison (high hardening)

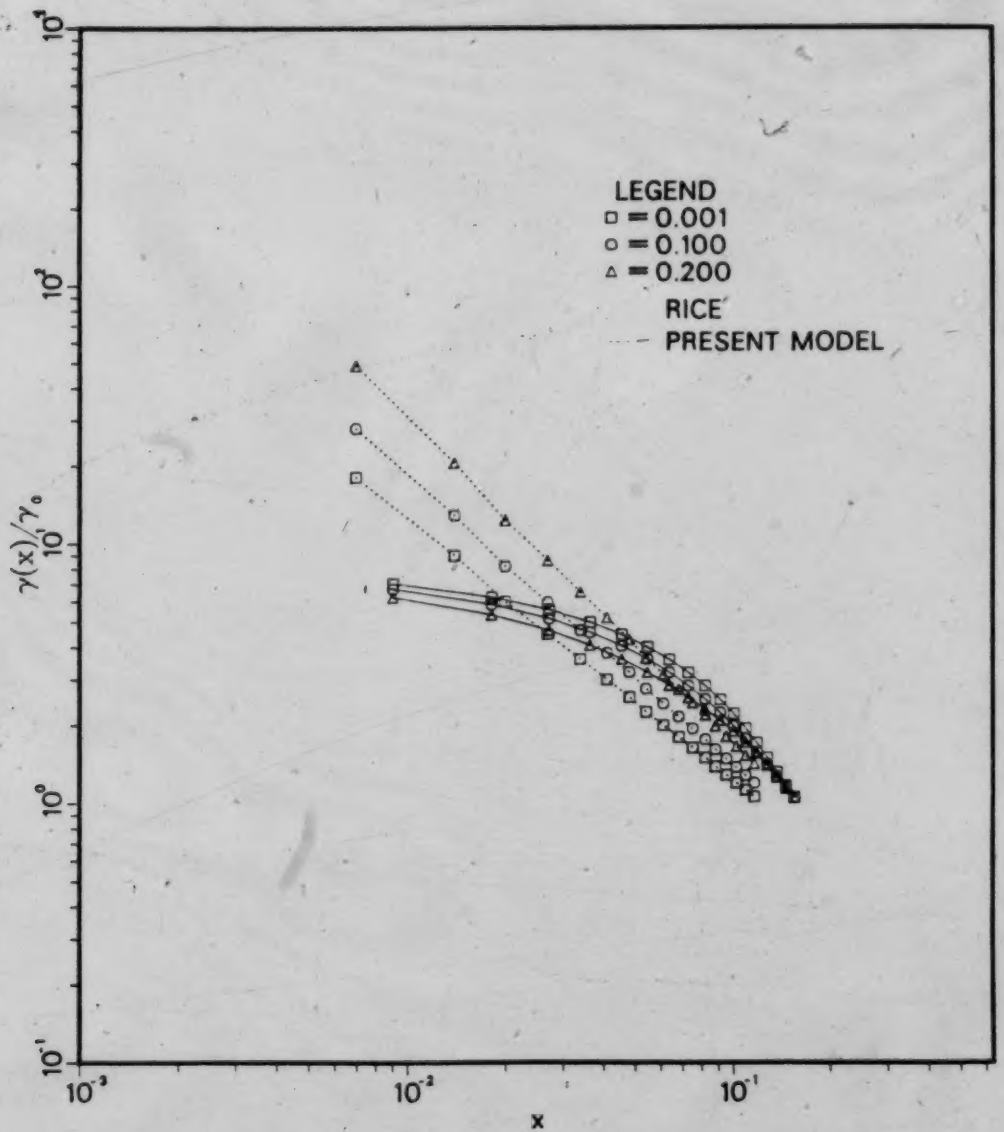

Figure 4.15 Crack-line strain comparison with continuum results on log-log scale

first 15% of the plastic zone size. This results mainly from the singularity predicted by the latter at the crack-tip. This dislocation model predicts finite values of stress/strain at this point for the various values of the hardening exponent. If this first part of the plastic zone is ignored,the prediction the two models are close. Figures 4.6 to 4.8 are for n'=0.001, which is practically elastic-perfectly plastic. The other two sets of Figures, 4.9 to 4.11 and 4.12 to 4.14, represent n'=0.1 and 0.2 respectively. These correspond to mild and high hardening cases. It can be seen that the predicted strains in the two models become closer as the hardening exponent increases. The results for the stresses are even better in general. The Strain Energy Density predicted from these two are also close to each other. These two models thus result in similar predictions for the stress/strain field if the first 15% of the plastic zone size is ignored. We shall discuss this disparity region shortly.

It is significant that the predictions at the ends of the plastic zone are very similar in both models despite the fact that there is a significant diference in the plastic zone sizes in the two models.The values of the strain, stress and the strain energy density predicted by the two models are very close to each other.

We now return to the first 15% of the plastic zone size where the two models differ most. Figure 4.15 shows the plot of the strain distribution versus the

crack-tip distance on a log-log scale. As expected, the greatest difference is observed as $x \to 0$. Available experimental results, however, support this model rather than Rice's in this part of the plastic zone. The crescent shape of this dislocation model prediction is exactly the same as has been observed by Davidson and Lankford [59] for various metals with differing hardening exponents. These investigators have shown that the strain distribution at the origin flattens out in the same way as this dislocation model behaves. This also justifies the singularity removal method used in chapter 3 where the stress/strain distribution at the crack-tip neghbourhood was assumed approximately constant.

Chapter 5

UNLOADING FIELD AND CYCLIC J-INTEGRAL

5.1 Introduction

The dislocation model developed in the previous chapter can be applied to the problem of a crack that is first loaded, and then unloaded to a specified value. This can be further applied to the case of the cyclically loaded crack. The application of dislocation to fatigue loading is not entirely new. Weertman [36], and later Lardner [35], have extended the original BCS [17] monotonic loading model to the case of cyclic loading. In these works, attention is restricted to the displacement at the crack-tip. Crack growth either results from the attainment of a critical value of the crack-tip displacement, or in the fatigue cycling case, when the sum of the displacements at the tip attains a critical value.

From the results in chapter 4, it was seen that work-hardening does not change the crack-tip displacement considerably. Since work-hardening usually leads to a reduction in the value of crack-tip displacement, applying the fatigue ductility failure criterion (as in ref. [7] for instance) would lead to a conclusion then that work-hardening should lead to a lower crack growth rate. Stated differently, this means that the plastic damage rate at the crack-tip should be lower, the higher the work-hardening rate in a given material.

It should be noted that these models presume that the crack-tip stress is always at the yield level. As a result of this limitation, it is not possible to obtain a criterion for cyclic crack growth based on crack-tip stress, or any other stress related quantity. Using the results of Chapter 4, we find that if the crack growth theory is based on the attainment of a critical stress value, a higher work-hardening material would lead to higher crack growth, and higher plastic damage rate. This is a diametrically opposite conclusion from the displacement based criterion. It is therefore evident that, neither the crack tip stress, nor the crack-tip displacement is a consistent measure of the crack-tip plastic damage.

It is desirable to have a crack growth criterion that is not restricted to the crack-tip values. A consideration of the entire plastic zone will be necessary to account for the plastic damage ahead of the crack which results in crack propagation. Such a criterion is the cyclic J-integral proposed by Tanaka [39]. Unfortunately, the evaluation of this quantity has been presented using the classical dislocation theory - limited to the elastic perfectly plastic situation where the entire plastic line is assumed to be maintained at the material yield stress. This is therefore again a quantity based on the plastic displacement considerations only, even though in this case attention is no longer restricted to the crack-tip values.

Applying the complete work-hardening dislocation model to the cyclic case will facilitate the evaluation of a cyclic J-integral dependent both on the plastic displacement as well as the stress field ahead of the crack-tip. Using such a quantity as a crack growth criterion, one would expect to avoid the inconsistency already noted in the use of either a displacement or stress based criterion.

In ref. [39] the plastic superposition method of Rice [19] was used to obtain the stress/strain field ahead of an unloaded crack. The dislocation modelling of the unloaded crack here can be viewed as a generalization of Rice's method. Moreover, one major inconsistency of the plastic superposition method is avoided. This inconsistency arises in the fact that the stress-strain relationship in the plastic zone is nonlinear. This implies that the superposed stress obtained from Rice's method is no longer related to a similarly obtained superposed strain through the stress/strain relationship. While the dislocation modelling of the unloading yields identical results with Rice's superposition method, its premises are different, and they can be extended naturally to the case of work-hardening, as we shall do shortly.

5.2 Work Hardening Unloading Problem

(a) Hardening Laws

In the post yield behaviour of any material, the loading funtion, ℓ, defines the yield surfaces beyond the

initial one in the form of:

$$\ell(\sigma_{ij}, \varepsilon^{p}_{ij}, K) = 0 \qquad 5.1$$

where, σ_{ij} are the stress components, ε^{p}_{ij} are the plastic strain components, and, K represents the way work-hardening enters the loading function.

Equation 5.1 is a general equation defining the changes in the yield surface as a result of the strain hardening. It is the manner in which ε^{p}_{ij} enters the equation that is of concern here. For the purpose of explaining the work-hardening dislocation model of unloading, it is sufficient to consider the one dimensional case here. This is depicted in Fig. 5.1.

After an initial loading to the yield point, (or surface), depicted as τ_o, continued loading leads to plastic strain $\gamma_p(x)$. This leads to the creation of a subsequent yield point at stress equal to $\tau_1(x)$. The difference between the initial yield point and the final yield point is τ_p. When the material is unloaded as shown, the incipience of the plastic strain depends on the hardening law. It is generally accepted that, due to Bauschinger effects, plasticity would begin earlier than the value of the negative initial yield stress, $-\tau_o$. It is convenient to represent this reduction in the negative yield point in terms of τ_p. Clearly, from the Figure, the value $\beta = 0$ represents a situation where there is no

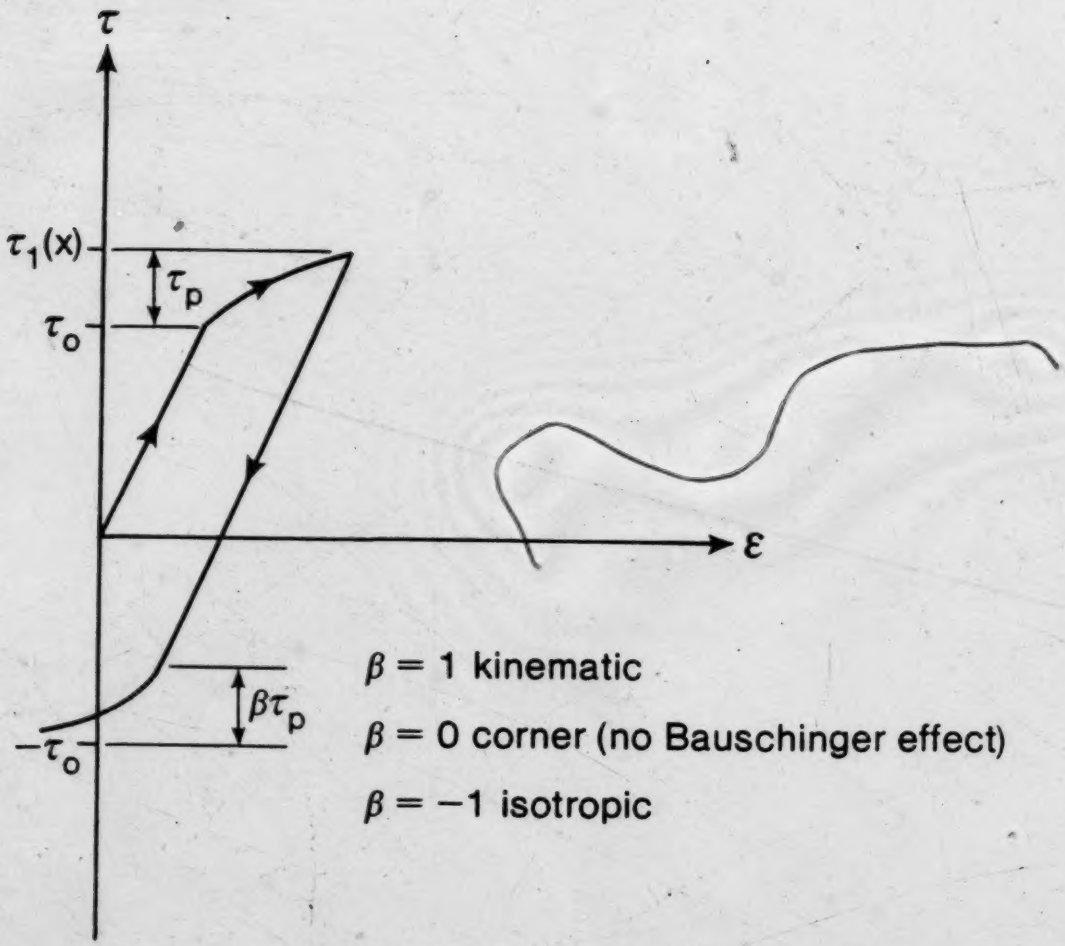

Figure 5.1 Reversed yield point for various hardening rules - one dimensional case

Bauschinger effect, in which case the yield surface is "anchored" at the stress level of $-\tau_o$. This is also called "CORNER HARDENING". The two simplest cases considered in the literature are, $\beta = \pm 1$, called kinematic and isotropic hardening respectively. In the former case, the yield surface is merely translated without any distortion (at least in the direction of loading), while the second case corresponds to a uniform expansion in the axis under consideration. In general, the hardening law is such that the yield surface is both translated and distorted. In this study, attention is restricted to the situation where $|\beta| \leq 1$.

(b) The Unloading Problem

For a work-hardening material loaded to a specified level of stress as described in chapter 4, consider a reduction in the applied stress of magnitude τ. The non-equilibrium created by this reduction leads to reversed forces on the dislocations along the plastic line. The friction stress at each point will then be adjusted in magnitude and direction to oppose dislocation motion. In some locations, near the crack-tip, the reversed forces will be sufficient to move some of the dislocations back into the crack-tip reducing the dislocation density (just as an increase in the applied stress would have led to a dislocation density increase). For the positions closer to the end of the plastic line, $x = \pm a$, the reversed forces may not be sufficient to cause reversed motion. For all

such locations, the dislocations already embedded during the loading are "locked" into their positions until the applied loading is sufficiently high to overcome the initial friction stresses present. Therefore, there is a reduction in the dislocation density from the crack-tip to a point "δ" (Fig. 5.2), while the density function between δ and a remains unchanged. Since the change in the plastic displacement is caused by the amount of reduction in the dislocation density, the functional form of the friction stress is assumed unchanged from Eq. 4.6, i.e.

$$\tau_{11}(x) = F(\Delta\phi(x)) - \beta\, \tau_p(x) \qquad 5.2$$

where $\Delta\phi(x)$ = the change in the plastic displacement due to the unloading at point x, $\tau_p(x) = \tau_1(x) - \tau_0$ and, $-1 < \beta < 1$.

The last term on the RHS of Eq. 5.2 is necessary to account for the displacement and the translation of the initial yield surface at each point due to the work-hardening. This is illustrated in Fig. 5.1. Since τ_0 is interpreted as the yield stress, $\beta\tau_p$ is the amount by which the initial yield stress is reduced in the reversed loading, to account for the Bauschinger effect. It is to be noted that β accounts for both translation and distortion of the yield surface in the one dimensional case. Let g(x) be the resultant dislocation density in the equilibrium state reached after the unloading. Provided

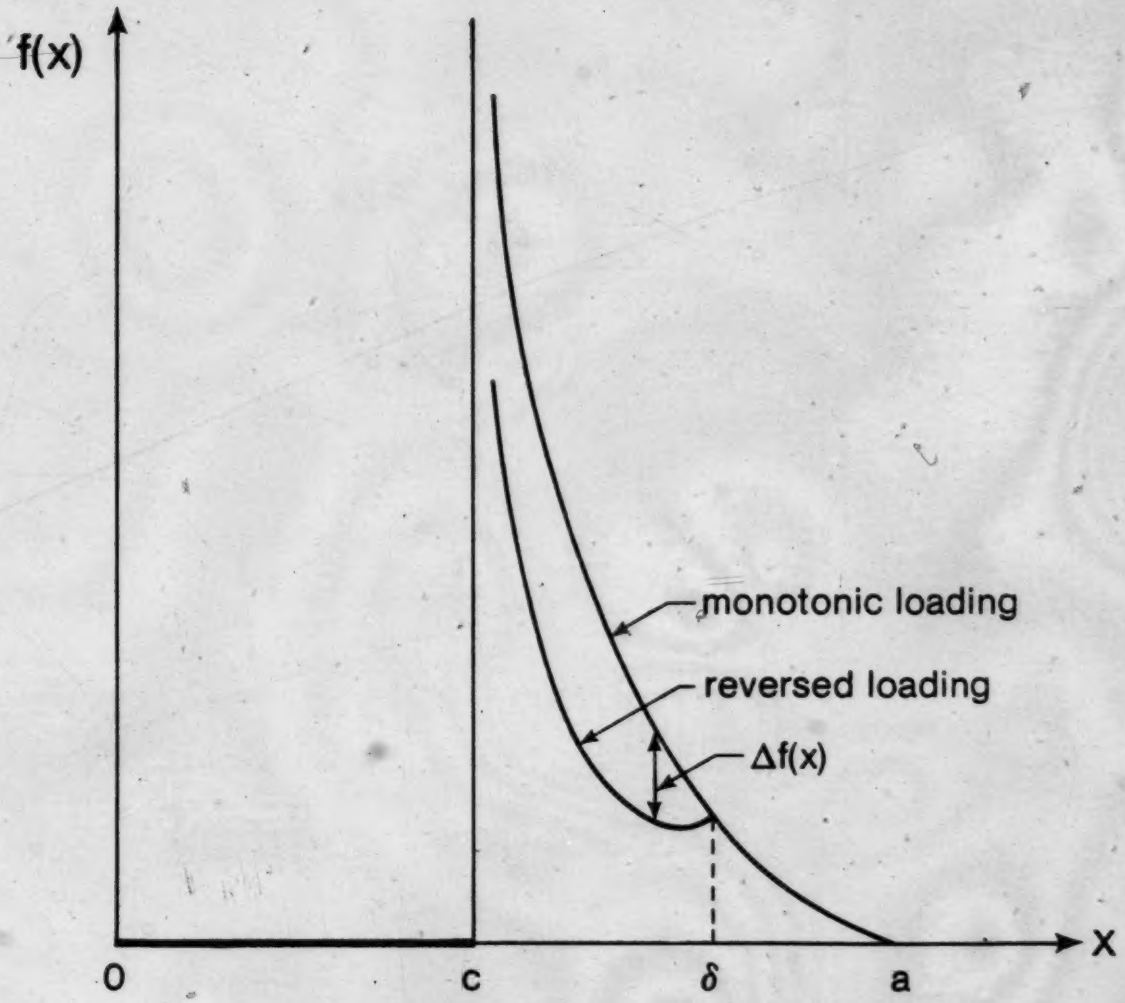

Figure 5.2 Loading and unloading dislocation density functions

$\delta < a$, application of equilibrium equation to the unloaded crack implies:

$$\int_{-a}^{a} \frac{g(x')dx'}{x-x'} + \frac{Q(x)}{A} = 0 \qquad 5.3$$

where

$$Q(x) = \begin{cases} \tau^{\infty} - \tau & |x| < c \\ \tau^{\infty} - \tau - \tau_{11}(x) & c < |x| < \delta \\ \text{unknown} & \delta < |x| < a \end{cases} \qquad 5.4$$

It has been assumed here that there is no contact between the two crack surfaces, so that only the effect of the far field loading contributes the non-dislocation forces at each point in the range $|x| < c$. The resistance of the friction stress in $\delta < |x| < a$ will vary from a value $\tau_{11}(x)$, opposing motion, to a value of $\tau_1(x)$, opposing the original motion of the dislocation, hence supporting the motion in the reversed direction. In this region therefore,

$$\tau^{\infty} - \tau - \tau_1(x) < Q(x) < \tau^{\infty} - \tau + \tau_{11}(x) \qquad 5.5$$

Subtracting equation 5.3 from 4.7, one gets,

$$\int_{-\delta}^{\delta} \frac{f(x')-g(x')}{x-x'} + \frac{H(x)}{A} = 0 \qquad 5.6$$

where
$$H(x) = \begin{cases} \tau & |x| < c \\ \tau - \tau_1(x) - \tau_{11}(x) & c < |x| < \delta \end{cases}$$

$$= \begin{cases} \tau & \\ \tau - 2\tau_0 & \end{cases} - \begin{cases} 0 & \\ (1-\beta)\{F(\phi(x)) - \tau_0\} & \end{cases} - \begin{cases} 0 & |x| < c \\ F(\Delta\phi(x)) - \tau_0 & c < |x| < \delta \end{cases}$$

$$H(x) = H_1(x) - H_2(x) - H_3(x) .$$

Using $H_1(x)$ instead of $H(x)$, Eq. 5.6 becomes the elastic-perfectly plastic unloading equilibrium equation, derived by Lardner [35].

The inversion of 5.6 follows the same pattern as already described in section 4.3. Substituting $f(x') - g(x')$ for $f(x')$ and $H(x)$ for $D(x)$ in Eq. 4.45, assuming that $f(x') - g(x')$ belongs to the class H^*, and $H(x)$ belongs to the class H, then,

$$f(x) - g(x) = \frac{2(1-\nu)}{\pi\mu b} \int_{-\delta}^{\delta} R_1(x, y)\, H(y)\, dy \qquad 5.7$$

where
$$R_1(x,y) = \frac{1}{x - y} \sqrt{\left\{\frac{\delta^2 - x^2}{\delta^2 - y^2}\right\}}$$

The change in the plastic displacement due to the

unloading can then be derived,

$$\Delta\phi(x) = \int_{-\delta}^{\delta} b\{f(x') - g(x')\}dx'$$

$$= \Delta\phi_0(x) - B(1-\beta)\int_{c}^{\delta}\{(\frac{\phi(y)}{\alpha\gamma_0} + 1)^{n'} - 1\}K_1(x,y)dy$$

$$- B\int_{c}^{\delta}\{(\frac{\Delta\phi(y)}{\alpha\gamma_0} + 1)^{n'} - 1\}K_1(x,y)dy, \qquad 5.8$$

where $\Delta\phi_0(x) = \int_{x}^{\delta}\frac{b}{\pi^2 A}\int_{-\delta}^{\delta} R_1(x';y)H_1(x')dx'dy$

is the elastic-perfectly plastic unloading displacement distributions [35],

$$R_1(x,y) = \frac{1}{x-y}\sqrt{\frac{\delta^2-x^2}{\delta^2-y^2}},$$

$$K_1(x,y) = \int_{x}^{\delta}\{R_1(x';y) + R_1(x';-y)\}dx \qquad 5.9$$

and

$$\frac{1}{2B}\Delta\phi_0(x) = (x+c)\cosh^{-1}\left|\frac{\delta^2-x^2}{\delta(x+c)} + \frac{x}{\delta}\right|$$

$$- (x-c)\cosh^{-1}\left|\frac{\delta^2-x^2}{\delta(c-x)} + \frac{x}{\delta}\right|$$

The second term on the RHS of equation 5.8 contains $\phi(x)$, the plastic displacement at each position at maximum loading, while the last term contains $\Delta\phi(x)$, the change in plastic displacement at each position. Therefore, it follows that the change in plastic displacement is dependent on both the range of unloading, as well as the amount of the maximum loading in the range. Other parameters affecting the change in plastic displacement are, of course, the hardening exponent n', and the "cyclic hardening factor", β. Setting n'=0, equation 5.8 becomes identical to the elastic-perfectly plastic solution of Lardner [35], irrespective of the value of the parameter β. This is to be expected because the term containing β cannot take any other value than zero when n'=0. In order to see this, consider the fact that this non work-hardening case corresponds to a retention of the original yield surface, so that there is no reduction of the yield stress in the unloading situation, therefore $\tau_p(x)$, defined in Fig. 5.1, is equal to zero.

It is necessary that the change in the dislocation density be bounded at the points $\pm\delta$. The conditions for this to be the case can be derived in a similar way as in equation 4.35. If H(x) in 5.6 is substituted for F(x) in 4.35, one obtains, after some rearrangements,

$$\int_{-c}^{c} \frac{\tau dx}{(\delta^2 - x^2)^{\frac{1}{2}}} + \left(\int_{-\delta}^{-c} + \int_{c}^{\delta}\right) \frac{\tau - \tau_I(x) - \tau_{II}(x)}{(\delta^2 - x^2)^{\frac{1}{2}}} dx = 0 \qquad 5.10$$

This is the cyclic equivalent of the boundedness condition in Eq. 4.35.

5.3 Solution of the Unloading Displacement Equations

The two unknown quantities in equations 5.8 and 5.10 are the change in plastic displacement, $\Delta\phi(x)$, and the extent of the cyclic plastic zone δ. The integral equation 5.8, and the boundary condition, 5.10 can be solved simultaneously for these two quantities as outlined in section 4.4. The expansion method, used in the latter was also employed with two main modifications. Firstly, it was found that the change in the monotonic plastic zone (compared to the perfectly plastic case) was insignificant. Hence, the elastic-perfectly plastic zone size was used in this analysis. This can be obtained from 5.10 by setting n'=0;

$$\int_{-c}^{c} \frac{\tau dx}{(\delta^2 - x^2)^{\frac{1}{2}}} + \left(\int_{-\delta}^{-c} + \int_{c}^{\delta}\right) \frac{\tau - 2\tau_o}{(\delta^2 - x^2)^{\frac{1}{2}}} dx = 0 \qquad 5.11$$

which means, $c/\delta = \cos(\pi\tau/4\tau_o)$.

This approximation leads to a great simplification of the computational procedure, and, judging from the results

obtained in section 4.4, the reduction in accuracy is minimal. Secondly, analogous to the procedure in chapter 4, the unknown change in plastic displacement was approximated by a perturbation of the elastic-perfectly plastic unloading fuction (Eq. (5.1)),

$$\frac{1}{2B}\Delta\phi(x) = \alpha_1(x+c)\cosh^{-1}\left[(1+|\alpha_2|)\left|\frac{\delta^2-c^2}{\delta(c+x)}+\frac{c}{\delta}\right|\right.$$

$$\left.-\alpha_3(x-c)\cosh^{-1}\left[(1+|\alpha_4|)\left|\frac{\delta^2-c^2}{\delta(c-x)}+\frac{c}{\delta}\right|\right]\right. \qquad 5.12$$

where the exponential-Gaussian background in Eq. 4.58, has been removed. This was done because there was little change to the initial parameter input for both the exponential and the Gaussian terms in the monotonic solution.

Apart from these two modifications, the solution method here is as described earlier, so no further details are given. Various values of the hardening exponents as well as values of the parameter β, depicting the cyclic hardening rule, were considered in the ranges, $0 < n' < 0.2$, and $-1 < \beta < +1$. For an initial maximum loading of $0.4\tau_o$, the values of unloading in the range $0.0\tau_o \leq \Delta\tau \leq 0.6\tau_o$ were considered. This was used to study the effect of hardening on the unloading displacement distribution as well as other relevant crack-tip

parameters. In order to study the effect of the mean applied stress in the range, the value of unloading was fixed (here at 0.35 τ_o), and various mean applied stresses were chosen.

The convergence characteristics of the unloading problem was found to be similar to the monotonic loading problem considered in chapter 4. The convergence was faster for lower values of applied unloading, and lower values of the work-hardening exponent n'. The reverse was the case when the applied unloading was higher.

5.4 The Unloading J-Integral

Consider the loading sequence depicted in Fig. 5.3. For any two loading states i → j, following Tanaka [39], the J-integral can be defined as:

$$\Delta J_{j/i} = \int_{\Gamma} (\Delta W dy - \Delta T_m \frac{\partial \Delta u_m}{\partial x} ds) \qquad 5.13$$

where Γ is a suitable integration path around the crack-tip plastic zone.

$\Delta W = \int_{(\varepsilon_{k\ell})_i}^{(\varepsilon_{k\ell})_j} \left(\sigma_{k\ell} - (\sigma_{k\ell})_i \right) d\varepsilon_{k\ell}$ = change in the strain energy density, and,

$\Delta T_m = (T_m)_j - (T_m)_i$ is the change in the traction vector, while, $\varepsilon_{k\ell}$ and $\sigma_{k\ell}$ are the strain and stress tensors

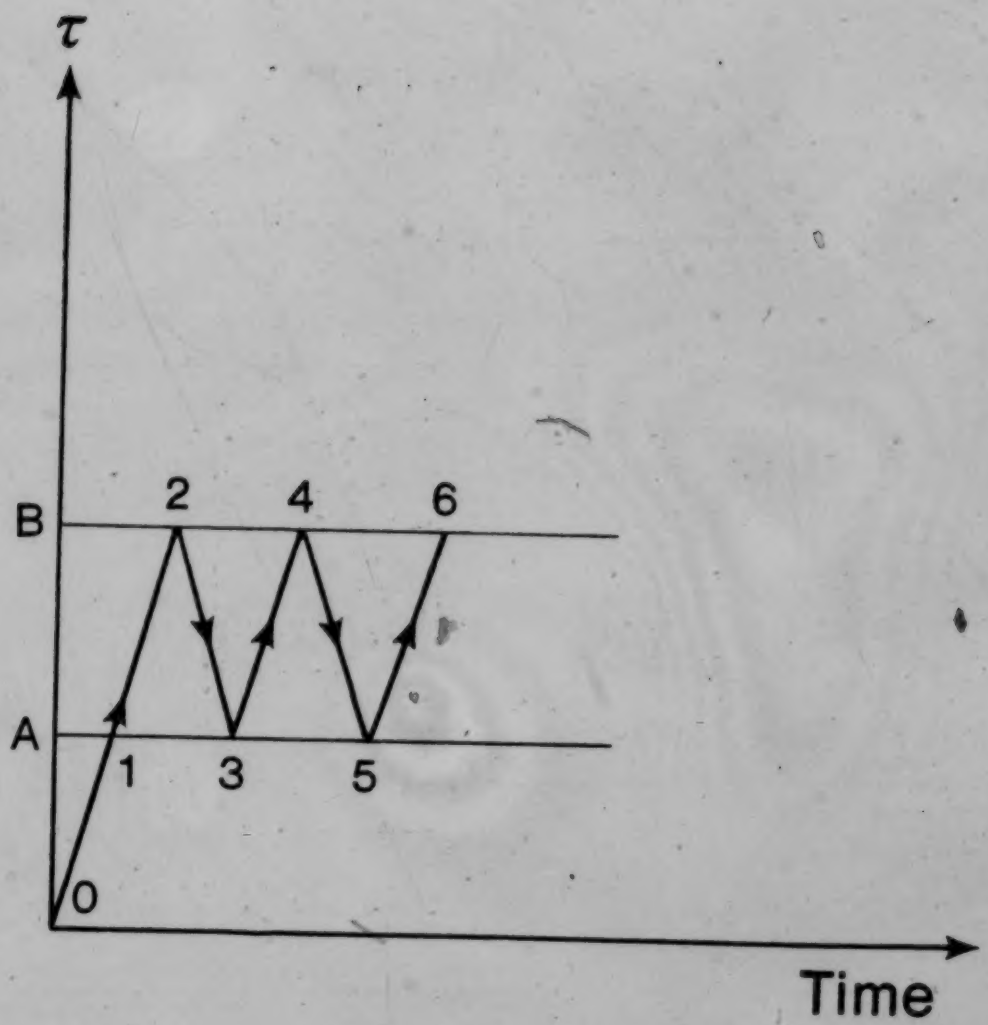

Figure 5.3 Loading sequence

respectively, and $\Delta u_m = (u_m)_2 - (u_m)_1$ is the change in the displacement vector. Equation 5.13 has been shown (see appendix) to be path independent just like Rice's J-integral.

Let us consider for the meantime the unloading from 2 → 3. For the plastic line of the dislocation model, taking Γ as the upper and lower surfaces of the plastic zone implies that $dy = 0$. Hence the first term in Eq. 5.13 vanishes, and $ds = dx$.

On the plastic line,

$$\Delta T_m = (T_m)_2 - (T_m)_1 = \tau_{11}(x) - \tau_1(x)$$

which, using 4.6 and 5.2 becomes

$$= \tau_0 \{(\frac{\sigma_{22}(x)}{\sigma_0} + 1)^{n'} + (1 - \beta)(\frac{\sigma(x)}{\sigma_0} + 1)^{n'} + \beta\} \qquad 5.14$$

and,

$$\Delta u_m = \Delta\sigma(x) = b \int_{\delta}^{c} \{f_3(x') - f_2(x')\} dx' \qquad 5.15$$

where $f_2(x)$ and $f_3(x)$ are the respective dislocation densities at the states 2 and 3, so that,

$$\Delta J_{3/2} = -\int_{c}^{\delta} \tau_o\{(\frac{\Delta\phi(x)}{\alpha\gamma_o} + 1)^{n'} + (1-\beta)(\frac{\phi(x)}{\alpha\gamma_o} + 1)^{n'} + \beta\}\frac{\partial\Delta\phi(x)}{\partial x}\, dx \qquad 5.16$$

Equation 5.16 can be evaluated when the parameters (a_1, a_2, a_3, a_4) have been supplied from the least squares optimization solution of equation 5.8 using the function $\Delta\phi(x)$ defined in 5.12, and $\phi(x)$ from 4.58.

For a given level of the initial loading, state 2, (Fig. 5.3) Eq. 5.16 can be used in evaluating the unloading J-integrals for various amounts of unloading, $\Delta\tau$, values of n', and of the parameter β. The effects of the unloading and hardening on the J-integral to mean loading can also be quantified by fixing the amount of unloading stress, $\Delta\tau$ while evaluating $\Delta J_{j/i}$ for various values of initial loading (state 2).

5.5 Results and Discussion

(a) Relationship between unloading and cyclic J-integrals

The procedure outlined in the the last section shows how the unloading J-integral is obtained. It is important to see how this is related to the cyclic J-integral. Figure 5.4 depicts the changes in the dislocation density for the loading sequence in Fig 5.3. The functions $f_1(x)$ and $f_2(x)$ the dislocation densities for states 1 and 2 are of the same shape, and can both be evaluated from the monotonic dislocation solution, Eq. 4.45. The density

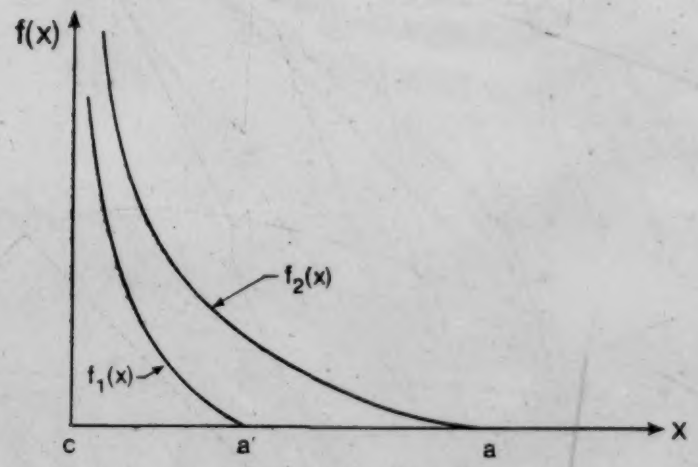

(a) Monotonic Loading

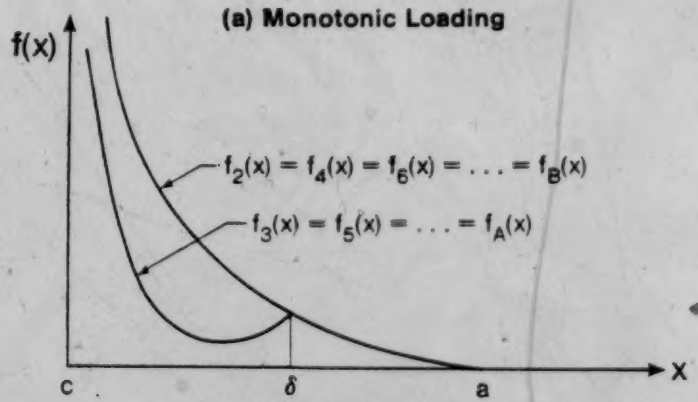

(b) Kinematic Hardening, $\beta = 1$

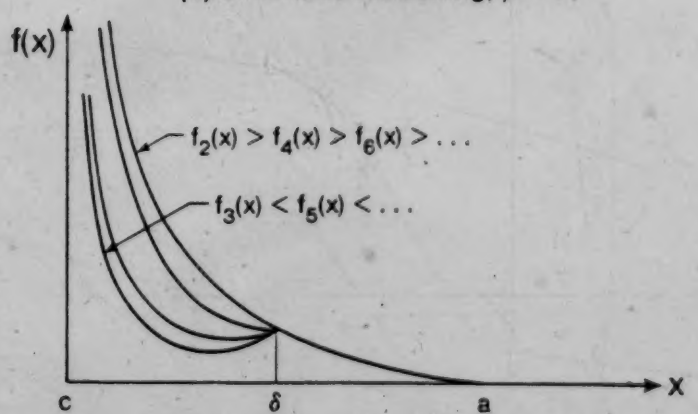

(c) Non Kinematic Hardening, $\beta < 1$

Figure 5.4 Variation of dislocation density with monotonic and cyclic loading

function after the unloading to state 3, is as depicted in Fig. 5.4b. If the τ in equation 5.4 is replaced by the unloading stress range $\Delta\tau$, then, $f_3(x) = g(x)$ in Eq. 5.8. In the reversed plasticity portion (i.e. where some of the dislocations return to the crack-tip, causing a negative change in plastic displacement due to the unloading), there is a reduction in the dislocation density. Outside this region, the unloading is elastic and there is no reversed plasticity. By reloading to state 4, the new dislocation density will depend on the magnitude of the friction stress opposing the return of the dislocations. If the friction stress is the same in state 4 as in state 2 (as in the case of kinematic hardening, $\beta = 1$) the dislocation density would return to its former value at state 2, so that in the sequence we can have $f_2(x) = f_4(x) = f_6(x)$...etc. In this case, $\Delta J_{3/2}$ obtained from Eq. 5.13 is the unique value that quantifies the J-integral in the loading range τ_A and τ_B. . In other cases (non-kinematic hardening, $|\beta| < 1$), the friction stress in state 4 will be greater than that in state 2. Unloading to state 5 would also lead to a reversed friction stress of greater amount than before. The resulting dislocation density will be depicted in Fig. 5.4c. $\Delta J_{3/2}$ does not uniquely quantify the J-integral for the range of loading in this case. Its value is the J-integral at the maximum plastic displacement range. This is a reference cyclic J-integral for the loading range in this particular cyclic

hardening law.

(b) Non-Work Hardening Case

In Ref. [5] the cyclic J-integral was expressed as a linear combination of the elastic and plastic strain energy density range. Similar results follow in the dislocation model in the case of constant friction stress provided the applied stress range is small enough. This is shown below.

The relevant cyclic J-integral is obtained from Eq. 5.16 by setting n' = 0, so that,

$$\Delta J_{3/2} = - \int_{c}^{\delta} 2\tau_0 \frac{\partial[\Delta\phi(x)]}{\partial x} dx \, . \qquad 5.17$$

A closed form solution exists for the displacement range function $\Delta\phi(x)$ in this case. It is the same as Eq. 5.12 with $\alpha_1 = 1$, $\alpha_2 = 0$, $\alpha_3 = 1$ and $\alpha_4 = 0$. Since $\Delta\phi(x)$ depends on x alone, from Eq. 5.17, we get

$$\begin{aligned} \Delta J_{3/2} &= 2\tau_0 \{\Delta\phi(c) - \Delta\phi(\delta)\} \\ &= 2\tau_0 \, \Delta\phi(c) \, , \end{aligned} \qquad 5.18$$

as $\Delta\phi(\delta) = 0$. But for the elastic-perfectly-plastic case, from 5.11,

$$\frac{c}{\delta} = \cos\left(\frac{\pi(\Delta\tau)}{4\tau_0}\right) \qquad 5.19$$

Using the values of the α_i's already specified in 5.17,

$$\Delta\phi(c) = 4Bc \log\left(\frac{\delta}{c}\right) , \qquad 5.20$$

And, now, a substitution from 5.19 in 5.20 leads to,

$$\Delta\phi(c) = 4Bc \log\left[1 + \frac{\pi^2}{32}\left(\frac{\Delta\tau}{\tau_0}\right)^2\right]$$
$$= 4Bc\left[\frac{\pi^2}{32}\left(\frac{\Delta\tau}{\tau_0}\right)^2\left\{1 - \frac{\pi^2}{64}\left(\frac{\Delta\tau}{\tau_0}\right)^2\right\}\right] \qquad 5.21$$

where we have ignored all terms expcept the first two in a Taylor's series expansion of the logarithmic and secant functions. The relevant J-integral in this range can be written as,

$$\Delta J_{3/2} = \eta(\Delta W)c \qquad 5.22$$

where $\Delta W = (\Delta\tau/2\mu)^2$ is the far field strain energy density, c is half crack length, and

$$\eta = (1-\nu)\pi \left[1 - \frac{\pi^2}{64}\left(\frac{\Delta\tau}{\tau_0}\right)^2\right] \qquad 5.23$$

It follows therefore, that, provided $\Delta\tau \ll \tau_0$, η is practically constant, so that, the cyclic J-integral is proportional to the far field strain enery density range.

(c) Effect of Hardening

In the calculations presented, typical alloy steel properties used are μ = 400GPa, τ_0 = 200MPa, and ν = 0.3. Figure 5.5 is a plot of the cyclic J-integral against the far field applied strain energy density on a log-log scale. For moderate levels of the applied stress range, $\Delta\tau$, (keeping the maximum nominal stress at $0.4\tau_0$) the curves are approximately linear for β in the range $-1 < \beta < 1$. Only the two extreme cases ($\beta = \pm 1$) are shown here (as in other places in this chapter) for clarity. The approximate linearity on a log-log scale in this case obviously shows that the relationship between ΔJ and the far field strain energy density range is, in general, of a power law type. For each cyclic hardening law (that is, the value of β), the effect of work hardening is quite significant. The magnitude of ΔJ varies by a factor of up to 5 as n' varies from 0.0 to 0.2. For β = 1 (kinematic hardening) the curves are approximately parallel. For a power law relationship of the type,

$$\Delta J = a(\Delta W)^b, \qquad 5.24$$

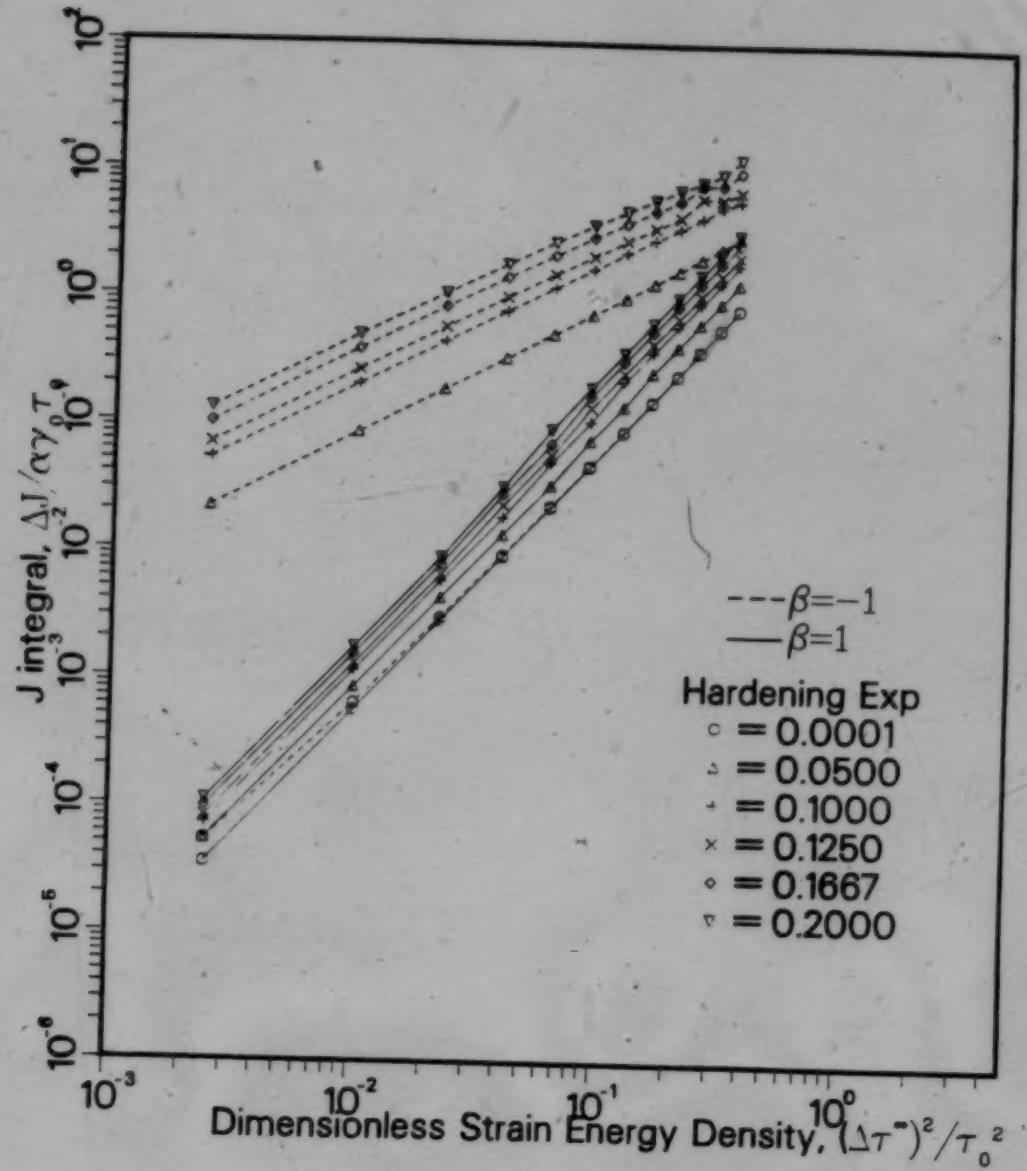

Figure 5.5 Cyclic J-integral vs applied strain energy density

the parameter b is quite insensitive to work-hardening in this case. Most of the work hardening influence is carried through the coefficient parameter a. This is not the case in the non-kinematic work-hardening cases, represented by isotropic hardening $\beta = -1$. These curves change both in slope and intercept as the hardening exponent varies.

Figure 5.6 is the plot of the cyclic crack-tip strain energy density, SED, versus the applied far field stress range. In all cases, the SED increases with applied stress as well as the hardening exponent. The apparent contradiction in the use of either stress or strain to characterise the plastic damage (see section 4.5) can be avoided by basing the cyclic damage on the SED.

In the next set of Figures, the applied stress range is kept fixed at the value of $\Delta\tau = 0.35\tau_o$, while the mean applied stress was allowed to vary between $0.05\tau_o$ and $0.3\tau_o$. In this case, a mean stress value of 0.175 corresponds to the case of complete unloading, $\tau_{min}/\tau_{max} = 0$. In Fig. 5.7, the crack-tip displacement was plotted against the mean applied stress, $(\tau_{max} + \tau_{min})/2\tau_o$. In general, as expected, the crack-tip displacement range decreases with the hardening exponent. This variation is more pronounced in the isotopic hardening case. The exact opposite behaviour is observed when the crack-tip stress is plotted against the mean applied stress (Fig. 5.8). When these two quantities are combined to form the crack-tip SED, Fig. 5.9, it turns out that the latter increases with

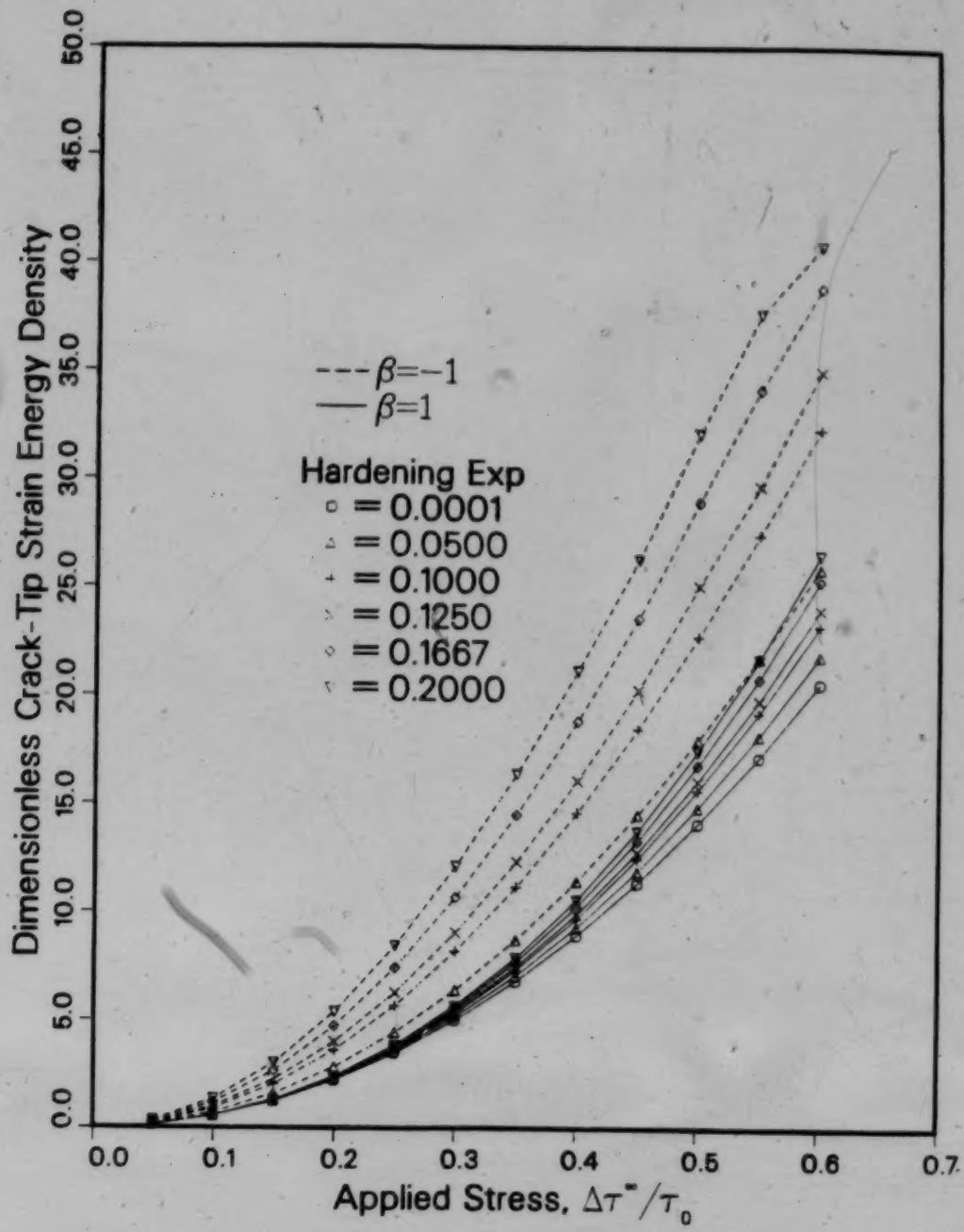

Figure 5.6 Effect of hardening on the crack-tip strain energy density

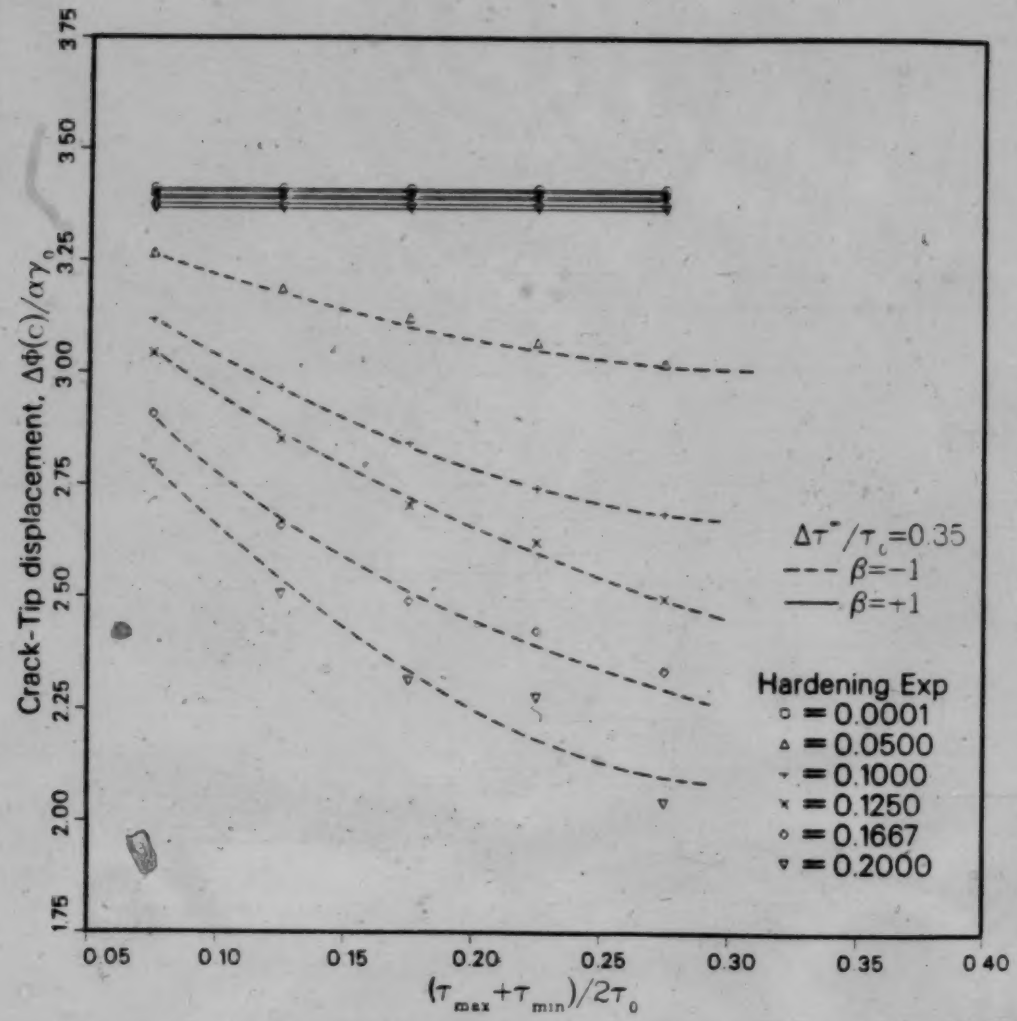

Figure 5.7 Variation of crack-tip displacement range with hardening and mean applied stress

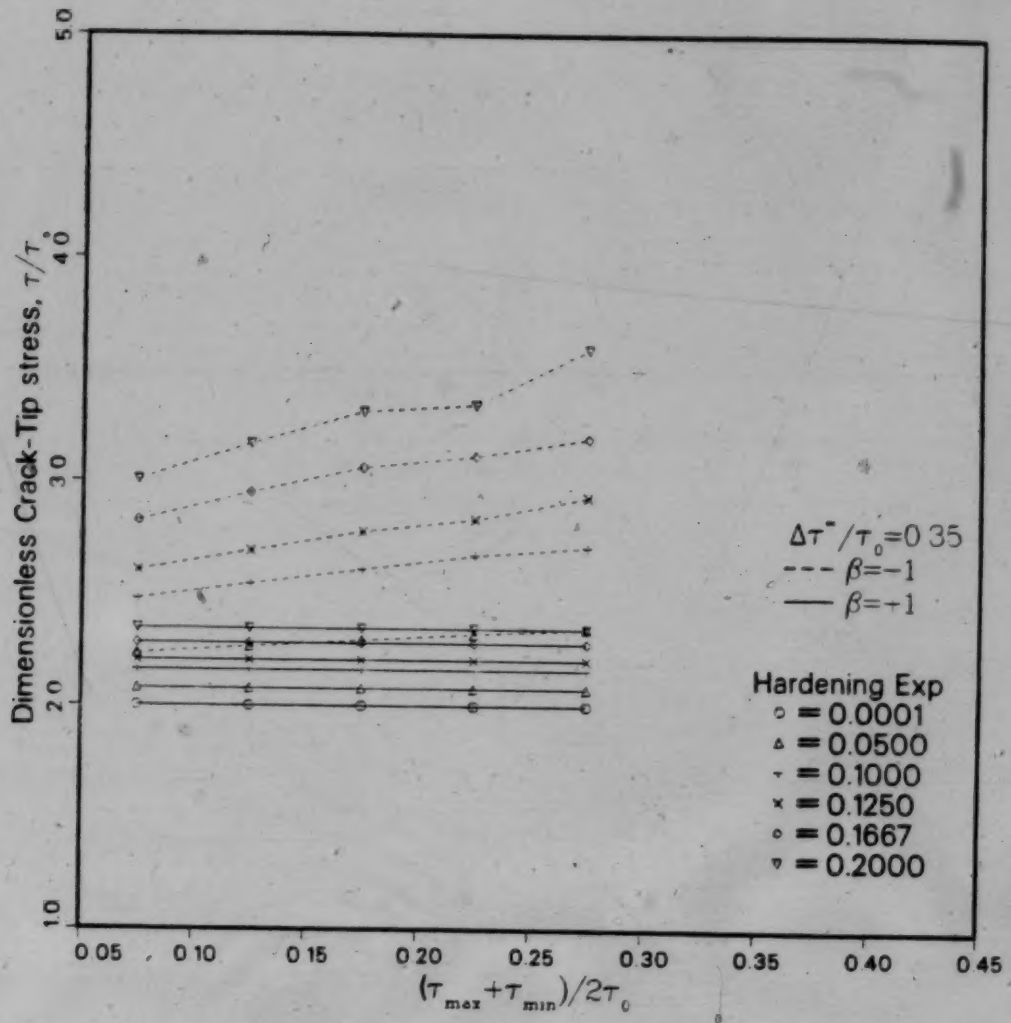

Figure 5.8 Variation of crack-tip stress range with hardening and mean applied stress

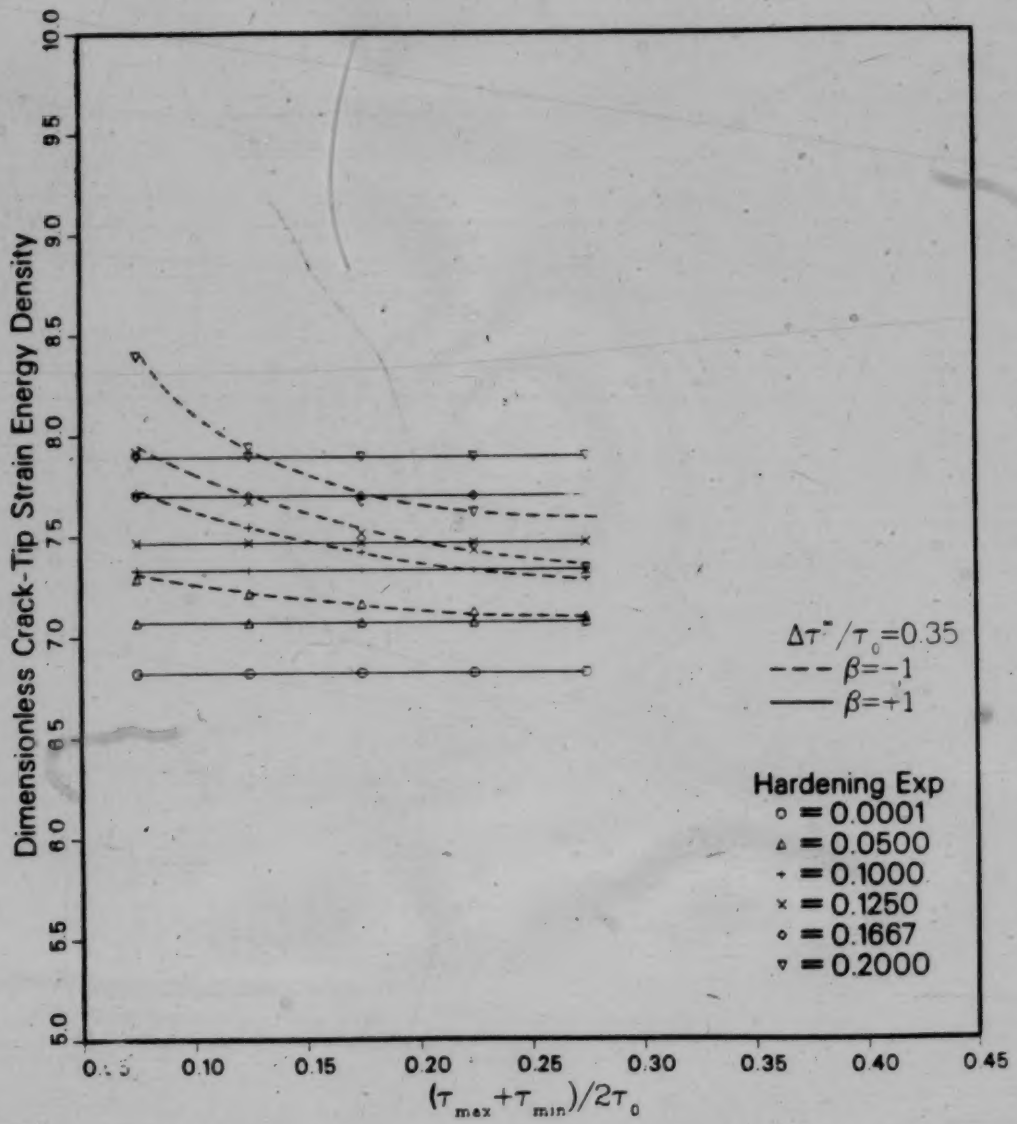

Figure 5.9 Variation of crack-tip strain energy density range with hardening and mean applied stress

hardening for both cases ($\beta = \pm 1$). Note that for the elastic-perfectly plastic case (i.e. hardening exponent, $n' = 0$) the results for all cases $|\beta| = \leq 1$ coincide as expected. In the kinematic hardening case, the variations in the displacement, J-integral and other field quantities cosidered are practically independent of the applied mean stress, while there is a decrease with the applied mean stress for the isotropic hardening case. Fig. 5.10 shows the variation of the cyclic J-integral with the applied mean stress. As in the previous case, the effect of work-hardening is to increase the cyclic J-integral. This variability is also not sensitive to the mean stress for the kinematic hardening case. However, for isotropic hardening, the cyclic J-integral increases with the applied mean stress.

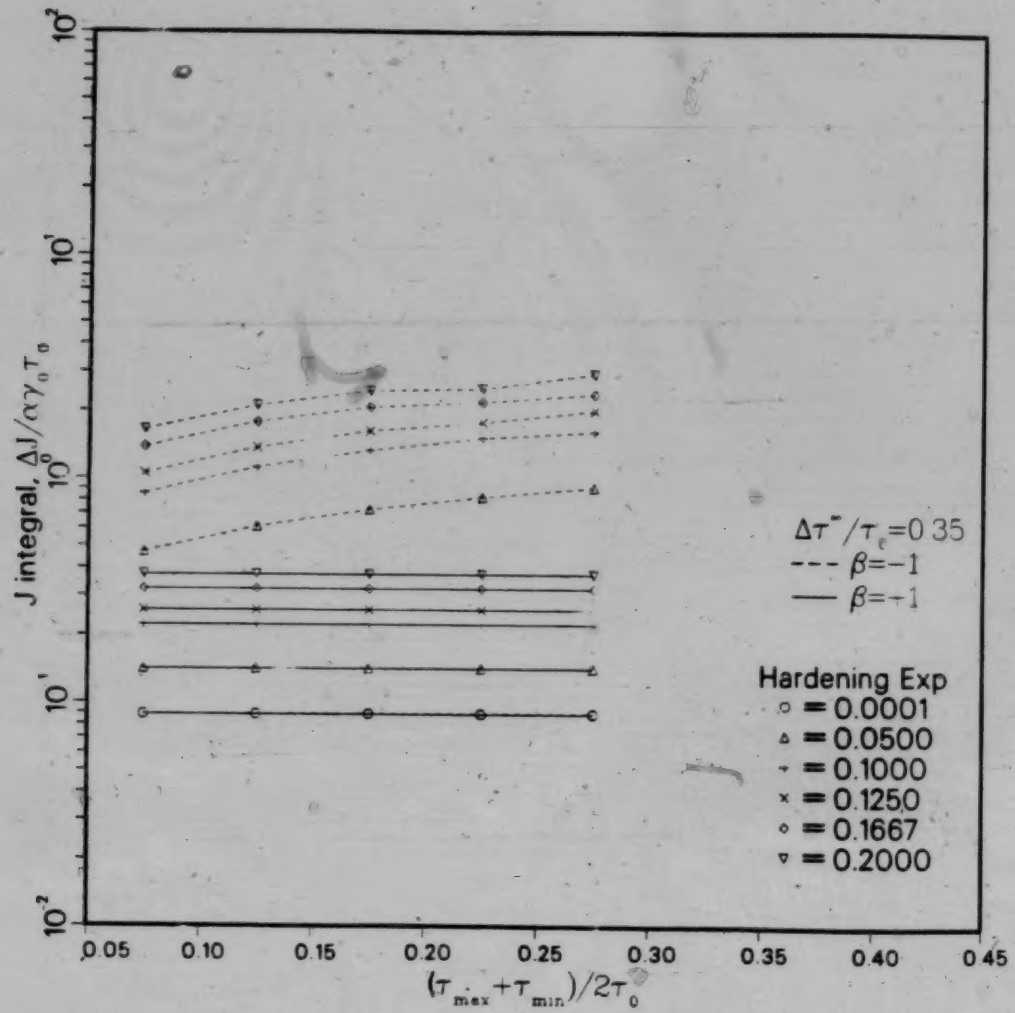

Figure 5.10 Variation of cyclic J-integral with hardening and mean applied stress

Chapter 6

DISCUSSION AND CONCLUSIONS

6.1 Deterministic Model

The main unresolved problem in the damage accumulation modelling of the fatigue crack-tip has been the treatment of the crack-tip fatigue element. Some authors (e.g. [20]) have completely ignored the damage contribution in this region, while others (e.g [21]) have considered it to be the only important aspect of damage accumulation. The seeming contradiction is resolved in the approach presented in this thesis. By including the two contributions, a crack growth rate law has been obtained that fully accounts for the total damage contribution in the fatigue damage zone. The singularity at the origin was removed by noting the experimental evidence that the stress/strain levels sustainable on the fatigue elements cannot be higher than the fatigue strength and ductility coefficients respectively. By assuming that this is attainable only at the critical value of the stress intensity factor, it was possible to determine the extent to which the plastic superposition method for deriving the cyclic stress/strain levels, can be applied. In the region immediately ahead of the crack-tip, due to non-proportional plasticity, the plastic superposition method for obtaining the cyclic stress and strain is not used. Instead of removing this region from the analysis as

in [20], it was included on the assumption that the stress/strain gradient is small, so that the cyclic stress strain levels could be taken as approximately constant as in [21]. However, unlike [21], the failure criterion was applied to this (region I) in a way cognizant of the damage already accumulated in region II (see fig. 3.1). The resulting crack growth law contains the results from the two works cited as special cases. The results from using this law (as earlier demonstrated elsewhere [44]) shows that the contribution from both regions to damage accumulation is of the same order of magnitude. The error, therefore, in ignoring either part is about a factor of 2. Considering the usual scatter in crack growth data, this may not show much significant effect. This explains why the models in [20] and [21] give similar results even through they are based upon seemingly opposite premises.

6.2 Probabilistic Simulation

The main feature that distinguishes the probabilistic simulation model presented is its capability of accounting for the damage accumulation in each fatigue element throughout its damage history. This is a departure from the earlier model by Oh [7] where the system "resets" itself after each crack advance so that the fatigue elements sort of "forget" some of the previously accumulated damage. This is not the first attempt to rectify this deficiency in the memoriless probabilistic

model. Tsurui and Igarashi [33] had earlier suggested that the fatigue element could be treated as random variables whose location factor can be taken as a function of position - in order to account for historical damage. However, there is no obvious *a priori* reason that can lead to a suitable functional form for this location factor. In our approach, the historical damage is simulated once some statistical equilibrium is attained. In this way, it becomes possible to quantify this parameter and to show that its contribution to the damage process is significant. The median growth rate obtained from this simulation has also been shown to approximate the growth rate obtained from the experimental data in some structural alloys.

No attempt was made to obtain a closed form solution for the probability distribution of the growth rate. Previous attempts at closed form crack growth distributions have led to complex densities that could not be approximated by the simple density functions used in practice. Considering the approximate nature of the several factors involved in the derivation of these distributions, it was considered more important to seek the form of the distribution function. Moreover, the inclusion of the historical damage in the model presented, significantly complicates the problem. The resulting growth rate distributions were compared to some of the commonly used density functions in the literature, using

probability plots. The resulting distributions are closer to the Log-normal density than the other two: Extreme Value and Weibull densities. A further indication of the Log-normality of the data was obtained by using a Shapiro-Wilk normality test on the logarithm of the simulated crack growth rate.

6.3 Dislocation Modelling of the Cyclic Field

The dislocation model was presented as an alternative to the unresolved problem of the unloading field. Even though the dislocation modelling of crack-tip plasticity is known to be an extreme simplification of reality, it use still gives some important results comparable to that derived from contiumum considerations. The BCS [17] dislocation model was extended to the case of work-hardening by using a friction stress (opposing the dislocation motion) in the plastic line, as a nonlinear function of strain. The functional form chosen is a modified form of the Ramberg-Osgood stress-strain law. In the unloading field, by assuming that the functional form of the friction stress is retained, work-hardening was treated in a way that allows for the inclusion of the Bauschinger effect.

The inclusion of hardening in this model shows some new insights into the use of failure criterion in crack propagation modelling. While the crack-tip displacement decreases with the hardening exponent, the crack-tip

stress follows the opposite trend. To use either as the measure of fatigue damage would lead to opposite results with respect to hardening. This justifies the use (in the crack-tip modelling used in this thesis) of the product of the stress and strain ranges as a measure of cyclic plastic damage in each fatigue cycle. This measure is closely related to the cyclic strain energy density at each point.

The work-hardening dislocation model is also suitable for the evaluation of the unloading and the cyclic J-integral. This quantity unlike the stress intensity factor used in linear elastic fracture mechanics, is dependent, not only on the range of applied far-field stresses, but also on the applied mean stress. Its dependence on the latter quantity has been found to be closely related to the way Bauschinger effect enters the analysis. For instance, in the case of the elastic-perfectly plastic material where Bauschinger effect can be ignored, as well as when the yield surface is assumed to be translated without distortion (i.e. $\beta = 1$, or kinematic hardening), the mean stress effects are negligible. However, for other values of the parameter β, the mean stresses have quite significant effects on the unloading and cyclic J-integrals, as well as other stress dependent quantities like the strain energy density. We could thus conclude, on the basis of this model, that the observed mean stress dependency well documented in the

literature, can be associated with the departure from kinematic behaviour. Even though the stable cyclic behaviour of a material is usually modelled by the kinematic yield surface, the results here show that there are certain other factors affecting cyclic material damage, that are better modelled from a non-kinematic viewpoint. This is consistent with earlier results by Ellyin and Neale [61] who showed that the yield surface in a cyclically loaded material both expands and translates.

6.4 Future Work

In the failure analysis of the fatigue elements in the statistical crack growth model in chapter 3, the use of a normal distribution was justified by asymptotic considerations. While the burden of experimental evidence supports the use of unity mean, there is no *a priori* considerations for the distribution variance. The use of the standard normal distribution in this circumstance is thus a first approximation only. Experimental and analytical investigations need to be done on the variance of the distribution used.

It would also be helpful if the results of the work-hardening unloading dislocation model of chapter 5 could be extended to the case of tensile loading. The results of the analysis presented here can be formally extended to tensile loading as pointed out by Lardner [35]. The dislocation motion into the crack-tip would then

be interpreted as a "climb" instead of the sliding explanation in the shear case. It is difficult to find similar physical explanation for the former as have been done in the latter. Several alternative models have been proposed for the tensile case. Dugdale [34], Goodier and Field [56], and Bilby and Swinden [18], models are available for the elastic-perfectly plastic loading case. It would be instructive to extend these works for the unloaded crack and the nonlinear work-hardening case.

List of References

1. Hutchinson, J.W., "Fundamentals of the Phenomenological Theory of Nonlinear Fracture Mechanics", ASME Journal of Applied Mechanics, Vol. 50, 1983, pp. 1042-1052.
2. Rice, J.R., "A Path Independent Integral and Approximate Analysis of Strain Concentration by Notches and Cracks," ASME Journal of Applied Mechanics, Vol. 35, 1968, pp. 379-386.
3. Shih, C.F., "J-Integral Estimates for Strain Hardening Materials in Antiplane Shear Using Fully Plastic Solution", Mechanics of Crack Growth, ASTM STP 590, American Society For Testing and Materials, 1976, pp. 3 26.
4. Shih, C.F. and Hutchinson, J.W., "Fully Plastic Solutions and Large Scale Yielding Estimates for Plane Stress Crack Problems", ASME Journal of Engineering Materials and Technology, Vol. 98, 1976, pp. 289-295.
5. Dowling, N.E., "Crack Growth During Low Cycle Fatigue of Smooth Axial Specimens", Cycle Stress-Strain and Plastic Deformation Aspects of Fatigue Crack Growth, ASTM STP 637. American Society For Testing and Materials, 1977, pp. 97-121.
6. Miner, M.A., "Cumulative Damage in Fatigue", ASME Journal of Applied Mechanics, Vol. 12A, 1945, pp. 159-164.
7. Oh, K.P., "A Weakest-Link Model for the Prediction of

Fatigue Crack Growth Rate", ASME Journal of Engineering Materials and Technology, Vol. 100, 1978, pp. 170-174.

8. Sih. G.C. and Madenci, E., "Fracture Initiation Under Gross Yielding: A Strain Energy Denstity Criterion", Engineering Fracture Mechanics, Vol. 18, 1983,pp. 667-677.

9. Bolotin, V.V., "Statistical Methods in Structural Mechanics", Holden Day Inc., 1965.

10. Griffith, A.A., "The Phenomenon of Rupture in Solids", Philosophical Transactions of the Royal Society", Vol. 221, 1920, pp. 163-198.

11. Paris, P.C. and Erdogan, F., "A Critical Analysis of Crack Propagation Laws", Trans ASME, Vol. 85D, 1963, pp. 528-534.

12. Ellyin, F., "A Strategy for Periodic Inspection Based on Defect Growth", Theoretical and Applied Fracture Mechanics, Vol. 4, No. 2, 1985.

13. McClintock, F.A. and Zavel, Jr., F., "An Analysis of the Mechanics and Statistics of Brittle Crack Fracture", International Journal of Fracture, Vol. 15, 1979, pp. 107-118.

14. Hunt, R.A. and McCartney, L.N., "A New Approach to Weibull's Statistical Theory of Brittle Fracture", International Journal of Fracture, Vol. 15, 1979, pp. 365-375.

15. Harlow, D.G. amd Phoenix, S.L., "Bounds on the

Probability of Failure of Composite Materials, "International Journal of Fracture, Vol. 15, 1979, pp. 321-336.

16. Bogdanoff, J.L., "A New Cumulative Damage Model, Part I", ASME Journal of Applied Mechanics, Vol. 45, 1978, pp. 246-250.

17. Bilby, B.A., Cottrell, A.H., and Swinden, K.H., "The Spread of Plastic Yield from a Notch", Proceedings of the Royal Society, Vol. A 272, 1963, pp. 304-314.

18. Bilby, B.A. and Swinden, K.H., "Representation of Plasticity at Notches by Linear Dislocation Arrays", Proceedings of the Royal Society, Vol. A285, 1965, pp. 22-33.

19. Rice, J.R., "Mechanics of Crack-tip Deformation and Extention by Fatigue", Fatigue Crack Propagation, ASTM STP 415, American Society For Testing and Materials, 1967, pp 247-311.

20. Majumdar, S. and Mor J., "Correlation Between Fatigue and Low Cycle Fagitue Properties", Fracture Tougness and Slow Stable Cracking, ASTM STP 559, 1974, pp. 159-182.

21. Glinka, G., "Cumulative Model of Fatigue Crack Growth", International Journal of Fatigue, Vol. 4, 1982, pp. 59-67.

22. Schutz, W., "The Prediction of Fatigue Life in the Crack Initiation and Propagation Stages - a state of the Art Survey", Engineering Fracture Mechanics, Vol.

11, 1979, pp. 405-421.

23. Hult, J.A. and McClintock, F.A., "Elastic-Plastic Stress and Strain Distribution Around Sharp Notches Under Repeated Shear", Ninth International Congress of Applied Mechanics, Vol. 8, Brussels, 1956.

24. Rice, J.R. "Plastic Yielding at a Crack-Tip", Proceedings, International Conference on Fracture, Sendai, Japan, 1965.

25. Lehr, L.R. and Liu, H.W., Fatigue Crack Propagation and Strain Cycling Properties", International Journal of Fracture Mechanics, Vol. 5, 1969, pp. 45-53.

26. Challant, G. and Remmy, L., "Model of Fatigue Crack Propagation by Damage Accumulation at the Crack-tip", Engineering Fracture Mechanics, Vol. 18, 1983, pp. 939-952.

27. Antolovitch, S.D. Saxena, A. and Chanani, G.R., "A Model for Fatigue Crack Propagation", Engineering Fracture Mechanics, Vol. 7, 1976, pp. 649-652.

28. Chakrabortty, S., "A Model Relating Low Cycle Fatigue Properties and Microstructure to Fatigue Crack Propagation Rates", Fatigue of Engineering Materials and Structures, Vol. 2, 1979, pp. 331-334.

29. Head, A.K., "The Growth of Fatigue Cracks", Philosophical Magazine, Vol. 44, 1953, pp. 925-958.

30. Rice, J.R. and Rosengren, G., "Plane Strain Deformation near a Crack-tip in a Power-Law Hardening Material", Journal of the Mechanics and Physics of

Solids, Vol. 16, 1968, pp. 1-12.

31. Hutchinson, J.W., "Singular Behaviour at the end of a Tensile Crack in a Hardening Material", Journal of the Mechanics and Physics of Solids, Vol. 16, 1968, pp. 13-31.
32. Weibull, W., "A Statistical Theory of the Strength of Materials", Ing Vetenskaps Hkad Handl, No 151, 1939.
33. Tsurui, A. and Igarashi, A., "Probabilistic Approach to Fatigue Crack Growth Rate", ASME Journal of Engineering Materials and Techology", Vol. 102, 1980, pp. 300-302.
34. Dugdale, D.S., "Yielding of Steel Sheets Containing Slits", Journal of the Mechanics and Physics of Solids, Vol. 8, 1960, p100.
35. Lardner, R.W., "A Dislocation Model For Fatigue Crack Growth in Metals", Philosophical Magazine, Vol. 17, 1968, pp. 71-82.
36. Weertman, J., "Continuum Distribution of Dislocations on Faults with Finite Friction", Bulletin of the Seismological Society of America, Vol. 54, 1964, pp. 1035-1058.
37. Goldman, N.L. and Hutchinson, J.W., "Fully Plastic Crack Problems: The Centre-Cracked Strip Under Plane Strain", International Journal of Solid Structures, Vol. 11, 1975, pp. 575-591.
38. Mowbray, D.F., "Derivation of Law cycle Fatigue Relationship Employing the J-Integral Approach to

Crack Growth", Cracks and Fracture, ASTM STP 601, American Society For Testing and Materials, 1976, pp. 33-46.

39. Tanaka, K., "The Cyclic J-Integral as a Criterion for Fatigue Crack Growth", International Journal of Fracture, Vol. 22, 1983, pp. 91-104.

40. Baker, C.T.H., "Expansion Methods" in Numerical Solution of Integral Equations, L.M. Delves and L. Walsh, Editors, Claredon Press, Oxford, 1974.

41. Shih, C.F., DeLorenzi, H.G., and Andrews, W.R., "Studies in Crack Initiation and Stable Crack Growth", Elastic-Plastic Fracture, ASTM STP 668, American Society For Testing and Materials.

42 Kujawski, D. and Ellyin, F., "A Fatig. Crack Propagation Model", Engineering Fracture Mechanics, Vol. 20, 1984,pp. 695-704

43. Ellyin, F.,"The Effect of Tensile-Mean-Strain on Plastic Strain Energy and Cyclic Response", ASME Journal of Engineering Materials and Technology, Vol 107, pp.119-125

44. Ellyin, F. and Fakinlede, C., "Crack-tip Growth Rate Model for Cyclic Loading", Modelling Problems in Crack-tip Mechanics, CFC 10, Waterloo, Ontario, 1983.

45. Ellyin, F. and Li, H.P., "Fatigue Crack Growth in Large Specimens with Various Stress Ratios", ASME Journal of Pressure Vessel Technology, Vol. 106, 1984, pp. 255-260.

46. McClintock, F.A., "On the Plasticity of the Growth of Fatigue Cracks", Fracture of Solids, D.C. Drucker and J.J. Gilman, Editors, Interscience, New York, 1963, pp. 65-102.

47. Feller, W., "An Introduction to Probability Theory and its Applications", Vol. II, John Wiley, pp. 262-265.

48. Shimokawa, T. and Tanaka, S., "A Statistical Consideration of Miner's Law", International Journal of Fatigue, Vol. 2, 1980.

49. Rolfe, S.T. and Barsom, J.M., "Fracture and Fatigue Control in Structures", Prentice Hall Inc., 1977.

50. Bury, K.V., "Statistical Models in Applied Science", John Wiley, 1975.

51. Betrand, M., Lefvebre, D. and Ellyin, F., "Statistical Analysis of Crack Initiation and Fatigue Fracture of Thin Walled Tubes, Using the Weibull Law", Journal of Mecanique Theorique et Appliques, Vol. 1, 1983, pp. 49.-510.

52. Hudson, C.M., and Scardina, J.T., "Effect of Stress Ratio on Fatigue Crack Growth in 7076-T6 Aluminum-Alloy Sheet", Engineering Fracture Mechanics, Vol. 1, 1969, pp. 429-446.

53. Newman, Jr., J.D., "Finite Element Analysis of Fatigue Crack Closure", ASTM STP 590, 1976, pp. 281-301.

54. Gakhov, F.D., "Boundary Value Problems", Trans. I.N. Sneddon, Pergammon Press, New York, 1966.

55. Muskhelishvili, N.I., "Singular Integral Equations",

English Translation, Noordhoff, Groningen, Holland, 1953.

56. Mayers, D.F., "Quadrature Methods for Fredholm Equations of the Second Kind", Numerical Solution of Integral Equations, L.M. Delves and J. Walsh, Editors, Claredon Press, Oxford, 1974, pp. 64-79.

57. IMSL, International Mathematical and Statistical Library, Houston, Texas, 1982.

58. Swinden, K., "Applications of the Theory of Internal Stresses in Crystals", PhD Thesis, University of Sheffield, 1964.

59. Davidson, D. L. and Lankford, J., "Fatigue Crack Tip Plastic Strain in High Strength Aluminum alloys", Fatigue of Engineering Materials and Structures, Vol. 3, 1980, pp.289-303

60. Guerra-Rosa, L.,Moura Branco, C. and Radon, J. C., "...otonic and cyclic crack-tip plasticity", International Jou...al of Fatigue, Vol. 6, 1984 pp. 17-25.

61. Ellyin, F. and Neale, K. W., "Effect of Cyclic Loading on the Yield Surface", ASME Journal of Pressure Vessel Technology, Vol. 101, 1979, pp. 59-63.

62. Goodier, J.N. and Field, F.A., "Plastic Energy Dissipation in Crack Propagation", Fracture of Solids, D.C. Drucker and J.J. Gilman, Editors, John Wiley, New York, 1963, pp. 103-118.

APPENDIX

A1. Distribution of sums of random variables

Let X_1 and X_2 be jointly continuous random variates with the joint distribution function

$$f(x_1,x_2) \qquad \text{A1.1}$$

The random variable $Y = X_1 + X_2$ is also continuously distributed. The distribution function of the latter is,

$$F(y) = P[X_1 + X_2 \leq y] \qquad \text{A1.2}$$

$$= P[\{(x_1,x_2): x_1 + x_2 \leq y\}] \qquad \text{A1.3}$$

$$= \iint_{\{(x_1,x_2):x_1 + x_2 \leq y\}} f(x_1,x_2)dx_1dx_2 \qquad \text{A1.4}$$

$$= \int_{-\infty}^{\infty} dx_1 \int_{-\infty}^{y-x_1} dx_2\, f(x_1,x_2) \qquad \text{A1.5}$$

$$= \int_{-\infty}^{\infty} dx_1 \int_{-\infty}^{y} dx_2' \, f(x_1, x_2' - x_1) \qquad \text{A1.6}$$

If in addition, it is known that X_1 and X_2 are independent, then,

$$f(x_1, x_2) = f_1(x_1) f_2(x_2) \qquad \text{A1.7}$$

where $f_1(x_1)$ and $f_2(x_2)$ are the individual density functions respectively. It follows from A1.6 and A1.7 that,

$$F(y) = \int_{-\infty}^{\infty} dx_1 \int_{-\infty}^{y} dx_2' \, f_1(x_1) f(x_2' - x_1) \qquad \text{A1.8}$$

Differentiating equation A1.8 leads to an expression for the density of Y, f(y) given by

$$f(y) = \int_{-\infty}^{\infty} f_1(x_1) f_2(y - x_1) \, dx = \int_{-\infty}^{\infty} dx_1 \int_{-\infty}^{} dx_2' \, f_1(x_1) f_2(x_2' - x_1) \qquad \text{A1.9}$$

$$f(y) = \int_{-\infty}^{\infty} f_1(y - x_1) f_2(x_1) dx$$

The last expression is called a convolution of the functions f_1 and f_2. This idea can be extended to the case of a random variable which is the sum of more than two random variates. Mutual independence will lead to a density function involving a convolution of the initial random variate densities.

A2. The Integral $\int_x^a R(x',y) + R(x' - y)dx'$ (Section 4.5)

Let

$$H(a,x,v) = \cosh^{-1} \left| \frac{a^2 - x^2}{a(x - y)} + \frac{x}{a} \right| \qquad \text{A2.1}$$

It has been shown by Swinden [58] that,

$$H(a,x,y) = H(a,y,x) \qquad \text{A2.2}$$

and that

$$\frac{\partial}{\partial y} H(a,x,y) = R(x,y) \qquad \text{A2.3}$$

It will be shown here that the integral,

$$\int_x^a R(x',y) + R(x',-y)dx' = K(x,y) \qquad \text{A2.4}$$

where

$$K(x,y) = \cosh^{-1} \left| \frac{a^2 - x^2}{a(x-y)} + \frac{x}{a} \right| + \cosh^{-1} \left| \frac{a^2 - x^2}{a(x+y)} + \frac{x}{a} \right|$$

$$- 2\sqrt{\frac{a^2 - x^2}{a^2 - y^2}} \qquad \text{A2.5}$$

From A2.3 it follows that,

$$\frac{\partial}{\partial x} H(a,y,x) = R(y,x) \qquad 2.6$$

Using the symmetry property (Eq. A2.2) we have,

$$\frac{\partial}{\partial x} H(a,x,y) = R(y,x) \qquad A2.7$$

and,

$$\frac{\partial}{\partial x} H(a,x,-y) = R(-y,x) \qquad A2.8$$

$$\frac{\partial K(x,y)}{\partial x} = \frac{\partial}{\partial x} \{H(a,x,y) + H(a,x,-y) - 2\sqrt{\frac{a^2 - x^2}{a^2 - y^2}}\} \qquad A2.9$$

which from the above can be written,

$$R(y, \quad + R(-y,x) + 2\sqrt{\{(a^2 - x^2)(a^2 - y^2)\}} \qquad A2.10$$

$$= -\left\{\frac{1}{x+y} + \frac{1}{x-y}\right\} \sqrt{\frac{a^2 - y^2}{a^2 - x^2}} + \frac{2}{\sqrt{\{(a^2 - x^2)(a^2 - y^2)\}}} \qquad A2.11$$

which after some rearrangements can be shown to be

$$= - R(x,y) - R(x,-y) \qquad \text{A2.12}$$

This and the fact that $K(a,y)=0$ completes the proof.

A3. Path Independence of The Cyclic J-integral [39].

The cyclic J-integral is defined as

$$\Delta J = \int_{\Gamma} \left(\Delta W dy - \Delta T_m \frac{\partial u_m}{dx}\right) ds \qquad \text{A3.1}$$

where

$$\Delta W = \int_{(\varepsilon_{k\ell})_i}^{(\varepsilon_{k\ell})_j} [\sigma_{k\ell} - (\sigma_{k\ell})_i] \, d\varepsilon_{k\ell} \qquad \text{A3.2}$$

is the strain energy density range between states i and j, $\Delta T_m = (T_m)_j - (T_m)_i$ is the change in the traction vector, and $\Delta u_m = (u_m)_j - (u_m)_i$ is the change in the displacement vector. Consider any two paths Γ_1 and Γ_2 and suppose Γ_1 encloses Γ_2. Let ΔJ_1 and ΔJ_2 be the associated cyclic J-integrals with these paths. On the assumption that the stress and strain feilds in the enclosed region are known for an initial state i,

$$\Delta J_2 - \Delta J_1 = \int_{A(\Gamma_2,\Gamma_1)} \left\{ \frac{\partial \Delta W}{\partial x_{k\ell}} - \Delta\sigma_{k\ell} \frac{\partial \Delta\varepsilon_{k\ell}}{\partial x} \right\} dxdy \qquad \text{A3.3}$$

where $A(\Gamma_2,\Gamma_1)$ is the region contained in these curves. Green's theorem has been used to convert the line integral in Eq. A3.1 to the surface integral A3.3. Now,

$$\frac{\partial \Delta W}{\partial x} = \frac{\partial}{\partial x} \int_{(\varepsilon_{mn})_i}^{(\varepsilon_{mn})_j} \{\sigma_{k\ell} - (\sigma_k \qquad \text{A3.4}$$

$$= \frac{\partial}{\partial x}\left\{ \int_0^{(\varepsilon_{mn})_j} \sigma_{k\ell}\, d\varepsilon_{k\ell} - \int_0^{(\varepsilon_{mn})_i} \sigma_{k\ell}\, d\varepsilon_{k\ell} - (\sigma_{mn})_i (\varepsilon_{mn})_j + (\sigma_{mn})_i (\varepsilon_{mn})_i \right\} \quad \text{A3.5}$$

Differentiating under the integral sign leads to

$$\frac{\partial \Delta W}{\partial x} = (\sigma_{mn})_j \frac{\partial (\varepsilon_{mn})_j}{\partial x} - (\sigma_{mn})_i \frac{\partial (\varepsilon_{mn})_i}{\partial x} - (\sigma_{mn})_j \frac{\partial (\varepsilon_{mn})_i}{\partial x}$$

$$- (\sigma_{mn})_i \frac{\partial (\varepsilon_{mn})}{\partial x} j + 2(\sigma_{mn})_i \frac{\partial (\varepsilon_{mn})}{\partial x} i \quad \text{A3.6}$$

$$= [(\sigma_{mn})_j - (\sigma_{mn})_i][\partial (\varepsilon_{mn})_j / \partial x - \partial (\varepsilon_{mn})_i / \partial x]$$

$$= \Delta \sigma_{k\ell}\, \partial \varepsilon_{k\ell} / \partial x \quad \text{A3.7}$$

Using A3.7 in A3.3, we obtain,

$$\Delta J_2 - \Delta J_1 = 0 \quad \text{A3.8}$$

Hence the cyclic J-integral is path independent.